the STEEL centre

Steel Centre Engineering Report No. 020 | May 2021

STANDARDIZATION AND TESTING OF EMBEDDED PLATES FOR DESIGN, FABRICATION, AND CONSTRUCTION ECONOMY

Ian Chong-Xian Chin

Robert G. Driver

Douglas Tomlinson

UNIVERSITY OF ALBERTA

Standardization and Testing of Embedded Plates for Design, Fabrication, and Construction Economy

by

Ian Chong-Xian Chin

Robert G. Driver

and

Douglas Tomlinson

Steel Centre Engineering Report No. 020

Department of Civil and Environmental Engineering

University of Alberta

Edmonton, Alberta, Canada

May 2021

Abstract

Embedded plates are commonly used to facilitate connecting structural steel members to reinforced concrete building elements such as walls and columns. Due to a lack of readily available industry-wide standard embedded plate designs, embedded plates are often custom designed for each project. This leads to many inefficiencies in the design, fabrication, and installation stages of the construction process. Additionally, the current Canadian design standard for concrete structures, CSA A23.3:19, requires many assumptions when evaluating embedded plate capacity, leading to inconsistency among designers. This research project aims to improve the efficiency of the embedded plate construction process by proposing standard embedded plates, and then testing selected embedded plates to verify the predicted capacities and key design assumptions.

Three standard embedded plates having four, six or eight end-welded stud anchors, with design tables developed using CSA A23.3:19, are proposed through collaboration with industry partners involved in the construction process. A small number of plate configurations were chosen to cover a wide variety of common placement and loading situations to improve the simplicity of the design guide. Also, the four- and six-anchor proposed standard embedded plates with shear tab connections were placed at four distances from the concrete edge (75, 125, 175, 250 mm) and tested in shear towards the edge. From the eight full-scale test results, A23.3 was deemed adequate in predicting the failure loads if the connection eccentricity, caused by the gap between the bolt line on the shear tab and the exposed surface of the plate, is considered in the capacity predictions. A test-to-predicted ratio of 0.92 was found when not considering connection eccentricity, compared to 1.11 when considering it. Additionally, embedded plate rotation during testing (0.01 to 0.02 rad at peak load, and further rotation post-peak), suggests connection eccentricity significantly affects the behaviour of the embedded plate and should be considered in design.

Acknowledgments

This research was funded by the Natural Sciences and Engineering Research Council (NSERC) Collaborative Research and Development program (CRDPJ 530162-18: Standardization of Embedded Plates for Steel-Concrete Connections in Buildings) and the Steel Centre at the University of Alberta. The in-kind donation of all the embedded plates and loading arm by Collins Steel, as well as the in-kind donation of concrete by LaFarge, is gratefully acknowledged.

Expertise regarding the design, fabrication and installation of embedded plates provided by DIALOG, Collins Steel, and Clark Builders was also crucial. The knowledge and expertise in the laboratory provided by Cam West and Greg Miller were instrumental for the experimental program. Thank you to the Tomlinson Research Group and the Steel Centre members for their constructive comments and technical advice.

Table of Contents

List of Tables

List of Figures

List of Symbols

A_{brg} = bearing area of the head of the anchor (mm)

A_{Nc} = projected concrete failure area of a single anchor or anchor group in tension (mm^2)

A_{Nco} = projected concrete failure area of a single anchor in tension with an edge distance greater than or equal to $1.5h_{ef}$ ($= 9h_{ef}^2$) (mm^2)

$A_{se,N}$ = effective cross-sectional area of an anchor in tension (mm^2)

$A_{se,V}$ = effective cross-sectional area of an anchor in shear (mm^2)

A_s = cross sectional area of the stud

A_{Vc} = projected concrete failure area of a single anchor or anchor group in shear (mm^2)

A_{Vco} = projected concrete failure area of a single anchor in shear in a deep member with distance from edges equal or greater than $1.5c_{a1}$ in the direction of the shear force ($= 4.5c_{a1}^2$) (mm^2)

$c_{a,min}$ = the minimum distance from the centre of an anchor to the edge of concrete

c_{a1} = if tension is applied, c_{a1} is taken as the minimum distance from the centre of the anchor to the edge of concrete (mm). If shear is applied, c_{a1} is taken as the distance from the centre of the anchor to the edge of concrete in the direction of the applied shear (see Figure 2.20) (mm)

c_{a2} = distance from the centre of the anchor to the edge of concrete in the direction perpendicular to the applied shear, or in the case of applied tension, perpendicular to c_{a1} (mm)

d_a = shaft diameter of the anchor (mm)

E_c = modulus of elasticity of concrete

E_s = modulus of elasticity of the steel anchor

e'_N = eccentricity of resultant tensile load (mm)

e'_V = eccentricity of resultant shear load (mm)

f'_c = specified compressive strength of concrete (MPa)

$f_{cc,200}$ = concrete cube compressive strength (MPa)

f_{uta} = specified tensile strength of anchor steel (MPa)

h_a = thickness of the concrete member that the anchor is installed in, measured parallel to the anchor's axis

h_{ef} = effective anchor embedment depth (mm)

k_c = coefficient for factored concrete breakout resistance in tension (10 for cast-in headed studs)

k_{cp} = coefficient for pryout resistance

$k_1 \cdot k_2 \cdot k_3$ = coefficients for factored concrete breakout resistance in tension before simplification into a single coefficient (k_c) (Fuchs et al. 1995)

l_e = load bearing length of the anchor, which cannot exceed $8d_a$ (mm)

N_{br} = factored concrete breakout resistance in tension of a single anchor in cracked concrete

N_{cbgr} = factored concrete breakout resistance in tension of an anchor group (N)

N_{cbr} = factored concrete breakout resistance in tension of a single anchor (N)

N_{cpr} = factored pullout resistance in tension of a single anchor (N)

N_f = factored tensile load

N_{no} = concrete breakout resistance in tension of a single anchor in cracked concrete proposed by Fuchs et al. (1995)

N_{pr} = factored pullout resistance in tension of a single anchor in cracked concrete (N)

N_r = factored tensile resistance

N_{sar} = factored resistance of an anchor in tension (N)

N_{sbr} = factored side-face blowout resistance of a single anchor (N)

Q_u = shear strength of stud connectors embedded in concrete proposed by Ollgaard et al. (1971)

R = resistance modification factor in CSA A23.3

R_{ACI} = resistance modification factor in ACI 318

s = centre-to-centre distance between anchors (mm)

s_{LVDT} = LVDT spacing

V_{br} = factored concrete breakout resistance in shear of a single anchor in cracked concrete (N)

V_{cbr} = factored concrete breakout resistance in shear of a single anchor (N)

V_{cbgr} = factored concrete breakout resistance in shear of an anchor group (N)

V_{cpr} = factored concrete pryout resistance of a single anchor (N)

V_{cpgr} = factored concrete pryout resistance of an anchor group (N)

V_f = factored shear load

V_r = factored shear resistance

V_{sar} = factored resistance of an anchor in shear (N)

α = test to calculated ratio of the resistance of an anchor in shear for 220 tests conducted by (W. Fuchs and R. Eligehausen, unpublished report, October 1986)

δ_1 = measurement at vertical LVDT 1 (see Figure 4.12)

δ_2 = measurement at vertical LVDT 2 (see Figure 4.12)

λ_a = factor to account for low-density concrete

ϕ_a = material resistance factor for the structural steel plate

ϕ_c = material resistance factor for concrete

ϕ_s = steel embedment material resistance factor for reinforcement

$\psi_{c,N}$ = modification factor for concrete breakout resistance in tension based on the presence or lack of cracks

$\psi_{c,P}$ = modification factor for pullout resistance of anchors based on the presence or lack of cracks

$\psi_{c,V}$ = modification factor for concrete breakout resistance in shear based on the presence or lack of cracks

$\psi_{cp,N}$ = post-installed anchor modification factor for anchors in tension (= 1.0 for cast-in welded headed studs)

$\psi_{ec,N}$ = eccentricity modification factor for anchors in tension

$\psi_{ec,V}$ = eccentricity modification factor for anchors in shear

$\psi_{ed,N}$ = edge distance modification factor for anchors in tension

$\psi_{ed,V}$ = edge distance modification factor for anchors in shear

$\psi_{h,V}$ = factor used to modify shear strength of anchors in concrete members with a depth less than $1.5c_{a1}$

1 Introduction

1.1 Background

The two most common materials used to construct large buildings are reinforced concrete and structural steel. Since these two materials are often used together, connections are required to attach steel members to concrete. Embedded plates are commonly used at connection points due to their relatively easy fabrication, installation, and high load-bearing capacity. Though common, currently there are disagreements among not only different design codes and standards, but also with different assumptions being made by different designers. Also, as designers and steel fabricators are pushed to complete projects faster and cheaper than ever, it is important to have design guides that are easy to use and provide safe designs.

Embedded plates provide a surface on concrete to which steel members can be connected easily using welds or bolts. Many types of embedded plates exist, but they typically consist of anchors that are welded or bolted to a steel plate; the anchors are either post-installed by drilling into the hardened concrete or installed into the concrete formwork prior to casting and the steel member can later be attached to the exposed plate surface. Embedded plates transfer forces from the connecting steel member to the concrete in a variety of ways, depending principally on the type of anchor used. Three common concrete anchors are: headed anchors/studs, expansion anchors, and adhesive or bonded anchors, which resist tension primarily through mechanical interlock, friction, and chemical interlock, respectively, as seen in Figure 1.1 (Eligehausen et al. 2006). Headed anchors transfer tensile load by mechanical interlock through bearing of the underside of the enlarged anchor head on the surrounding base material, typically concrete, as shown in Figure 1.2. Friction is used by expansion anchors, which expand during installation to increase frictional resistance. Finally, in chemical interlock, the anchor is bonded to the base material with an adhesive and tensile load is transferred through the bond. Shear is resisted by all the anchor types mostly by bearing against concrete. The upper part of the anchor bears against the concrete in the direction of the load and the lower part bears in the opposite direction (Figure 1.2) (Grosser 2012).

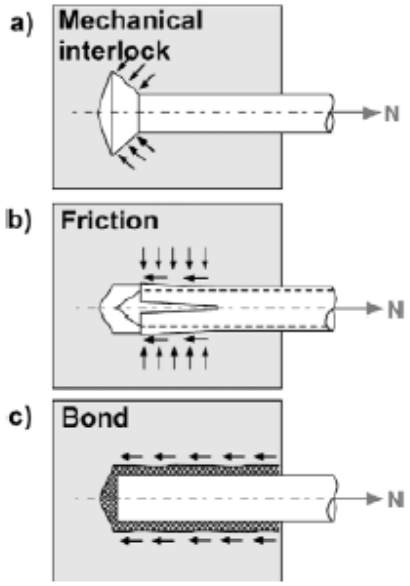

Figure 1.1 Anchor tensile load transfer mechanisms (Eligehausen et al. 2006)

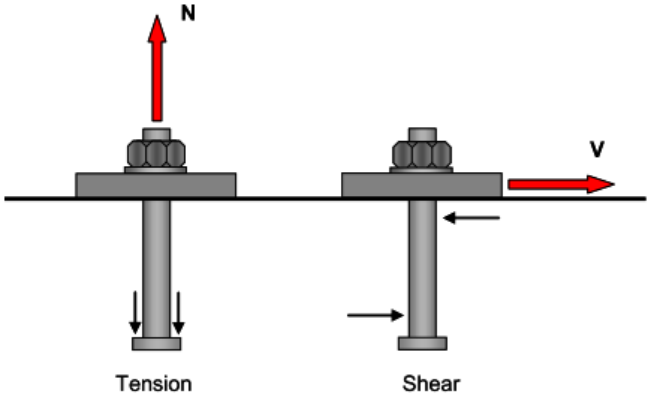

Figure 1.2 Anchor load transfer mechanisms (Grosser 2012)

Additionally, anchors can be differentiated by their installation methods: post-installed or cast-in. Post-installed anchors are installed after the concrete has sufficiently cured by drilling into the hardened concrete, while cast-in anchors are often placed in concrete by connecting the plate directly to the interior surface of the formwork. One of the most widely-used embedded plates is cast-in with welded headed studs, as depicted in Figure 1.3 prior to casting, that transfer loads primarily through mechanical interlock.

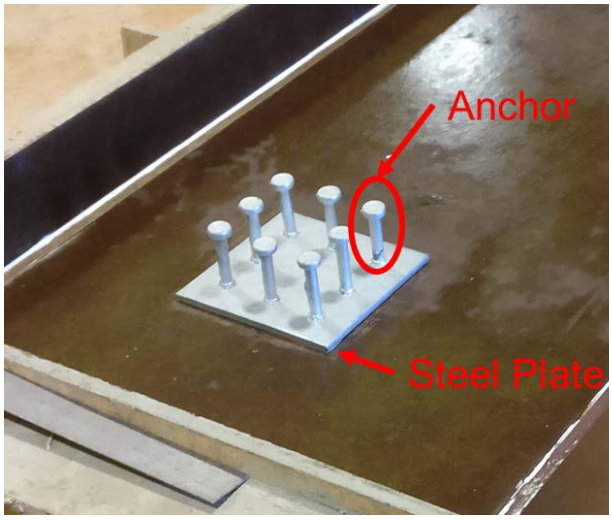

Figure 1.3 Embedded plate with welded headed stud anchors

The design method for concrete anchorage using embedded plates was codified in the American Concrete Institute's (ACI) building code (ACI 318) in 2011, and continues to be an appendix in the Canadian concrete design standard (CSA A23.3) as of 2019. There are also different design methods, such as the methods found in the Canadian Precast/Prestressed Concrete Institute's (CPCI) Design Manual (CPCI 2017), and ACI 349, which deals with the design of nuclear structures. The CPCI Design Manual has different provisions for calculating shear capacity compared those of CSA A23.3 (CSA 2019). Furthermore, many anchor applications are not covered in those design methods, since most of the research relates to a single or a small group (four or fewer) of anchors in tension (Grosser 2012). For example, for anchor groups welded to an attachment (such as an embedded plate with welded headed studs) that is loaded in shear towards the edge of a concrete element (shown in Figure 1.4), CSA A23.3 (CSA 2019) allows a commonly-used assumption that the row of anchors farthest from the edge carries all of the shear load. Although concrete breakout capacities measured experimentally are consistent with that assumption (Grosser 2012) the design provisions conservatively assume that after the anchors closer to the edge crack the concrete, no more load can be carried by those anchors. This may result in a conservative prediction of the steel anchor group capacity in reinforced concrete if only the row of anchors farthest from the edge is considered.

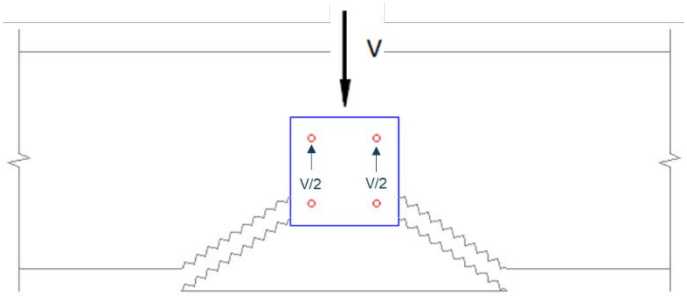

Figure 1.4 Concrete breakout failure of embedded plate with welded headed studs loaded in shear towards an edge.

1.2 Objective and Scope

The main objective of this research is to improve the embedded plate construction process, from design to fabrication to installation, by creating an easy-to-use design guide of a set of standardized embedded plates that produces safe designs. To achieve the objective, the following tasks were completed:

1. Conduct a literature review to understand current embedded plate design methods;
2. Propose a family of standard embedded plates with welded headed studs through consultations with designers, fabricators, and installers;
3. Create design tables using current design provisions found in CSA A23.3 (CSA 2019) for the proposed standard embedded plates; and
4. Conduct eight experimental tests of selected standard embedded plates loaded in shear towards an edge to ensure the reliability of the design tables and verify key assumptions used in the calculation of the design table capacities.

The scope of the research is limited to embedded plates with welded headed studs loaded monotonically under pseudo-static loads. Furthermore, the design of the embedded plates focuses on the Canadian design standard, CSA A23.3 (CSA 2019). Design methods for other kinds of anchors and seismic applications are not considered. The proposed design tables address embedded plates with 4, 6 or 8 anchors in 30 MPa concrete, loaded in shear or tension with a 25 mm lateral eccentricity to allow for some accidental misplacement. Also, shear load design tables assume that load is applied 75 mm from the exposed face of the embedded plate to simulate the use of a fairly rigid connection such as a shear tab. The experimental testing focuses on the

evaluation of two representative standard embedded plates, complete with a shear tab, loaded in shear towards an edge, each placed at four different distances from the edge (75, 125 175 and 250 mm).

1.3 Organization of Report

This report is divided into five chapters. To gain an understanding of the state of the art of embedded plate design, Chapter 2 is a review of literature regarding experimental tests of embedded plates and a review of the design methods provided in Annex D of CSA A23.3 (CSA 2019). Chapter 3 presents the proposed standard embedded plates and their design tables; the design decisions and capacity calculation assumptions are also discussed. Also, experimental test data of anchors close to an edge and loaded towards the edge are aggregated from the literature review in Chapter 2 and compared with design capacities predicted using Annex D. Chapter 4 describes the experimental testing program used to ensure that the design table capacities, calculated with Annex D of A23.3:19, are adequate. Finally, Chapter 5 summarizes the conclusions drawn from this study and recommendations future studies regarding both standardizing embedded plate designs and embedded plate design methods.

2 Literature Review

2.1 Introduction

In this chapter, an overview of research conducted on concrete anchor capacity for embedded plates is presented. Selected investigations performed by researchers are discussed and some history regarding the development of design codes and standards for concrete is provided to give context to the development of the current Canadian design standard, CSA A23.3:19, used to calculate design capacities in the tables presented in Chapter 3. Additionally, design guidelines provided in Annex D are discussed.

2.2 Headed Anchors

One major component of an embedded plate is the anchor. Cast-in headed anchors are typically made of a cylindrical steel rod, with a larger diameter "head" at one end and welded to a fixture at the other end, as shown in Figure 2.1. When the anchor is cast into concrete, loads are transferred from the fixture to the concrete through the anchor.

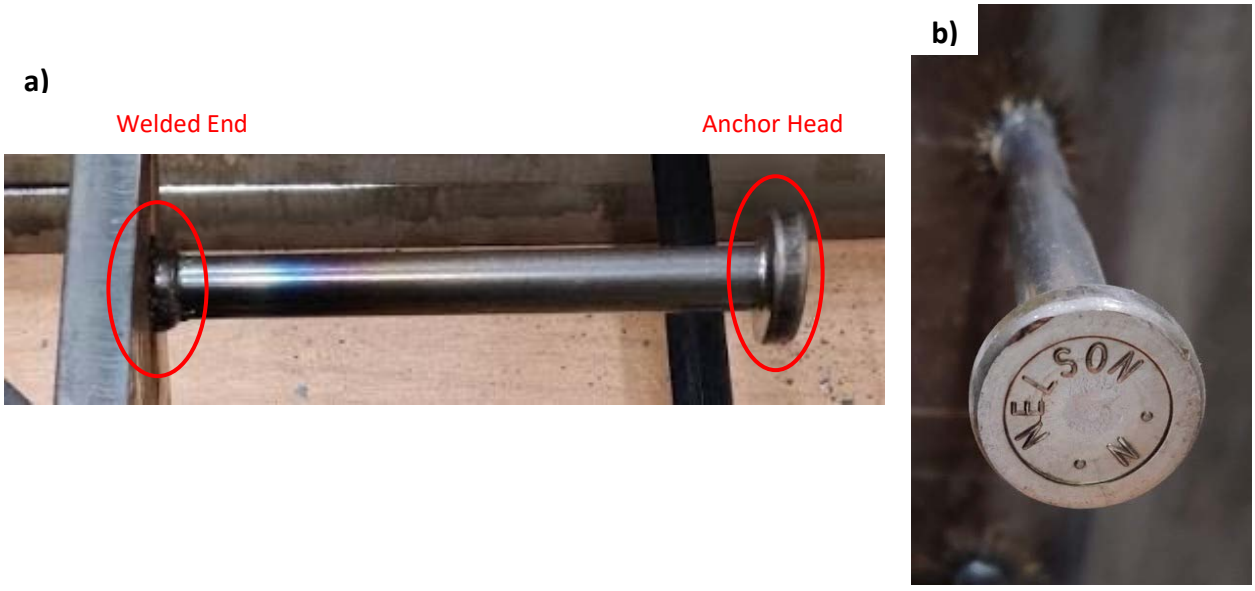

Figure 2.1 Anchor welded to a steel plate (a) viewed from the side, and (b) viewed from the anchor head

This section highlights some of the relevant studies conducted to predict concrete anchor capacity in tension and in shear. Due to the complexity of the geometry of embedded plates, the non-linearity of concrete behaviour, and complicated contact and bond formulations between the anchor and the concrete, much of the research conducted regarding concrete anchors has been

focused on experimental testing results used to develop empirical design equations. Additionally, studies regarding concrete breakout resistance and steel anchor resistance in shear are highlighted with more detail, as they are especially relevant to the experimental testing program presented.

2.2.1 Tension Failure Modes

Headed steel anchors loaded in tension can fail in four main modes: anchor failure, concrete breakout, anchor pullout, and side-face blowout.

2.2.1.1 Anchor Failure

Steel failure of an embedded welded headed stud is typically the most desirable failure mode because it is much more ductile than the concrete failure modes. As long as the weld and the steel plate have sufficient strength, the anchor will fail through tensile uniaxial stress. Methods to predict steel anchor failure are typically based on ultimate strength rather than yield strength, since the materials used in headed studs typically do not have a well-defined yield point (Anderson and Meinheit 2000). Thus, steel anchor failure capacity is much easier to calculate when it is based on an easier to measure material strength.

2.2.1.2 Concrete Breakout

The second failure mode for welded headed studs in tension is concrete breakout strength. This failure mode is characterized by the breakout of the concrete surrounding the anchor in a conical shape (seen in Figure 2.2).

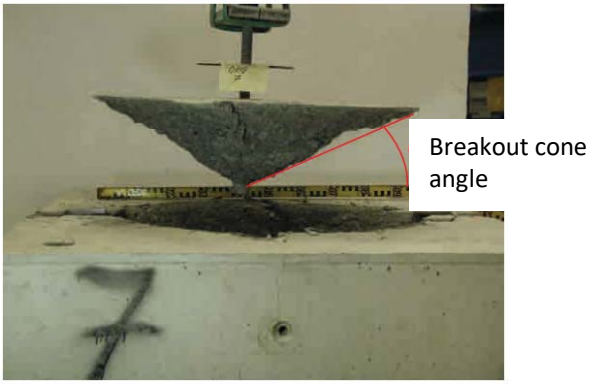

Figure 2.2 Concrete breakout in tension failure surface (adapted from Eriksson and Gasch 2011)

The concrete capacity design (CCD) method, outlined by Fuchs et al. (1995), is used in current building codes and standards such as ACI 318-19 and A23.3:19 to predict the failure load and

mode. Since the CCD method was introduced, further research has been conducted to expand and improve the CCD method. Specifically, the effects of reinforcement on concrete breakout failure loads were studied by Nilsson et al. (2011) and Nilforoush et al. (2018). Nilsson et al. (2011) tested single cast-in headed anchors in plain and reinforced concrete (reinforcement ratio of 0% to 1.2%) and found a significant increase (23% to 54% increase) in load bearing capacity when reinforcement is present. Furthermore, the amount of increase depended on the placement of the reinforcement. Thick concrete members were also found by both Nilsson et al. (2011) and Nilforoush et al. (2018) to increase the capacity of the anchors failing in concrete breakout. Thin slabs tended to deform and crack close to the failure load, accelerating failure, while thicker slabs did not deform as much; reinforcement also prevented cracks from forming until the peak load was reached (Nilforoush et al. 2018).

2.2.1.3 Anchor Pullout

Pullout failure of welded headed studs typically occurs when the anchor is deeply embedded into a member so as to develop a large force. The concentrated pressure at the bearing surface of the head of the stud causes local crushing of the concrete, which leads to significant displacement of the anchor, resulting in reduced concrete breakout failure capacity as predicted by the CCD method. Smaller anchor heads lead to larger pressures on the bearing area, leading to larger displacements, as shown in Figure 2.3.

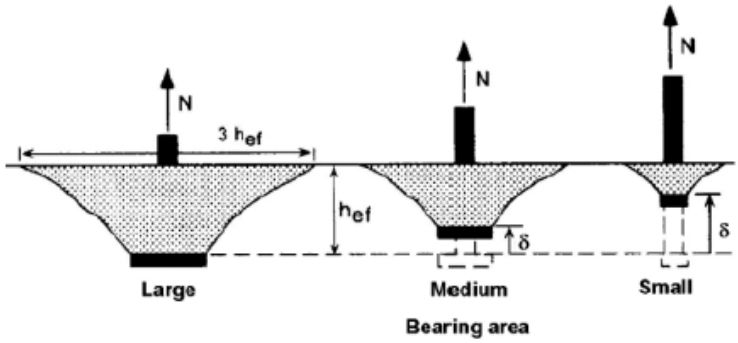

Figure 2.3 Pullout of a headed anchor in tension (Eligehausen et al. 2006)

Eligehausen et al. (1992) estimated the critical bearing pressure of headed studs to be approximately 15 times the concrete cube compressive strength ($f_{cc,200}$) from tests with embedment depths of 185 mm. Additionally, Nilforoush et al. (2018) conducted seven tests on cast-in headed anchors with three different head sizes to determine the effects of head size on

concrete breakout capacity. From the experiments, large-headed anchors had significantly increased concrete breakout capacities compared to small-headed anchors of the same length, while the small-headed anchors had increased ductility compared to the large-headed anchors. Notably, the small-headed anchors exhibited a pullout failure behaviour where they developed greater ductility and displacements after peak load, compared to the large-headed anchors. This means that because of the high concrete bearing stress against the anchor head, the concrete locally crushed, resulting in a gradual pullout of the anchor and a reduced concrete breakout capacity. The small-headed anchors had a bearing stress of approximately $14.7f_{cc,200}$, similar to the proposed critical bearing pressure of $15f_{cc,200}$ proposed by Eligehausen et al. (1992).

2.2.1.4 Side-face Blowout

When an anchor is deeply embedded near an edge of a concrete member, the side-face of the concrete can blow out laterally when the anchor is loaded in tension, as shown in Figure 2.4. According to Furche and Eligehausen (1991), this side-face blowout failure is caused by the quasi-hydrostatic pressure near the head of the stud producing a lateral force. This failure mode is independent of the embedment depth (h_{ef}), but is a concern when the anchor is close to an edge.

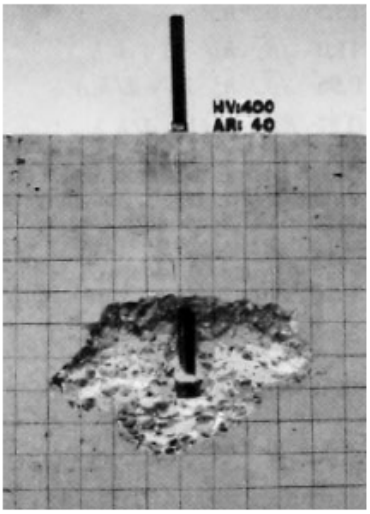

Figure 2.4 Concrete side-face blowout (Eligehausen et al. 2006)

Few studies have been published regarding this failure mode for headed anchors. Though there are studies examining headed reinforcement fabricated from deformed reinforcing steel bars, headed anchors differ from headed reinforcing bars in that the bond strength of reinforcement to concrete is significant, while the bonding of headed studs to concrete can typically be neglected.

Furche and Eligehausen (1991) conducted 35 tests on single headed anchors, varying embedment depth (100 to 500 mm), edge distance (40 to 60 mm), and head bearing area (264 to 1100 mm^2) in unreinforced concrete to study side-face blowout failure. The failure load increased with increasing edge distance, increasing bearing area of the anchor, and increasing concrete strength. Of their tests, 28 failed by side-face blowout and the equation proposed after these tests is used in Annex D of A23.3:19 (see Section 2.5.2.4). Notably, the effects of reinforcement are not included in the method found in A23.3 to calculate concrete side-face blowout resistance, even though confinement of the concrete failure surface has been shown to increase the anchor resistance to other failure modes such as concrete breakout in tension and in shear.

2.2.2 Shear Failure Modes

Anchors loaded under a predominantly shear force can fail in three main modes: anchor failure, concrete breakout, and pryout. Because of the complexity of the stresses developed in an anchor loaded in shear, discussed in Section 2.5.3.1, attempts to quantify welded headed stud's shear load bearing capacity have been largely empirical. Relevant studies regarding each mode of failure are presented in this section.

2.2.2.1 Anchor Failure

Typically, if an anchor or anchor group is embedded deep in concrete and far from an edge, steel anchor failure is the governing failure mode. Steel failure of anchors embedded in concrete and loaded in shear is complex, as shear, tension and bending stresses develop in the anchor (shown in Figure 2.5) (Eligehausen et al 2006).

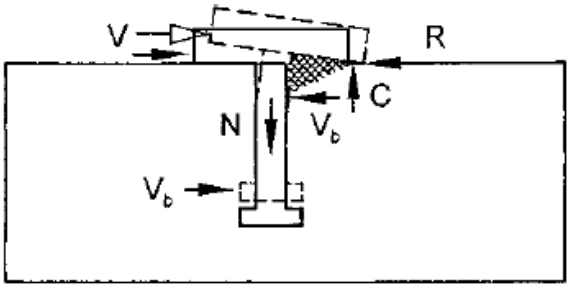

Figure 2.5 Load bearing mechanism of headed stud in shear (adapted from Eligehausen et al. 2006)

Currently, there is no widely accepted theoretical method to determine the steel failure load of an anchor loaded in shear, since these methods have generally been found to be inaccurate or have

high coefficients of variation in the ratio of measured-to-calculated failure loads (Eligehausen et al 2006). Thus, Fuchs and Eligehausen (1986) proposed Equation 2.1.

$$V_{sar} = \alpha \, A_{se,V} \, f_{uta} \qquad \textbf{2.1}$$

where:

V_{sar} = factored resistance of an anchor in shear

$A_{se,V}$ = effective cross-sectional area of an anchor in shear

α = test-to-calculated ratio of V_{sar} for 220 tests conducted by Fuchs and Eligehausen (1986)

f_{uta} = specified tensile strength of anchor steel

From Fuchs and Eligehausen (1986), α was determined to be 0.6 for post-installed anchors. Anderson and Meinheit (2000) performed 97 tests of cast-in welded headed anchors and anchor groups (with two or four studs) loaded in shear as a response by the Precast/Prestressed Concrete Institute (PCI) after new provisions for concrete anchors were introduced into the ACI 318-02 Building Code, even though the ACI provisions were based on post-installed anchor tests. Their report focuses on the steel-controlled failure mode of cast-in welded headed anchors loaded in shear. The anchors (12.7 and 15.9 mm in diameter) were cast into concrete slabs placed flat on the ground and loaded horizontally to be more representative of the conditions found in precast concrete construction. In all the tests studied, the anchors failed at either the weld or the stud shank. From the results, α was determined to be 1.0 for welded headed anchors. The higher coefficient, α, for welded headed studs—as compared to post-installed anchors—is attributed to the weld metal increasing the effective cross-sectional area in the region of highest stress, and the increased fixity at the welded end reduces bending stresses in the anchor (Eligehausen et al. 2006).

Equation 2.1 has been widely adopted for assessing steel anchor shear failure, notably in CSA A23.3:19. Further testing from other researchers such as Lin et al. (2014), who conducted six direct shear pushout tests of welded headed anchors in unreinforced concrete failing in the steel anchor, showed the equation provided accurate predictions of steel anchor shear failure.

2.2.2.2 Concrete Breakout

Concrete breakout typically occurs when anchors are placed close to an edge of the concrete and loaded in shear perpendicular to and toward an edge. It is characterized by the breakout of the concrete towards the edge in a half-conical shape, similar to the shaded region in Figure 2.6.

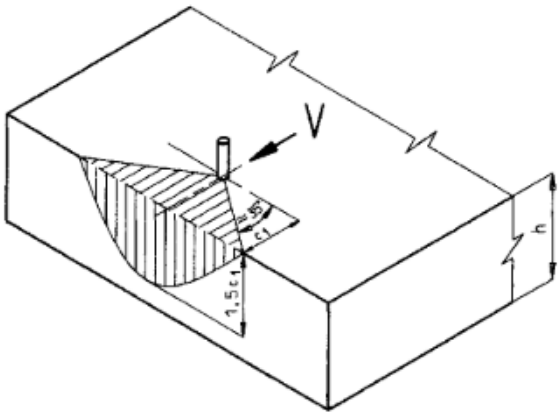

Figure 2.6 Concrete breakout in shear (Fuchs et al. 1995)

Although many studies have been published to develop and verify the CCD method used in Annex D to predict concrete breakout failure, research continues to improve on the method. For example, in a series of studies published by Sharma et al. (2016, 2017), a more detailed model of anchors embedded in reinforced concrete (than in current design codes such as ACI 318-19) is proposed.

Sharma et al. (2016) conducted 16 tests on anchor groups of two to eight anchors (with one to four anchor rows) loaded in shear perpendicular to the edge, with four reinforcement layouts (unreinforced, 12 mm stirrups, 16 mm stirrups, and bundled 16 mm and 14 mm stirrups, all at 200 mm spacing). In the tests, the steel plate to which the anchors are attached was restrained to prevent movement away from the concrete surface. The main purpose of this study is to experimentally investigate the influence of supplementary reinforcement on anchor groups with multiple rows loaded in shear toward the edge, failing by concrete breakout. Due to limited research in the area, current models only consider the contribution of the greater of either concrete or reinforcement to anchor capacity; they do not consider the combined effects of concrete and reinforcement. This leads to conservatism in current design approaches, such as in ACI 318-19. Furthermore, in ACI 318-19, when the failure crack is assumed to be at the farthest anchor row (as is typical for welded headed studs), the anchor steel failure load must be calculated based on the assumption that the entire shear load is carried by the furthest anchor row only. Neglecting the possible contribution of the closer anchor rows to steel anchor capacity also leads to more conservative predictions.

Sharma et al. (2016) also proposes an explanation of the behaviour of anchors close to an edge with supplementary reinforcement using a strut-and-tie model. The tensile forces are taken up by

the stirrups and edge reinforcement, and compression forces are taken by the concrete struts shown in Figure 2.7. From the results of the tests, Sharma et al. (2016) concluded that even small amounts of edge reinforcement and stirrups can significantly increase the capacity of anchor groups close to an edge loaded in shear towards the edge. For the reinforcement layout with 12 mm stirrups, anchor groups failed at loads up to 2.45 times those observed in unreinforced concrete. However, there was relatively little increase in capacity as the amount of reinforcement increased. An increase of only up to 2.62 times the failure load compared to unreinforced concrete was found for the tests in concrete with bundled 16 and 14 mm stirrups, since with large amounts of reinforcement, strut failure begins to become the governing failure mode. Additionally, for anchor groups with only one row placed close to the edge, the edge reinforcement and stirrups could not be reliably activated. Although there is an increase in their capacity, the increase caused by cable action of the edge reinforcement is unreliable, and should not be considered in design.

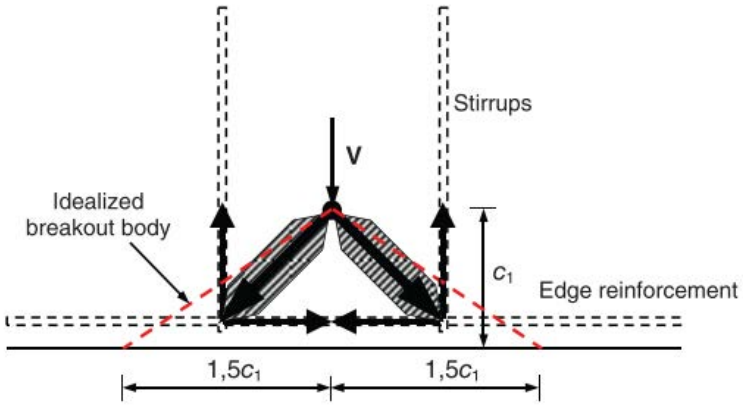

Figure 2.7 Strut-and-tie model for anchors with reinforcement close to an edge (Sharma et al. 2016)

In addition to research on improving the CCD method, there have also been studies on the ambiguities in how it applies to anchor groups. Specifically, the distribution of shear load to the anchors at the ultimate load relies heavily on assumptions made about the behaviour of the anchor groups after initial concrete cracking occurs around anchors closer to the edge. For example, Grosser (2012) conducted shear tests of anchor groups to determine what assumptions should be made when calculating concrete edge breakout capacities of anchor groups in different conditions. Post-installed, bonded anchors were installed in concrete slabs with only the minimum reinforcement required to lift it with a crane, to prevent the reinforcement from confining the concrete breakouts.

Anchor groups consisting of two to three rows of anchors with varying centre-to-centre spacings between the rows of anchors (s_1), and distances from the concrete edge to the closest anchor ($c_{1,1}$), loaded in shear toward the free edge, shown in Figure 2.8, were tested. For anchor groups with a large ratio of row spacing to front edge distance ($\frac{s_1}{c_{1,1}} = 2.0$) in unreinforced concrete, the ultimate concrete breakout failure occurred at the back anchor. Consequently, it can be assumed that the anchors closer to the edge have cracked the concrete and do not resist a significant amount of load and the ultimate load is controlled by the back anchors. Thus, only the back anchors should be used in the calculation of steel anchor shear capacity in unreinforced concrete. However, tests with $\frac{s_1}{c_{1,1}}$ approximately equal to 1.0 showed that this can be conservative as a higher steel anchor capacity was found, showing that the front anchor can resist a fraction of the applied shear load after initial concrete breakout. Furthermore, initial cracking of anchors closer to the edge in an anchor group were shown not to affect the ultimate capacity of the anchors farther from the edge. Additionally, the commentary for ACI 318-14 states that for anchors having a perpendicular spacing to front edge distance ratio ($\frac{s_1}{c_{1,1}}$) less than 0.6, both front and rear anchor rows may be assumed to fully participate in resisting the shear load.

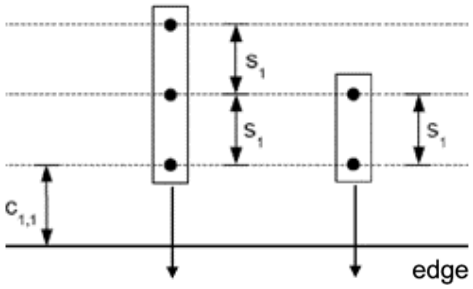

Figure 2.8 Anchor groups tested by Grosser (2012) in shear towards the concrete edge (adapted from Grosser 2012)

Anchor groups loaded in shear parallel to an edge were also tested by Grosser (2012) and results showed their load-bearing behaviour differs compared to the same group loaded in shear perpendicularly toward the edge. In contrast, ACI 318-14 simply calculates the capacity of an anchor group in shear parallel to the edge as being twice the capacity of the same anchor group if it were loaded in shear perpendicular toward the edge. For anchor groups such as those depicted in Figure 2.9, reference tests were conducted on each row of anchors (one closer to the edge, one further from the edge), and tests were also conducted on the full anchor group. From the failure

patterns shown in Figure 2.9, and comparing the reference tests to the full anchor group tests, it was suggested that the ultimate capacity of the anchor groups should be calculated as twice the concrete breakout resistance of the anchor row closer to the edge acting alone. Although load can be redistributed to the anchors farther from the edge after breakout of the first row of anchors, this redistribution is heavily affected by the torsional restraint of the fixture attached to the anchor group. Additionally, in narrow concrete members such as columns or edges of walls, where very few studies have investigated anchor group load bearing behaviours, Grosser (2012) shows similar findings through the anchor groups' failure patterns, shown in Figure 2.10, and comparison with reference tests.

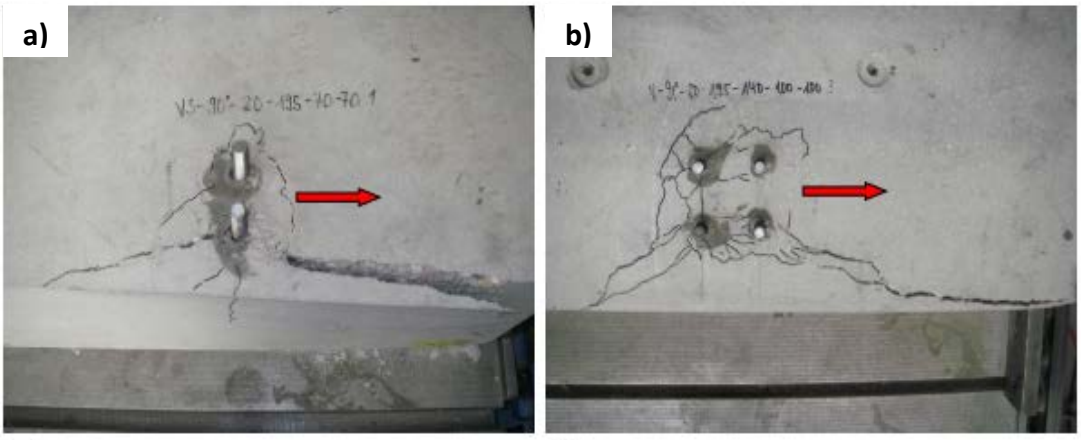

Figure 2.9 Failure patterns of anchor groups loaded parallel to the free edge failing in concrete breakout for (a) two-anchor group, and (b) four-anchor group (Grosser 2012)

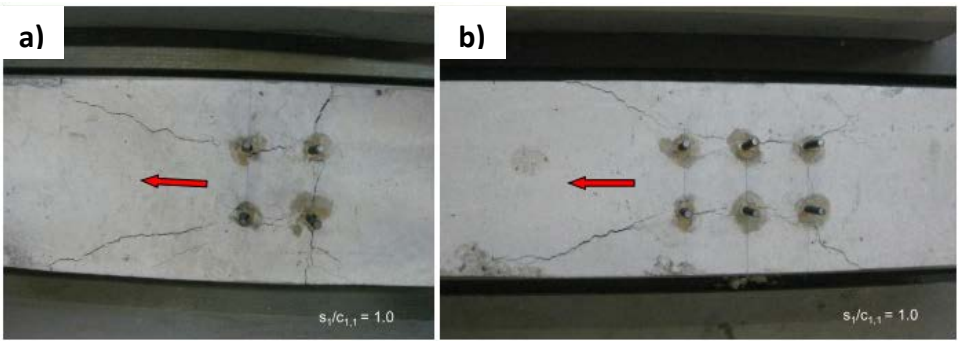

Figure 2.10 Failure patterns of anchor groups in narrow concrete members loaded parallel to free edge failing in concrete breakout for (a) four-anchor group, and (b) six-anchor group (Grosser 2012)

2.2.2.3 Pryout

The last failure mode of anchors embedded in concrete loaded in shear considered in Annex D is pryout. Figure 2.5 shows that when a headed anchor is loaded in shear, it bears against the concrete, resulting in spalling near the surface of the concrete. Thus, the reaction force (V_b), shifts downward as more shear load (V) is applied, resulting in an increasing moment that causes a compressive force (C) between the plate and the concrete surface, and tensile force (N) in the stud. If the tensile force (N) exceeds the tensile capacity associated with the maximum fracture surface that can be activated by the stud, the concrete will fail and a cone-shaped section of concrete behind the anchor will pry out (Eligehausen et al. 2006), as shown in Figure 2.11.

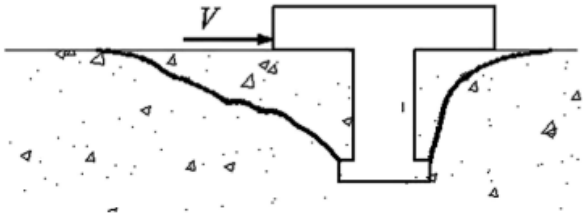

Figure 2.11 Concrete pryout failure (Jebara et al. 2015)

Different equations have been proposed to calculate pryout capacity of welded headed studs, such as Equation 2.2 proposed by Ollgaard et al. (1971) for a single stud, because of its prevalence in composite beams. Equation 2.2 is commonly used in steel design standards such as in CSA S16:19 to design welded headed studs used for composite beams with a solid slab because of its simplicity and accurate predictions. Ollgaard et al. (1971) tested 48 pushout specimens, varying the number of studs, stud diameter, and type of concrete used (light-weight and normal-weight). From the results, it was determined that the cross-section of the anchor, and concrete properties (strength and density) play an important role in predicting pryout capacity, Q_u. Since the density of concrete affects its elastic modulus, it is accounted for in Equation 2.2.

$$Q_u = \frac{1}{2} A_s \sqrt{f_c' \, E_c} \qquad \textbf{2.2}$$

where:

A_s = cross-sectional area of the stud

f_c' = concrete compressive strength

E_c = modulus of elasticity of concrete

Currently, in Annex D, the pryout failure capacity is the tension concrete breakout failure capacity multiplied by the coefficient for pryout resistance, k_{cp} (more information can be found in Section 2.5.3.3), which does not consider the effects of anchor diameter. However, more recent studies (Anderson and Meinheit (2005), Jebara et al. (2016)) have found this method to be overly conservative and it misses the contribution of anchor diameter to pryout capacity. Precast concrete members are often thin, such as in sandwich wall panels; thus, anchors are often shallowly embedded and therefore often fail by pryout. Anderson and Meinheit (2005), as a part of a PCI research program, analyzed pushout test data from several studies, and conducted eight tests on multiple-row anchor groups with welded headed studs. Notably, from the results, an equation was proposed that considers the anchor diameter, concrete properties (strength and density), embedment depth, and spacing of the anchors in the direction of the shear load ('y' spacing), while the equation proposed by Ollgaard et al. (1971) does not consider embedment depth or y spacing. Similarly, Jebara et al. (2016) investigated pryout capacity through 45 tests on single welded headed studs with varying embedment depth (30, 50 and 90 mm) and diameter (8 to 44 mm), and proposed Equation 2.3. Again, cross-sectional area (accounted for with anchor diameter (d_a)), concrete strength ($f_{cc,200}$) and embedment depth (h_{ef}) were shown to be significant factors in predicting concrete pryout strength.

$$V_{cp} = 6\, d_a^{0.5} f_{cc,200}^{0.5}\, h_{ef}^{1.5} \qquad \textbf{2.3}$$

2.2.3 Shear and Tension Interaction

When anchors are loaded in shear and tension simultaneously, the interaction of the two forces results in a capacity reduction. This interaction is complex as there are different failure modes to consider, as well as the shear and tension interaction. Different interaction models, shown in Figure 2.12, have been proposed in several different studies. A trilinear interaction diagram was proposed by Bode and Roik (1987), and elliptical interaction diagrams, common for shear and tension interaction of steel, have been studied by Lotze et al. (2001), Saari et al. (2004), and Lin et al. (2014).

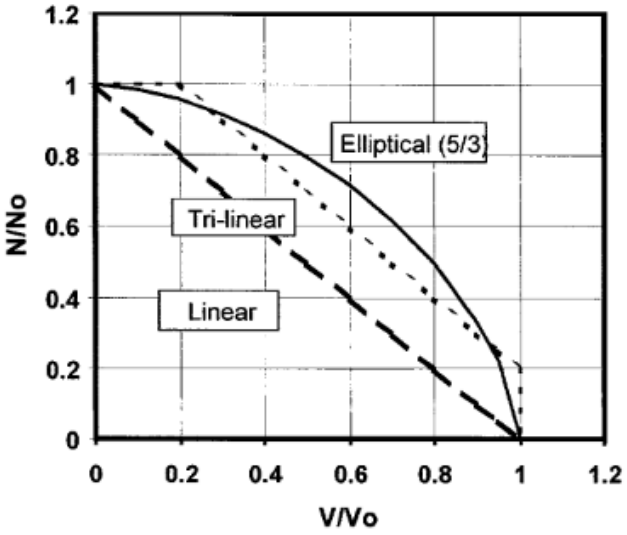

Figure 2.12 Different shear and tension interaction diagrams (Lotze et al. 2001)

Bode and Roik (1987) tested single headed anchors under combined shear and tension and proposed a trilinear equation, currently used in Annex D, because of its simplicity and relatively conservative predictions. For cases where there is little shear (less than 20% of applied tension when normalized by their respective capacities without interaction) in tension-dominated loading, or little tension (less than 20% of similarly normalized applied shear) in shear-dominated loading, no reduction in strength due to shear and tension interaction has to be considered. Furthermore, since the concrete specimens used in the testing were unreinforced or only lightly reinforced, they considered the trilinear method, shown in Figure 2.12, to be conservative in more practical cases with higher reinforcement ratios.

An elliptical interaction, such as Equation 2.4, has been used by several studies, such as those of Lotze et al. (2001) and Saari et al. (2004), to describe the shear and tension interaction of anchors. However, there have been varying recommendations for the exponent (k). Lotze et al. (2001) proposed exponents of 1.67 to 1.80 for failures in the steel anchors and 1.6 for concrete failure, while Saari et al. (2004) showed that an exponent of 1.0 may be more appropriate. Lin et al. (2014) proposed a modified elliptical interaction, where the simplicity of the trilinear equation is combined with an elliptical interaction.

$$\left(\frac{V_f}{V_r}\right)^k + \left(\frac{N_f}{N_r}\right)^k \leq 1.0 \quad \textbf{2.4}$$

where:

V_f = factored shear load

V_r = factored shear resistance

N_f = factored tensile load

N_r = factored tensile resistance

2.3 Plate Design

The steel plate to which anchors are welded is an important part of an embedded plate assembly. However, few studies been published regarding the steel plates used for embedded plates. Currently, there are no explicit design guidelines for the steel plate of an embedded plate in CSA A23.3:19 or S16:19. Although there are baseplate design guidelines in the Canadian Handbook of Steel Construction (CISC 2017), baseplates typically transfer predominantly compressive forces, while embedded plates typically transfer shear, tensile forces and moments. Furthermore, the CPCI Design Manual (CPCI 2017) specifies minimum plate thicknesses depending on the nominal diameter of the welded headed anchor used; the plate thickness is required to be at least half the anchor diameter. This required minimum, originally presented in the American PCI Design Manual, was based on experiments conducted by Goble (1968) (Anderson and Meinheit 2000). Increased plate thickness may be required for plate bending resistance or to ensure a uniform load distribution (Anderson and Meinheit 2000).

Goble (1968) conducted an experimental study to examine the behaviour of thin flange pushout specimens with diameters of 12.7, 15.9, and 19.1 mm welded stud shear connectors and determined when the shift in failure mode from stud shear to flange pullout occurs. From the 41 tests they conducted, using thin flange specimens with welded headed anchors loaded in shear, a shift in failure mode from stud shear to flange pullout occurred for tests exceeding an anchor diameter to flange thickness ratio of 2.7. Equivalently, the flange thickness must be greater than 0.37 times the anchor diameter to prevent failure in the steel flange.

Cook et al. (1989) investigated the behaviour of ductile multiple-anchor steel-to-concrete connections under combined shear and moment loads. Specifically, the objective was to create a

rational design procedure for ductile steel-to-concrete connections covering both cast-in and post-installed anchors. A steel-to-concrete connection is considered ductile if it fails by yielding and fracture of the steel anchors. Cook et al. (1989) conducted 44 friction tests, and 46 ultimate load tests of multiple anchor connections to study the coefficient of friction between a surface-mounted steel plate and hardened concrete, the shear and tension interaction relationships of the different anchor types, the distribution of tensile and shear forces to the anchors, and the effect of the steel plate's flexibility on the strength of the multiple-anchor connections. The connections were loaded in shear and moment with the test setup shown in Figure 2.13. From the friction tests, it was observed that the frictional force between the steel plate and concrete was significant due to the compressive reaction from the applied moment and, for design purposes, the coefficient of static friction should be taken as 0.40. From the ultimate load tests, an elliptical tension/shear interaction relationship is proposed, and a linear relationship is shown to be conservative. Furthermore, recommendations are provided on methods to distribute anchor forces depending on whether the applied load is dominated by moment or shear. Additionally, it is also determined that plate flexibility affects the location of the compressive reaction from the applied moment, and the location of the compressive reaction should be located conservatively as it affects the distribution of the tensile reaction from the applied moment to the anchors. Recommendations are also given to locate the compressive reaction conservatively.

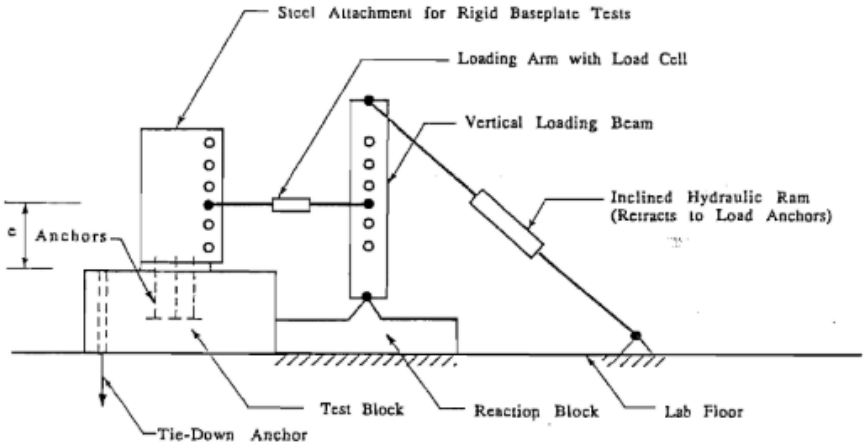

Figure 2.13 Schematic diagram of test-setup (Cook et al. 1989)

For embedded plates loaded with a combined shear and moment, Mallee and Burkhardt (1999) investigated the plate stiffness required to be able to calculate anchor forces using elastic theory

through experimental tests and finite element models. They conducted seven tests on embedded plates with post-installed anchors loaded with a combination of moment and tensile force. With the tests and their finite element models, they determined that anchor and concrete forces calculated by assuming elastic theory is sufficiently accurate to use linear finite element analysis to determine the required plate size. Furthermore, even with plates thinner than required based on the previous calculations (20 mm, compared to the calculated 25 mm), the plate still performed adequately and supported the use of elastic theory to determine anchor forces. Even if the selected plate is not fully rigid, resulting in a shortened resisting moment arm, the assumptions of negligible anchor displacement and triangular compressive stress block under the plate is conservative. In practice, when a moment is applied to an embedded plate, the plate rotates, causing a reduction in the length of the compressive stress block, leading to an increase in the resisting moment arm and thereby reducing anchor forces.

2.4 Development of Design Methods for Concrete Anchors

Concrete anchors have been used in construction since at least the 1950s. However, it was only in the 1970s where the kappa (κ) method, the precursor to the current CCD method, for designing concrete anchors was developed (Eligehausen 2017). Before that, manufacturers only published limited information for designers. Only properties such as mean failure loads of single anchors in concrete were provided, and the effects of edge distance, anchor spacing and concrete strength on failure loads were neglected (Eligehausen 2017). In 1985, ACI 349, a committee that develops the design code for concrete nuclear structures, incorporated the cone model published by Cannon et al. (1981) into the ACI 349 design code. Finally, in 1995, the CCD method for designing concrete anchors was published and subsequently adopted into an appendix in ACI 318-02 for designing concrete anchors. Some modifications to these provisions have been made since then, but the CCD method still continues to be used in newer editions of ACI 318. It became a chapter of ACI 318 in 2011. The CCD method, based on the κ method, differs from the cone model in calculating concrete breakout failure loads in several areas. The cone model assumes a 45° cone-shaped failure surface, compared to the CCD method's 35° pyramidal failure surface. Calculations with the CCD model are easier as it is more difficult to calculate overlapping areas of circles, and the assumption of a 45° cone leads to an incorrect assumed characteristic spacing of two times the embedment depth (h_{ef}), compared to $3h_{ef}$ found in experimental tests and assumed in the 35° pyramidal failure surface. The characteristic spacing of an anchor is the centre-to-centre distance

between anchors at which the full capacity of the anchor may be used; anchors spaced more than the characteristic spacing do not affect the capacity of adjacent anchors. Thus, the influence of anchor spacing and edge distance on failure load is underestimated in the cone model (Fuchs et al 1995). Furthermore, the cone model does not account for the size effect in its design method unlike the CCD method, preventing its extension to anchors with deep embedment (Fuchs et al 1995). Ultimately, the CCD method, used in the current ACI 318, is now commonly used around the world.

Annex D of CSA A23.3, which is the focus of this research, is essentially a Canadian version of ACI 318's "Chapter 17: Anchoring to Concrete". Some differences exist due to the use of different resistance modification factors for ductile and brittle failure modes in ACI 318, which is discussed in Section 2.5; otherwise, they are nearly identical.

Other design methods for concrete anchors are available in the CPCI Design Manual (2017). It uses Annex D for tension capacity calculations, but uses the Precast/Prestressed Concrete Institute (PCI) design method for shear capacity calculations. The PCI method for shear design of concrete anchors is similar to the CCD method; however, it considers some additional and different factors in the design calculations compared to the ones used in Annex D. For example, in the PCI method, for anchors loaded in shear, an x-spacing (spacing of anchors parallel to an edge) factor is used; Annex D does not include this factor. Even the modification factors, such as for anchors in thin concrete members ($\psi_{h,V}$), are calculated differently in the two methods. Thus, differences in the design methods for concrete anchors for embedded plates are still present.

2.5 Annex D in CSA A23.3:19

As previously stated, Annex D is very similar to ACI 318 Chapter 17 and many studies have been done on the capacities of concrete anchors to develop the current code. Annex D is a normative annex of CSA A23.3:19, specifying the design requirements for anchors in concrete used to transmit tension, shear, or a combination thereof, between connected structural elements (CSA 2019). Specifically, Annex D applies to cast-in anchors and post-installed expansion, undercut, and adhesive anchors that are not predominantly subjected to high-cycle fatigue or impact loading. Cast-in welded headed studs are the focus of this research, and are therefore the main subject of this section.

When designing, the anchor or anchor group capacity is determined by checking all the relevant failure modes using the procedures outlined in Annex D. For anchors loaded in tension, the relevant failure modes for welded headed anchors are steel strength in tension, concrete breakout strength in tension, pullout strength in tension, and concrete side-face blowout strength. For welded headed anchors loaded in shear, the relevant failure modes are steel strength in shear, concrete breakout strength in shear, and concrete pryout strength. It is also important to note that the design equations used in Annex D are based on the 5% fractile of anchor resistances found in the supporting experimental tests (also known as characteristic resistances). This means that there is a 95% chance that the actual strength exceeds the calculated design capacity.

2.5.1 Resistance Modification Factor (R)

Before presenting the design equations of Annex D, it is important to clarify the material resistance factors ϕ_s and ϕ_c, for steel and concrete, respectively, and the resistance modification factor, R. Annex D is adapted from ACI 318, which adjusts the material resistance factors according to failure mode, while CSA A23.3 typically adjusts according to the material. Ductile failure by yielding of the steel anchor before concrete breakout is typically more desirable than the brittle failure of the concrete. Furthermore, because of the possibility of a non-uniform distribution of shear to the anchors, the resistance modification factor is slightly lower for shear loads compared to tension loads for anchors governed by the strength of a steel element. Additionally, when supplementary reinforcement—i.e., reinforcement surrounding the anchor or anchor group—is used to tie in the potential concrete failure surface (known as Condition A in CSA A23.3), additional capacity can be gained (Eligehausen et al. 2006), resulting in a capacity increase. Thus, the resistance modification factors shown in Table 2.1, are used to adjust the calculated capacities of embedded plates for use in design. When supplementary reinforcement is not supplied, or when pullout or pryout strength governs, it is known as Condition B in CSA A23.3. Notably, in ACI 318, the resistance modification factor (R_{ACI}) includes failure mode resistance factors, while the resistance modification factor (R) in CSA A23.3 does not include material resistance factors, resulting in the apparent discrepancies between the two design standards seen in Table 2.1. When the resistance modification factor (R) in CSA A23.3 is multiplied by the appropriate material resistance factor, ϕ_s or ϕ_c, for steel or concrete failure modes, respectively (shown in Table 2.2), Annex D provides 0% to 9% lower modification factors for the same situation compared to ACI 318; ϕ_s is taken as 0.85 and ϕ_c is taken as 0.65.

Table 2.1 Resistance Modification Factors, R and R_{ACI} (CSA 2019 and ACI 2019)

a) Anchors governed by strength of ductile steel element		
	A23.3:19	**ACI 318-19**
Tension Loads	0.8	0.75
Shear Loads	0.75	0.65
b) Anchors governed by strength of brittle steel element		
	A23.3:19	**ACI 318-19**
Tension Loads	0.70	0.65
Shear Loads	0.65	0.60

c) Anchors governed by concrete failure				
	A23.3:19		**ACI 318-19**	
	Condition A	Condition B	Condition A	Condition B
Shear Loads	1.15	1.0	0.75	0.70
Tension Loads (Cast-in welded headed studs)	1.15	1.0	0.75	0.70

Table 2.2 Effective Resistance Modification Factor (ϕR) (CSA 2019)

a) Anchors governed by strength of ductile steel element	
	A23.3:19
Tension Loads	0.68
Shear Loads	0.64
b) Anchors governed by strength of brittle steel element	
	A23.3:19
Tension Loads	0.60
Shear Loads	0.55

c) Anchors governed by concrete failure		
	A23.3:19	
	Condition A	Condition B
Shear Loads	0.75	0.65
Tension Loads (Cast-in welded headed studs)	0.75	0.65

2.5.2 Embedded Plates Loaded in Tension

The methods provided by Annex D to calculate the capacity of the four basic failure modes of welded headed studs embedded in concrete loaded in tension are detailed in the following section. The resistance of an anchor group is the resistance of the weakest failure mode.

2.5.2.1 Resistance of Steel Anchors

The steel anchor strength in tension can be determined using Equation 2.5.

$$N_{sar} = A_{se,N}\phi_s f_{uta} R \qquad \textbf{2.5}$$

where:

N_{sar} = factored resistance of an anchor in tension (N)

$A_{se,N}$ = effective cross-sectional area of an anchor in tension (mm^2)

ϕ_s = steel embedment material resistance factor for reinforcement (0.85)

f_{uta} = specified tensile strength of anchor steel (MPa)

R = resistance modification factor

For welded headed studs, the effective cross-sectional area is the cross-sectional area of the stud shaft. Furthermore, the anchor specified tensile strength (f_{uta}) must not be taken as greater than the smaller of 1.9 times the anchor yield strength or 860 MPa to prevent yielding during service load conditions, and to limit the use of the equation based on the scope of the tests used in its development, where only anchors with up to 860 MPa specified tensile strength (f_{uta}) are included.

2.5.2.2 Concrete Breakout Resistance

Although experimental testing shows the concrete failure surface is cone-shaped (Fuchs et al. 1995), Annex D uses the concrete capacity design (CCD) method where the failure surface is a 35° square pyramid, shown in Figure 2.14, to simplify the design calculations. Equations 2.6 to 2.8 are used in Annex D to calculate concrete breakout strength in tension.

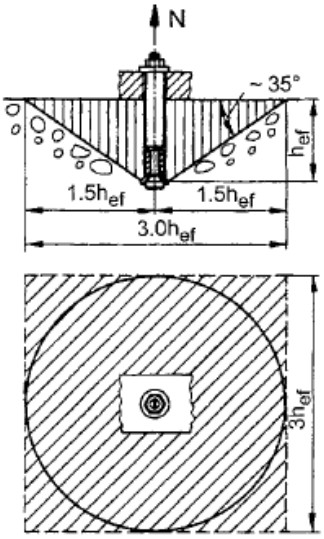

Figure 2.14 CCD concrete breakout pyramid (idealised) (Eligehausen et al. 2006)

For a single anchor:

$$N_{cbr} = \frac{A_{Nc}}{A_{Nco}} \psi_{ed,N} \psi_{c,N} \psi_{cp,N} N_{br} \quad \textbf{2.6}$$

For an anchor group:

$$N_{cbgr} = \frac{A_{Nc}}{A_{Nco}} \psi_{ec,N} \psi_{ed,N} \psi_{c,N} \psi_{cp,N} N_{br} \quad \textbf{2.7}$$

where:

N_{cbr} = factored concrete breakout resistance in tension of a single anchor in (N)

N_{cbgr} = factored concrete breakout resistance in tension of an anchor group (N)

A_{Nc} = projected concrete failure area of a single anchor or anchor group in tension (mm^2)

A_{Nco} = projected concrete failure area (= $9h_{ef}^2$) of a single anchor in tension with an edge distance greater than or equal to $1.5h_{ef}$ (mm^2)

$\psi_{ec,N}$ = eccentricity modification factor for anchors in tension

$\psi_{ed,N}$ = edge distance modification factor for anchors in tension

$\psi_{c,N}$ = modification factor for concrete breakout resistance in tension based on the presence or lack of cracks

$\psi_{cp,N}$ = post-installed anchor modification factor for anchors in tension (= 1.0 for cast-in welded headed studs)

$$N_{br} = k_c \phi_c \lambda_a \sqrt{f'_c} h_{ef}^{1.5} R \quad \textbf{2.8}$$

where:

N_{br} = factored concrete breakout resistance in tension of a single anchor in cracked concrete

k_c = coefficient for factored concrete breakout resistance in tension (= 10 for cast-in headed studs)

ϕ_c = material resistance factor for concrete

λ_a = factor to account for low-density concrete

f'_c = specified compressive strength of concrete (MPa)

h_{ef} = effective anchor embedment depth (see Figure 2.14) (mm)

As shown in Equations 2.6 and 2.7, in lieu of multiplying the factored concrete breakout resistance in tension of a single anchor in cracked concrete (N_{br}) by the number of studs present in a group, the $\frac{A_{Nc}}{A_{Nco}}$ ratio takes into account the overlapping projected failure areas, shown in Figure 2.15, to account for the influence of adjacent anchors on the anchor group capacity.

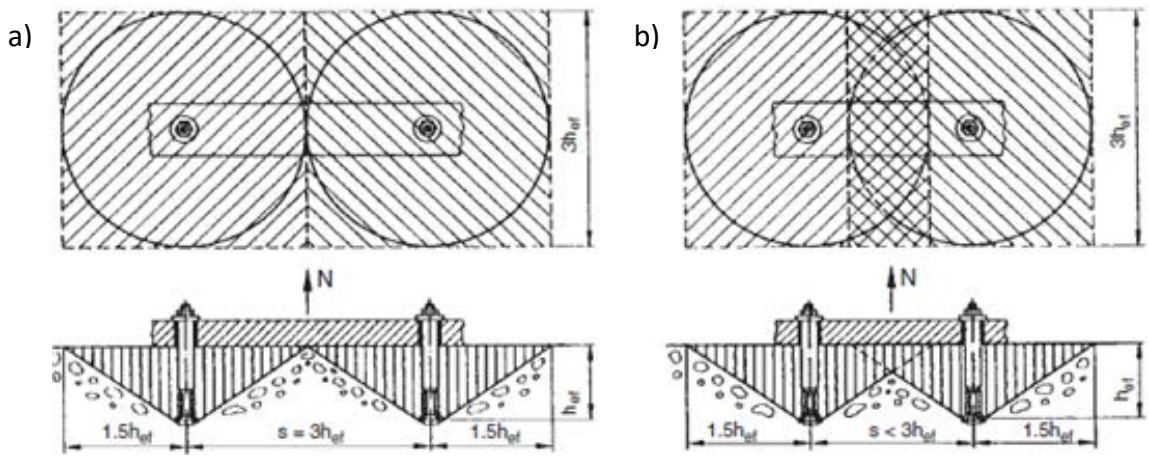

Figure 2.15 Failure area of an anchor group (Eligehausen et al. 2006): (a) large spacing with no overlapping area; (b) small spacing with overlapping area

The eccentricity modification factor ($\psi_{ec,N}$), calculated using Equation 2.9, accounts for anchor groups that are loaded eccentrically, unequally distributing the load.

$$\psi_{ec,N} = \frac{1}{(1 + \frac{2e'_N}{3h_{ef}})} \quad \textbf{2.9}$$

where:

e'_N is the eccentricity from the anchor group centroid of the resultant tensile load (mm)

and all other symbols have been defined previously.

The eccentricity of the resultant load (e'_N) is the distance between the resultant tensile force and the centroid of the anchors, shown in Figure 2.16. If the load is eccentric in two axes, a conservative method is used where the eccentricity modification factor is calculated for both axes and multiplied together. This equation is only valid for $e'_N \leq s/2$, where s is the centre-to-centre distance between the outermost anchors. Further analysis of the load distribution to the anchors is required if the load is applied a distance greater than $s/2$ from the centroid of the anchors.

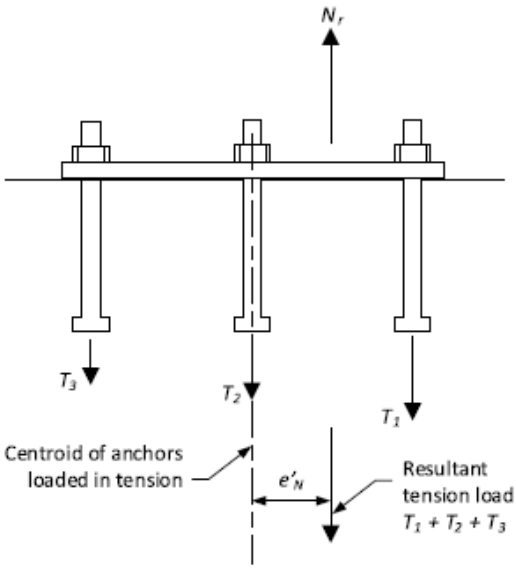

Figure 2.16 Eccentricity of an anchor group (CSA 2019)

The edge distance modification factor ($\psi_{ed,N}$) is calculated using Equation 2.10, in addition to using the $\frac{A_{Nc}}{A_{Nco}}$ ratio to take into account the proximity of the anchors to an edge of the concrete member. The reduced projected concrete area (A_{Nc}), when an anchor or anchor group is close to

an edge, reduces the $\frac{A_{Nc}}{A_{Nco}}$ ratio, thus reducing the capacity of the anchors. Furthermore, for anchors that are closer to an edge than their projected failure cone radius of $1.5h_{ef}$, the axisymmetric state of stress present for anchors far from an edge is disturbed (Fuchs et al. 1995). With this disturbance, the concrete breakout strength in tension of the anchors is reduced and is accounted for by using the edge distance modification factor ($\psi_{ed,N}$), proposed by Fuchs et al. (1995). Figure 2.17 illustrates the minimum distance from the centre of an anchor to the edge of concrete ($c_{a,min}$) used in Equation 2.10 and the reduced projected failure area (A_{Nc}) for anchors close to an edge.

$$\psi_{ed,N} = \begin{cases} 1.0, & c_{a,min} \geq 1.5h_{ef} \\ 0.7 + 0.3\frac{c_{a,min}}{1.5h_{ef}}, & c_{a,min} < 1.5h_{ef} \end{cases} \quad \textbf{2.10}$$

where:

$c_{a,min}$ = minimum distance from centre of an anchor to edge of concrete

and all other variables are as previously defined.

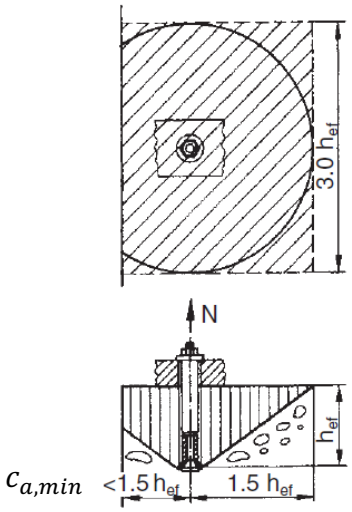

Figure 2.17 Influence of edge distance on concrete cone failure surface (adapted from Eligehausen et al. 2006)

The cracked concrete modification factor ($\psi_{c,N}$) is either 1.25 or 1.0 for cast-in anchors, where there is no cracking at service loads and where there is cracking at service loads in the concrete member, respectively. The lower cracked concrete modification factor ($\psi_{c,N}$), which means lower failure loads for the cracked concrete, are due to the cracks changing the stress distribution from axisymmetric to irregular, as shown in Figure 2.18 (Eligehausen et al. 2006).

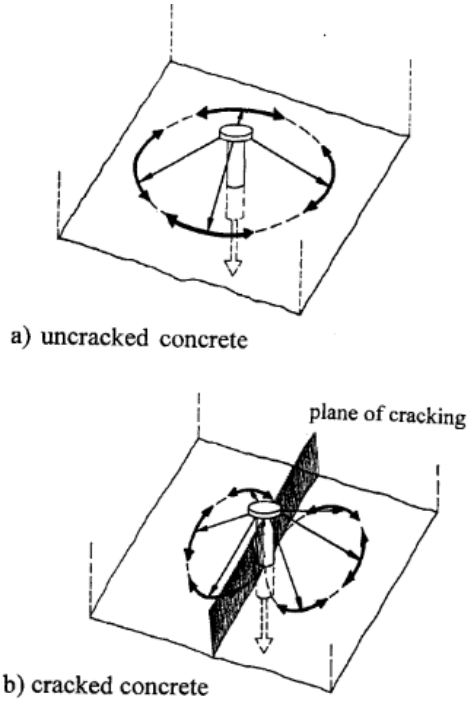

Figure 2.18 Effect of cracked concrete on the stress distribution in concrete (Fuchs et al. 1995)

The last modification factor in Equations 2.6 and 2.7 is the post-installed anchor modification factor ($\psi_{cp,N}$). Since the focus of this research is cast-in welded headed studs, $\psi_{cp,N}$ is 1.0. Details of its use for post-installed anchors will not be discussed. More information can be found in Annex D regarding the post-installed anchor modification factor.

The final component used to calculate concrete breakout strength in tension (N_{cbr} or N_{cbgr}) is the factored concrete breakout resistance in tension of a single anchor in cracked concrete (N_{br}), calculated using Equation 2.8. As mentioned previously, Annex D uses the CCD method but is presented slightly differently than the method proposed by Fuchs et al (1995). The coefficient for factored concrete breakout resistance in tension (k_c) is a combination of multiple factors. To show the specific factors more clearly, Equation 2.11 (Fuchs et al. 1995) shows Equation 2.8 before it was simplified and adopted by ACI 318, and subsequently by Annex D.

$$N_{no} = k_1 \cdot \sqrt{f'_c} \cdot k_2 \cdot h_{ef}^2 \cdot k_3 \cdot h_{ef}^{-0.5} \qquad \textbf{2.11}$$

where:

N_{no} = concrete breakout resistance in tension of a single anchor in cracked concrete

$k_1 \cdot k_2 \cdot k_3$ = coefficients for factored concrete breakout resistance in tension (k_c in Equation 2.8)

To calculate the mean concrete breakout resistance in tension of a single anchor in cracked concrete (N_{no}), the coefficient k_c is taken as 16.8. From Equation 2.11, $k_1 \cdot \sqrt{f'_c}$ represents the nominal concrete tensile stress at failure over the failure area, which can be calculated based on experimental testing. The size of the failure area is represented by the term $k_2 \cdot h_{ef}^2$, and the term $k_3 \cdot h_{ef}^{-0.5}$ accounts for the size effect (Fuchs et al 1995). Size effect is a property of all concrete members with a strain gradient, where the failure load increases less than the member size; this means that the maximum stress at failure decreases as the concrete member increases in size. This is a phenomenon that can be seen, for example, through the lower shear stress at failure of deeper beams compared to shallower beams. The size effect has also been verified to be present through experimental and theoretical studies for concrete anchors (Fuchs et al 1995). A more detailed explanation of size effects relating to concrete anchors can be found in the study by Ozbolt et al. (1998).

From Equations 2.6, 2.7 and 2.8, it is clear that the effective anchor embedment depth (h_{ef}) is critical for determining concrete breakout strength in tension, as it affects many of the variables in the design equations.

2.5.2.3 Pullout Resistance

Equations 2.12 and 2.13 are provided in Annex D to calculate the anchor pullout strength.

$$N_{cpr} = \psi_{c,P} N_{pr} \quad \textbf{2.12}$$

$$N_{pr} = 8 A_{brg} \phi_c f'_c R \quad \textbf{2.13}$$

where:

N_{cpr} = factored pullout resistance in tension of a single anchor (N)

$\psi_{c,P}$ = modification factor for pullout resistance of anchors based on the presence or lack of cracks

N_{pr} = factored pullout resistance in tension of a single anchor in cracked concrete (N)

A_{brg} = bearing area of anchor head (mm^2)

$\psi_{c,P}$ is taken as 1.4 when the concrete is uncracked, and 1.0 when the concrete is cracked. Finally, in general, pullout capacity is not affected by reinforcement unless the concrete the anchor head

bears on is locally confined, which is generally uncommon since the reinforcement would have to be specifically designed as such. Therefore, the resistance modification factor (R) in Equation 2.13 for pullout is typically treated as unreinforced (Condition B), even if there is supplementary reinforcement satisfying Condition A.

2.5.2.4 Concrete Side-face Blowout Resistance

In Annex D, the concrete side-face blowout failure mode only has to be checked when the effective embedment depth is greater than 2.5 times the shortest edge distance ($h_{ef} > 2.5c_{a1}$). Equation 2.14 is used to calculate the group side-face blowout resistance for single anchors and Equation 2.15 is used for anchor groups. Similar to concrete tension breakout, the side-face blowout cones of adjacent anchors can overlap, thus reducing the overall capacity of the anchor group. Thus, for anchor groups with close centre-to-centre spacings between studs, an adjustment factor is required (the parenthetic factor in Equation 2.15). Also, it is important to note that the equation assumes uncracked concrete.

For a single anchor:

$$N_{sbr} = 13.3c_{a1}\sqrt{A_{brg}}\phi_c\lambda_a\sqrt{f'_c}R \qquad \textbf{2.14}$$

For an anchor group:

$$N_{sbgr} = \left(1 + \frac{s}{6c_{a1}}\right)N_{sbr} \qquad \textbf{2.15}$$

where:

N_{sbr} = factored side-face blowout resistance of a single anchor (N)

N_{sbgr} = factored side-face blowout resistance of a group of anchors (N)

c_{a1} = minimum distance from centre of anchor to edge of concrete (mm)

s = centre-to-centre distance between adjacent anchors (mm)

2.5.3 Embedded Plates Loaded in Shear

The methods provided by Annex D to calculate the capacity of the three basic failure modes of welded headed studs embedded in concrete loaded in shear are detailed in the following sections. The resistance of an anchor group is the resistance of the weakest failure mode.

2.5.3.1 Resistance of Steel Anchors

For cast-in headed studs, the steel anchor's strength in shear is calculated using Equation 2.16.

$$V_{sar} = A_{se,N}\phi_s f_{uta} R \qquad \textbf{2.16}$$

where:

V_{sar} = factored resistance of an anchor in shear (N)

$A_{se,V}$ = effective cross-sectional area of an anchor in shear (mm^2)

Similar to determining the steel strength of an anchor in tension, f_{uta} is used since many anchor materials do not have a well-defined yield point. Furthermore, f_{uta} must not be taken as greater than 1.9 times the yield stress of the anchor or 860 MPa. The limits are to prevent the anchor from yielding under service loads, and to limit the equation's use to the maximum tensile strength of anchors tested in the studies the equation is based on, respectively.

2.5.3.2 Concrete Breakout Resistance

Similar to concrete breakout in tension, although the expected failure surface is a 35 degree half-cone shape, Annex D uses the CCD method where the failure surface is approximated as a 35 degree half-pyramid, shown in Figure 2.19, to simplify design calculations.

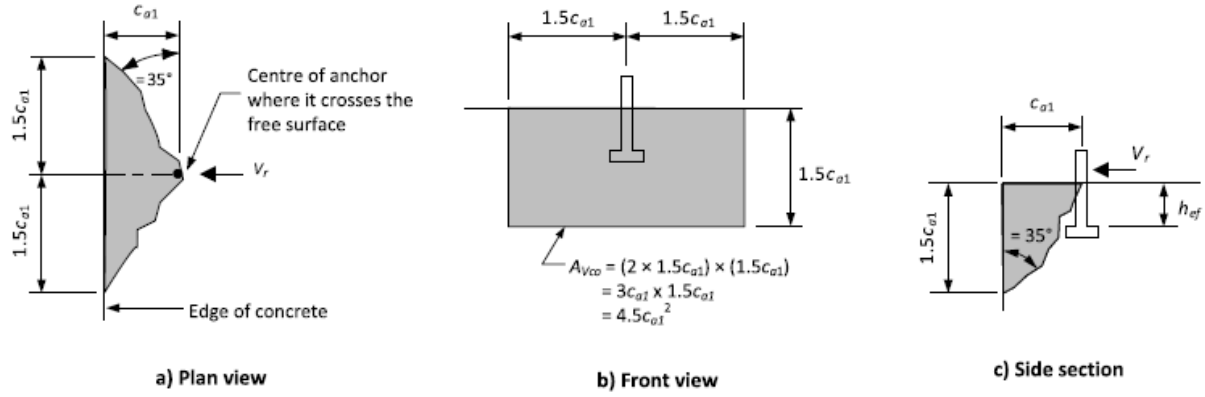

Figure 2.19 Annex D concrete breakout in shear failure surface (CSA 2019)

Equations 2.17 and 2.18 are provided in Annex D to calculate concrete breakout strength in shear. These equations are similar to Equations 2.6 and 2.7, used to calculate the concrete breakout strength in tension, since both concrete breakout strength calculations use the CCD method. The

main differences are in the different failure surfaces, modification factors, and basic (without modification factors) single anchor breakout resistance in cracked concrete (V_{br}).

For a single anchor:

$$V_{cbr} = \frac{A_{Vc}}{A_{Vco}} \psi_{ed,V} \psi_{c,V} \psi_{h,V} V_{br} \quad \textbf{2.17}$$

For an anchor group:

$$V_{cbgr} = \frac{A_{Vc}}{A_{Vco}} \psi_{ec,V} \psi_{ed,V} \psi_{c,N} \psi_{h,V} V_{br} \quad \textbf{2.18}$$

where:

V_{cbr} = factored concrete breakout resistance in shear of a single anchor (N)

V_{cbgr} = factored concrete breakout resistance in shear of an anchor group (N)

A_{Vc} = projected concrete failure area of a single anchor or anchor group in shear (mm^2)

A_{Vco} = projected concrete failure area (= $4.5c_{a1}^2$) of a single anchor in shear in a deep member with distance from edges equal or greater than $1.5c_{a1}$ in the direction of the shear force (mm^2)

$\psi_{ec,V}$ = eccentricity modification factor for anchors in shear

$\psi_{ed,V}$ = edge distance modification factor for anchors in shear

$\psi_{c,V}$ = cracked concrete modification factor for anchors in shear

$\psi_{h,V}$ = factor used to modify shear strength of anchors in concrete members with a depth less than $1.5c_{a1}$

V_{br} = factored concrete breakout resistance in shear of a single anchor in cracked concrete (N)

Similar to the concrete breakout resistance in tension of an anchor group, the factored concrete breakout resistance of an anchor group is multiplied by the ratio $\frac{A_{Vc}}{A_{Vco}}$ to account for both the number of anchors in the group, and the overlapping projected failure areas, as seen in Figure 2.20.

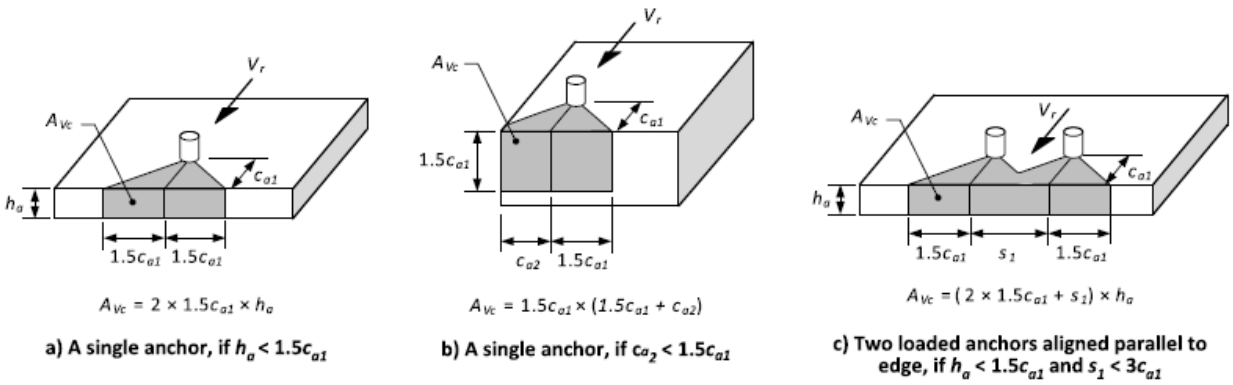

Figure 2.20 Concrete breakout failure area of single anchor and anchor group in shear (CSA 2019)

Similar to the eccentricity modification factor for concrete breakout in tension ($\psi_{ec,N}$), the eccentricity modification factor for concrete breakout in shear ($\psi_{ec,V}$) is calculated using Equation 2.19. It accounts for anchor groups that are loaded eccentrically, unequally distributing the load. Similar to concrete breakout in tension, this equation is only for eccentricities less than $s/2$.

$$\psi_{ec,V} = \frac{1}{(1 + \frac{2e'_V}{3c_{a1}})} \qquad \textbf{2.19}$$

where:

e'_V = eccentricity of resultant shear load measured from centroid of anchor group (see Figure 2.21) (mm)

c_{a1} = distance from the centre of anchor to edge of concrete in direction of applied shear (see Figure 2.20) (mm)

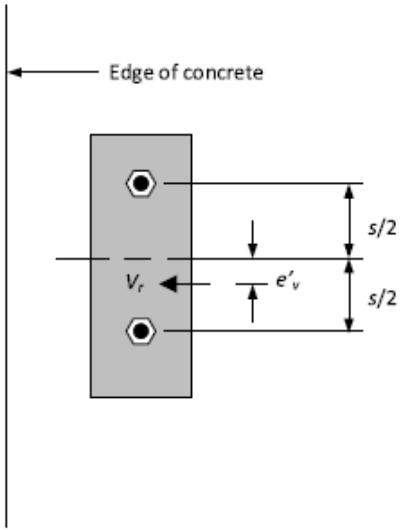

Figure 2.21 Eccentricity of shear load an anchor group (CSA 2019)

The edge distance modification factor ($\psi_{ed,V}$), calculated using Equation 2.20, and the $\frac{A_{Vc}}{A_{Vco}}$ ratio are used to take into account the proximity of the anchors to an edge of the concrete member. The disturbance of the failure area due to the anchor's proximity to the edge is taken into account by the edge distance modification factor ($\psi_{ed,V}$), proposed by Fuchs et al (1995).

$$\psi_{ed,V} = \begin{cases} 1.0, & c_{a2} \geq 1.5c_{a1} \\ 0.7 + 0.3\dfrac{c_{a2}}{1.5c_{a1}}, & c_{a2} < 1.5c_{a1} \end{cases} \qquad \textbf{2.20}$$

where:

c_{a2} = distance from centre of anchor to edge of concrete in direction perpendicular to applied shear (see Figure 2.20) (mm)

Because cracks in the concrete member can significantly reduce the anchor's breakout shear capacity, a cracking modification factor ($\psi_{c,V}$) is used to account for increased capacity when the concrete member is uncracked. Since the basic concrete breakout resistance in shear (V_{br}) is for anchors in cracked concrete, the cracking modification factor ($\psi_{c,V}$) is: 1.0 when the concrete is cracked; 1.2 when the concrete is cracked and there is reinforcement of a 15M bar or greater between the anchor and the edge of concrete; 1.4 when the concrete is cracked, and there is reinforcement of a 15M bar or greater between the anchor and the edge of concrete and they are enclosed within stirrups spaced less than 100 mm apart; and 1.4 when the concrete is uncracked.

The last modification factor for Equations 2.17 and 2.18 is for concrete member depth. For anchors in a shallow concrete member, with a depth less than $1.5c_{a1}$, the breakout area of the concrete is reduced. This reduction is partially accounted for by the $\frac{A_{Vc}}{A_{Vco}}$ ratio, but tests have shown that concrete breakout capacity in shear is less than proportional to the $\frac{A_{Vc}}{A_{Vco}}$ ratio in thin members (Eligehausen et al. 2006). Thus, the $\psi_{h,V}$ factor is used and is calculated using Equation 2.21.

$$\psi_{h,V} = \sqrt{\frac{1.5c_{a1}}{h_a}} \geq 1.0 \qquad \textbf{2.21}$$

where:

h_a = thickness of concrete member measured parallel to longitudinal anchor axis

The last component required to calculate the concrete breakout resistance of an anchor in shear is the basic cracked concrete breakout resistance in shear (V_{br}). Using Annex D, V_{br} shall not exceed the smaller of Equations 2.22 or 2.23; or for cast-in headed studs, V_{br} shall not exceed the smaller of Equations 2.23 or 2.24 provided that:

- for anchor groups, the resistance is based on the row of anchors farthest from the edge;
- anchor spacing is greater than 65 mm; and
- supplementary reinforcement is provided if the distance between the concrete edge and the closest anchor perpendicular to the applied shear (c_{a2}), shown in Figure 2.20, is less than 1.5 times the effective embedment depth (h_{ef}).

For cast-in headed anchors welded to a steel plate, Annex D allows for higher shear strength than anchors not welded onto a fixture, since Shaikh and Yi (1985) showed that higher shear strength exists. This is possibly due to the stiffening of the anchors caused by the weld, but there is a similar limit imposed on both Equations 2.22 and 2.24 since: in large diameter anchors, it was found that the concrete breakout resistance in shear was not affected by anchor length or anchor diameter (Lee et al 2010); and tests on large diameter anchors welded to steel plates are not available (ACI 2019).

$$V_{br} = 0.58(\frac{l_e}{d_a})^{0.2}\sqrt{d_a}\phi_c\lambda_a\sqrt{f'_c}c_{a1}^{1.5}R \quad \textbf{2.22}$$

where:

l_e = load bearing length of anchor, which cannot exceed $8d_a$ (mm)

d_a = shaft diameter of anchor (mm)

$$V_{br} = 3.75\phi_c\lambda_a\sqrt{f'_c}c_{a1}^{1.5}R \quad \textbf{2.23}$$

$$V_{br} = 0.66(\frac{l_e}{d_a})^{0.2}\sqrt{d_a}\phi_c\lambda_a\sqrt{f'_c}c_{a1}^{1.5}R \quad \textbf{2.24}$$

To calculate the mean V_{br}, Equation 2.25 is used (Fuchs et al. 1995).

$$V_{br(mean)} = 0.9\left(\frac{l_e}{d_a}\right)^{0.2}\sqrt{d_a}\sqrt{f_{cc,200}}c_{a1}^{1.5} \quad \textbf{2.25}$$

where:

$f_{cc,200}$ = concrete cube compressive strength (f'_c is taken as $0.85f_{cc,200}$ in this report)

l_e = load bearing length of the anchor (= h_{ef} for anchors with constant stiffness over their lengths)

From Equation 2.25 it is clear that V_{br} is strongly affected by edge distance (c_{a1}), since it determines the size of the breakout surface used to calculate concrete breakout resistance in shear for the CCD method; this is analogous to h_{ef} for concrete breakout resistance in tension (Eligehausen et al. 2006). Similarly, the failure load is proportional to $c_{a1}^{1.5}$ rather than c_{a1}^2 (the breakout surface area) because of the size effect, as discussed in Section 2.2.1.2 (Eligehausen et al. 2006). The failure load is proportional to the tensile strength of concrete, assumed to be $\sqrt{f_{cc,200}}$, which is, again, similar to the concrete breakout resistance in tension (Eligehausen et al. 2006). Furthermore, the distribution of the bearing stresses along the anchor length also influences the failure load, which depends on the stiffness of the concrete and the flexural stiffness of the anchor (Eligehausen et al. 2006). The anchor diameter (d_a) and effective load transfer length (l_e) terms account for the bearing stress distribution (Eligehausen et al. 2006). It is also important to note that the coefficient in Equation 2.25 differs significantly from that of Equation 2.22 because

Equation 2.25 uses the cube compressive strength of concrete ($f_{cc,200}$) rather than the cylinder compressive strength of concrete (f'_c). Equation 2.25 is also based on mean concrete breakout resistance rather than the 5% fractile values.

So far, only shear loads perpendicular to the edge, in the direction toward the edge have been discussed regarding the concrete breakout in shear failure mode. However, if shear is applied parallel to the edge, a similar concrete breakout failure mode can occur, since a fraction of the applied shear force generates a splitting force in front of the anchor, determined to be approximately 50% of the applied shear load (Eligehausen et al. 2006). Thus, concrete breakout capacity in shear for anchors loaded parallel to an edge is twice the value for shear force determined by Equation 2.17 or 2.18 with the shear force assumed to act perpendicular to the concrete free edge.

2.5.3.3 Concrete Pryout Resistance

Equations 2.26 and 2.27 are used to calculate concrete pryout resistance in shear. Notably, the pryout resistance is based on the concrete breakout resistance of the anchor in tension because, as mentioned earlier, failure occurs when the tensile force in the stud exceeds the concrete's resistance.

For a single anchor:

$$V_{cpr} = k_{cp} N_{cbr} \qquad \textbf{2.26}$$

For a group of anchors:

$$V_{cpgr} = k_{cp} N_{cbgr} \qquad \textbf{2.27}$$

where:

V_{cpr} = factored concrete pryout resistance of a single anchor (N)

V_{cpgr} = factored concrete pyrout resistance of an anchor group (N)

k_{cp} = coefficient for pryout resistance taken as $\begin{cases} 1.0, & h_{ef} < 65\ mm \\ 2.0, & h_{ef} \geq 65\ mm \end{cases}$

2.5.4 Combined Shear and Tension Loads

When anchors are loaded in shear and tension simultaneously, Annex D recommends using a trilinear interaction approach (shown in Figure 2.22) to determine combined shear and tension resistance.

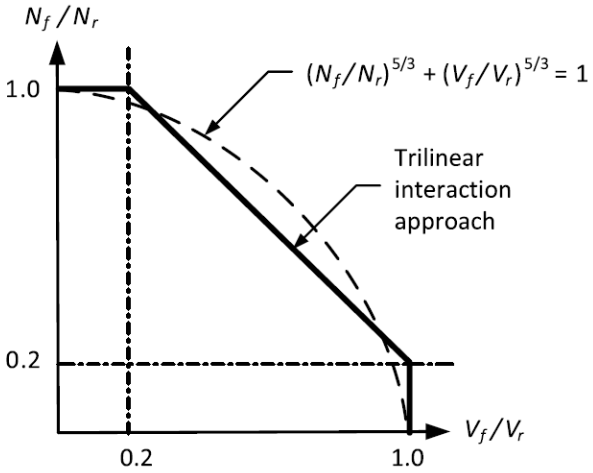

Figure 2.22 Shear and tension load interaction diagram (CSA A23.3:19)

When the ratio of $\frac{V_f}{V_r}$ or $\frac{N_f}{N_r}$ is less than 0.2, the full tension or shear resistance may be used, respectively; otherwise, Equation 2.28 applies.

$$\frac{V_f}{V_r} + \frac{N_f}{N_r} \leq 1.2 \qquad \textbf{2.28}$$

where:

V_f = factored shear load

V_r = factored shear resistance

N_f = factored tensile load

N_r = factored tensile resistance

Furthermore, this trilinear approach proposed by Bode and Roik (1987) is a simplification of the commonly-used interaction curve given by Equation 2.29, where the exponent (k) varies from 1.0 to 2.0, varying the interaction diagram from a straight line to a circle. The current recommended trilinear approach is based on a simplification of Equation 2.29 with k=5/3 (ACI 2019).

$$\left(\frac{V_f}{V_r}\right)^k + \left(\frac{N_f}{N_r}\right)^k \leq 1.0 \qquad \textbf{2.29}$$

2.5.5 Limitations of Annex D Regarding Embedded Plate Design

Presented in this section are some of the main limitations of Annex D regarding embedded plate design, highlighted through consultations with design engineers, and the making of the standard embedded plate design tables. Further discussion about how some of these limitations were overcome to calculate design capacities of embedded plates is presented in Section 3.3.

Using Annex D to calculate capacities for anchor groups can be challenging, as Annex D is complicated with its many variables and does not provide much guidance on the distribution and redistribution, after cracking, of load. This can cause confusion for designers. Specifically, for anchor groups welded to a plate loaded in shear parallel to a concrete edge (similar to Case B of the proposed standard embedded plate tables), two different concrete breakout failure capacities can be calculated, both adhering to Annex D. The ultimate concrete breakout resistance can be assumed to be achieved at the initial breakout of the anchor column closest to the edge, or after the initial breakout causing a redistribution of the load to the anchor column farther from the edge and its subsequent breakout. Choosing the correct failure surface is vital in determining the capacity of an embedded plate, and currently, with Annex D, it can be uncertain. Furthermore, anchor groups under shear loads that are neither perpendicular nor parallel to an edge are not discussed in Annex D.

Although reinforcement is prevalent in concrete structures, ACI 318-19 (upon which Annex D is based) does not provide methods to calculate its contribution to anchor capacity rigorously (Sharma et al. 2017). There are typically only a few values for modification factors concerning reinforcement, even though reinforcement can have a significant effect on concrete breakout capacity depending on size, spacing, and orientation (Sharma et al 2017).

While embedded plates, consisting of concrete anchors attached to a steel plate, are very commonly used, Annex D describes the design of only the concrete anchors. The effect of the steel plate on the distribution of loads in an anchor group is largely neglected, as is the assessment of the strength of the plate itself.

Finally, Annex D has a limit on anchor and concrete properties to prevent its use in cases that have not yet been tested. For example, cast-in anchors in high-strength concrete ($f_c' > 70$ MPa) and high-strength steel anchors ($f_u > 860$ MPa) are not covered under Annex D. However, as more research is conducted in those areas, Annex D can be further developed to cover those cases. For example, Nilforoush (2017) conducted a series of tension tests on single cast-in headed anchors in high-performance concrete ($f_c' = 81$ MPa) failing in concrete breakout and found that the CCD method provides a reasonable estimate of its ultimate failure load. However, the failure was more brittle than in normal-strength concrete, as there was significantly less displacement of the anchor in high performance concrete before peak load.

2.6 Previous Attempts at Standardization

Attempts to standardize embedded plates have been few, applicable only in narrow ranges of conditions, or unavailable publicly to the industry. For example, in the Concrete Design Handbook (CAC 2014), design capacities that consider static and cyclic load behaviour have been provided for three standard embedded plate connections used in concrete tilt-up panels, as shown in Figure 2.23. The scope of situations where these standard assemblies can be used is very narrow: only 1 or 2 capacities are given for each connection and they must be placed away from the edges of the concrete member, as the tests that were conducted to verify the capacities only looked at the connections away from any edges (Lemieux et al. 1998). These standard connections were proposed by Lemieux et al. (1998) after consultation with a committee consisting of designers and local contractors located in Vancouver, Canada, which reviewed commonly used connectors in the tilt-up panel industry. The embedded connectors used both welded headed studs and welded reinforcing bars, as the long reinforcing bars typically provided more ductility than the short welded headed studs that often failed in a concrete failure mode. Lemieux et al. (1998) then conducted 16 tension tests and 17 shear tests of the connectors in 140 mm thick, reinforced concrete slabs, which used static and cyclic loading to determine their load-bearing behaviour and capacity.

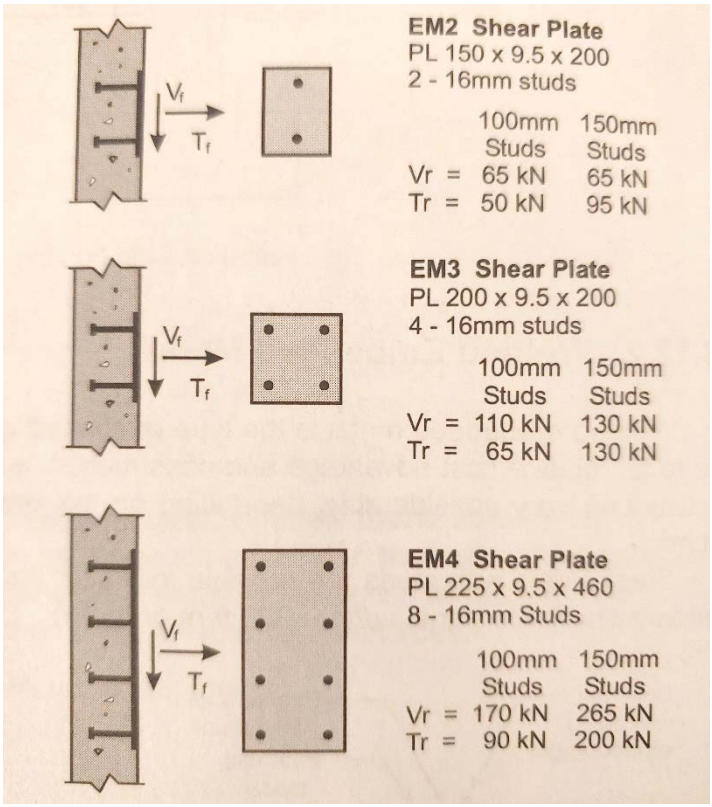

Figure 2.23 Standard tilt-up panel connectors (CAC 2014)

Design tables for anchors loaded in tension based on the methods of Annex D of CSA A23.3-14 are available in the CPCI Design Manual (2017); however, they are very limited in their application. Specifically, only concrete breakout capacity for only one anchor group configuration is shown in the design tables; thus, the tables are limited to a very narrow range of situations. Steel anchor, side-face blowout, and pullout capacities must also be checked. Furthermore, there are no design tables for anchors loaded in shear. Similarly, in the Concrete Design Handbook (CAC 2019), single anchor design capacities are provided in tables for shear and tension loading cases; however, single anchors are very rarely used in buildings since they lack redundancy and typically have low load bearing capacities. In-house standards for embedded plate design are commonly used in the industry, but they are often not widely available causing embedded plate designs to continue to vary from designer to designer. Ultimately, there have been few, and ineffective, attempts at an industry-wide standardization of embedded plate design.

3 Proposed Standard Embedded Plates

3.1 Introduction

To reduce the need to design embedded plates individually, standard designs are proposed in this chapter and the associated design selection tables can be found in Appendix A. Feedback from local (Edmonton, Alberta) designers, fabricators, and installers of embedded plates in the building construction industry was central to the process. The selection procedure and capacity calculations used for the design tables are also discussed.

3.2 Standard Embedded Plates and Selection Procedure

The proposed standard embedded plates are shown in Figure 3.1, and each is evaluated for its ability to resist shear (vertically in the figure) or tensile loads. The embedment depth (h_{ef}) is the distance from the outer surface of the plate to the underside of the stud head, and design capacities are presented for anchor lengths of 100, 150, and 200 mm. Recommended plate thicknesses to allow for the rigid plate assumption (discussed in Section 3.3.1.3) are: 16 mm for Standard Embedded Plate (SEP) 4, and 19 mm for SEP6 and SEP8. For each embedded plate there are separate design tables for different concrete edge conditions or cases. To reduce the number of standard embedded plates required and promote simplicity, the suite of embedded plates used in the shear and tension design tables are the same. The tables provide design capacities for a variety of common situations so that designers can choose an embedded plate quickly and easily once they determine the required capacity and distances to the surrounding concrete edges. The assumptions used to calculate the design table capacities are detailed in Section 3.3.

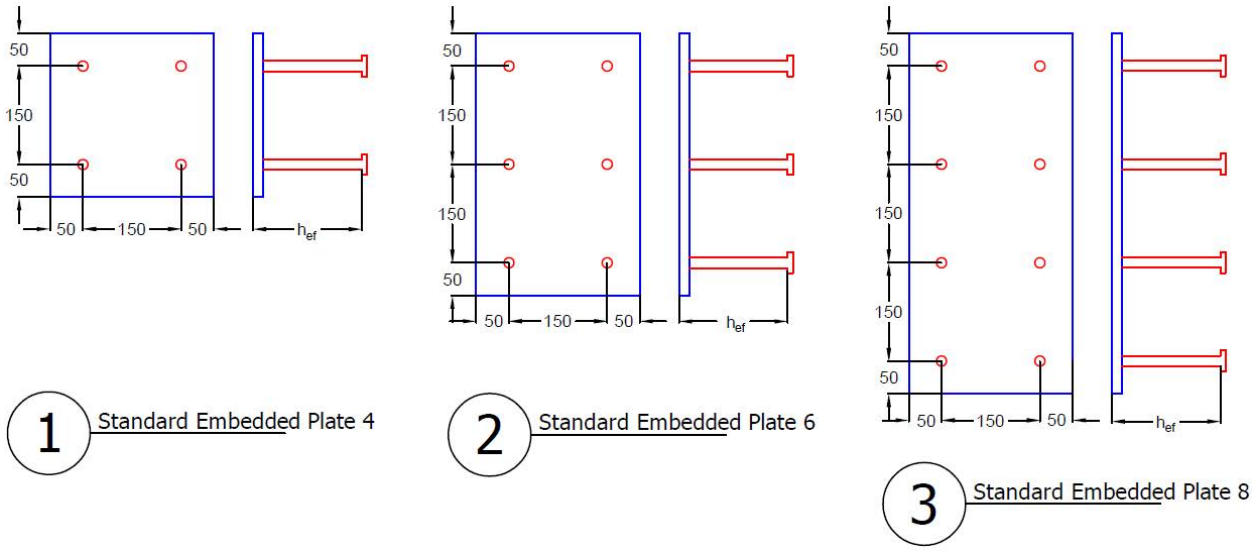

Figure 3.1 Proposed standard embedded plates (dimensions in mm)

3.2.1 Industry Input

Valuable input was gathered from construction industry professionals during an exploratory meeting that drove the objective towards the creation of design tables for a small set of standard embedded plates. Specifically, information was gathered about assumptions made during the design, and criticisms about current embedded plate design and installation procedures from a local designer, steel fabricator, and installer (general contractor). Their critical contributions are highlighted in this section.

Embedded plates are commonly custom-designed for each individual project, resulting in many different embedded plate designs. Although designs are sometimes scavenged from previous projects, a vast number of embedded plates normally need to be designed individually for a large project, resulting in a higher probability of errors just due to the sheer number of designs. This comment is the main driving force for creating design tables for a small set of standard embedded plates as fewer plate designs would be created, improving the efficiency of the design process. Additionally, many existing embedded plate designs were kindly provided by the designer. From those embedded plate designs and discussions with the designer, the great majority of embedded plates were designed for shear, with tension—and especially combined shear and tension—loading being much rarer. Therefore, the experimental testing of the proposed standard embedded plates was focused on shear load behaviour.

For the steel fabricator, a main attraction of standardizing embedded plates is that it is possible to have extras already made so that in the event that an embedded plate is discovered missing before a pour, one can readily be taken from the stockpile. Custom-designed embedded plates require lead time to produce, which causes delays, especially since concrete cannot be poured until the embedded plates are set in place. This further drove the objective towards standard embedded plates.

From the installer's perspective, embedded plates are challenging to place in their exact specified location due to factors such as tight reinforcement spacing clashing with the anchors, and embedded plate locations being laid out on formwork rather than the finished concrete member. This problem is exacerbated when the embedded plates are small, so allowing for tolerance during construction was a priority.

Additionally, embedded plates are sometimes placed in the correct location, but in the wrong orientation, resulting in delays during construction. Thus, the chosen standard embedded plates aim to prevent tight spacing of anchors, have a suitable steel plate size to increase the tolerance of their placement, and have either square or very apparently rectangular steel plates to diminish the probability of placement in the wrong orientation. Also, "nailer holes", small holes in the embedded plate used to attach it to the formwork, are very useful during installation, and were included in the embedded plates used in the experimental program presented in Chapter 4.

Considering all the industry input gathered, a set of standard embedded plates, along with their design tables for shear and tension loading, were created.

3.2.2 Embedded Plate Design Choices

To improve the simplicity of the design tables and reduce the number of different embedded plate designs, a small set of embedded plates are proposed to cover a variety of common use cases found in the building construction industry. Less common situations, such as embedded plates for circular columns or combined shear and tension loading, are excluded. Additionally, the proposed standard embedded plates should provide a solid foundation of embedded plates for future researchers who want to expand the scope of the standard plates/tables. Some of the rationale behind the design of the standard embedded plates is highlighted below.

For the standard embedded plates to cover a wide variety of situations, design-capacity tables are provided for the situations or cases shown in Figure 3.2 and Figure 3.3. These cases were determined to be common situations where embedded plates would likely be used. The term "In the Field" refers to an embedded plate that is not near any concrete edge. Additionally, variables that are not considered in Annex D when calculating the case's capacities are not included in the figures. For example, none of the embedded plate design cases for tension load, shown in Figure 3.3, include the concrete member thickness (h_a) since it is not considered in the design methods in Annex D used to calculate the capacities.

Practical considerations led to two eccentricities being included in the development of the design tables. First, a common assumption made by the embedded plate designer, who in Canada is typically not the connection designer, is that for shear loads the line of load application is 75 mm (3 in.) away from the face of the plate, resulting in a moment applied to the embedded plate in addition to the applied shear. This load eccentricity would be reasonable for many shear tab connections and would tend to be conservative for use with more flexible assemblies—such as single- or double-angle shear connections—that allow the point of zero moment to migrate toward the embedded plate under the ultimate design load. This eccentricity is considered in all the design tables for shear load. Also, after discussion with the installer and designer, a lateral eccentricity of 25 mm (10% of the plate width), as depicted in Figure 3.2 and Figure 3.3, is included in the calculation of all design table capacities and the steel plates were sized to increase the tolerance to slight misplacements. Although larger misplacements can occur during installation, it was not economical to design plates with very large eccentricities, as this reduces the capacity significantly. Situations where the plate is misplaced more than 10% of the plate width are therefore not covered by the standard embedded plate tables.

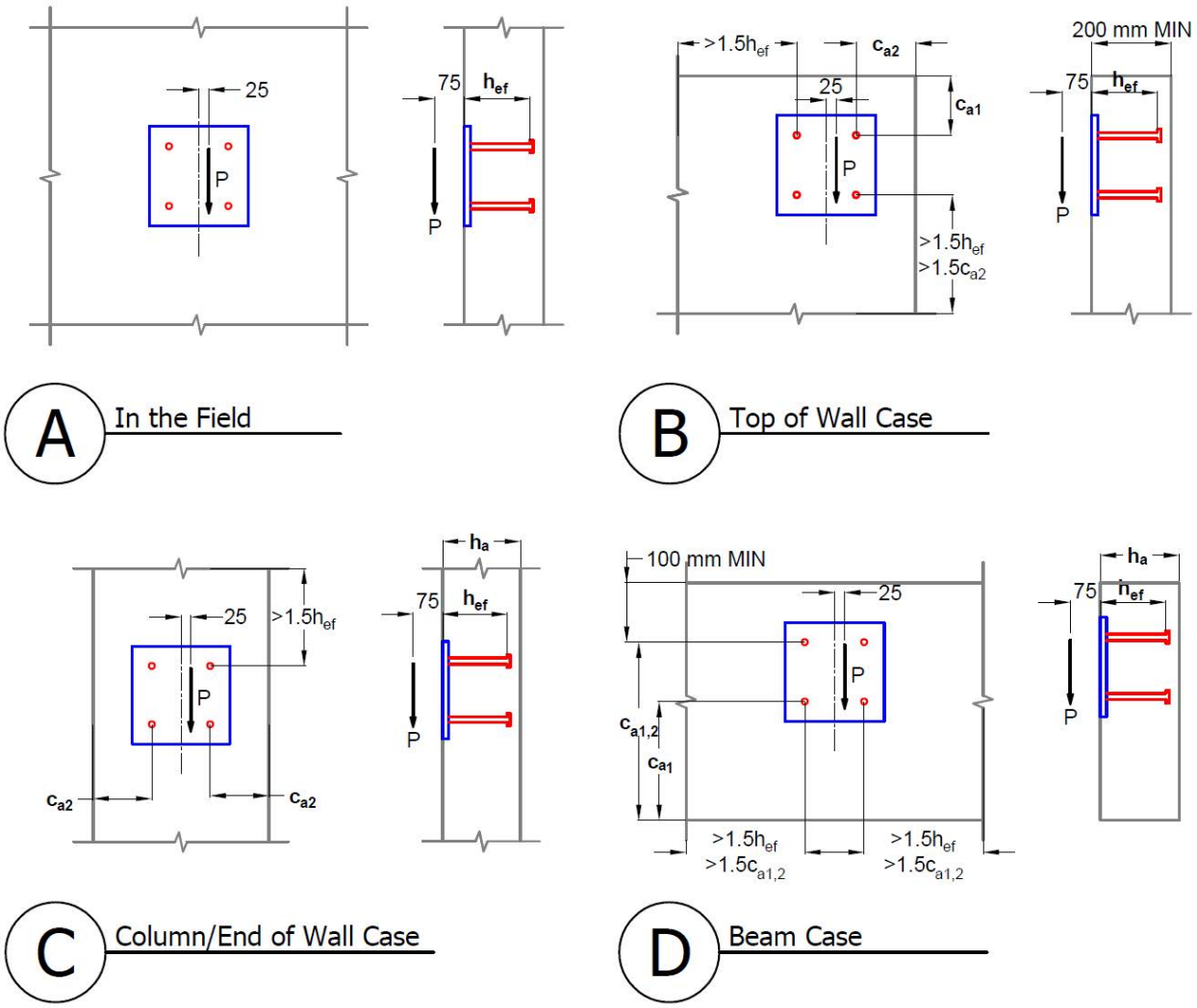

Figure 3.2 Embedded plate design cases for shear load

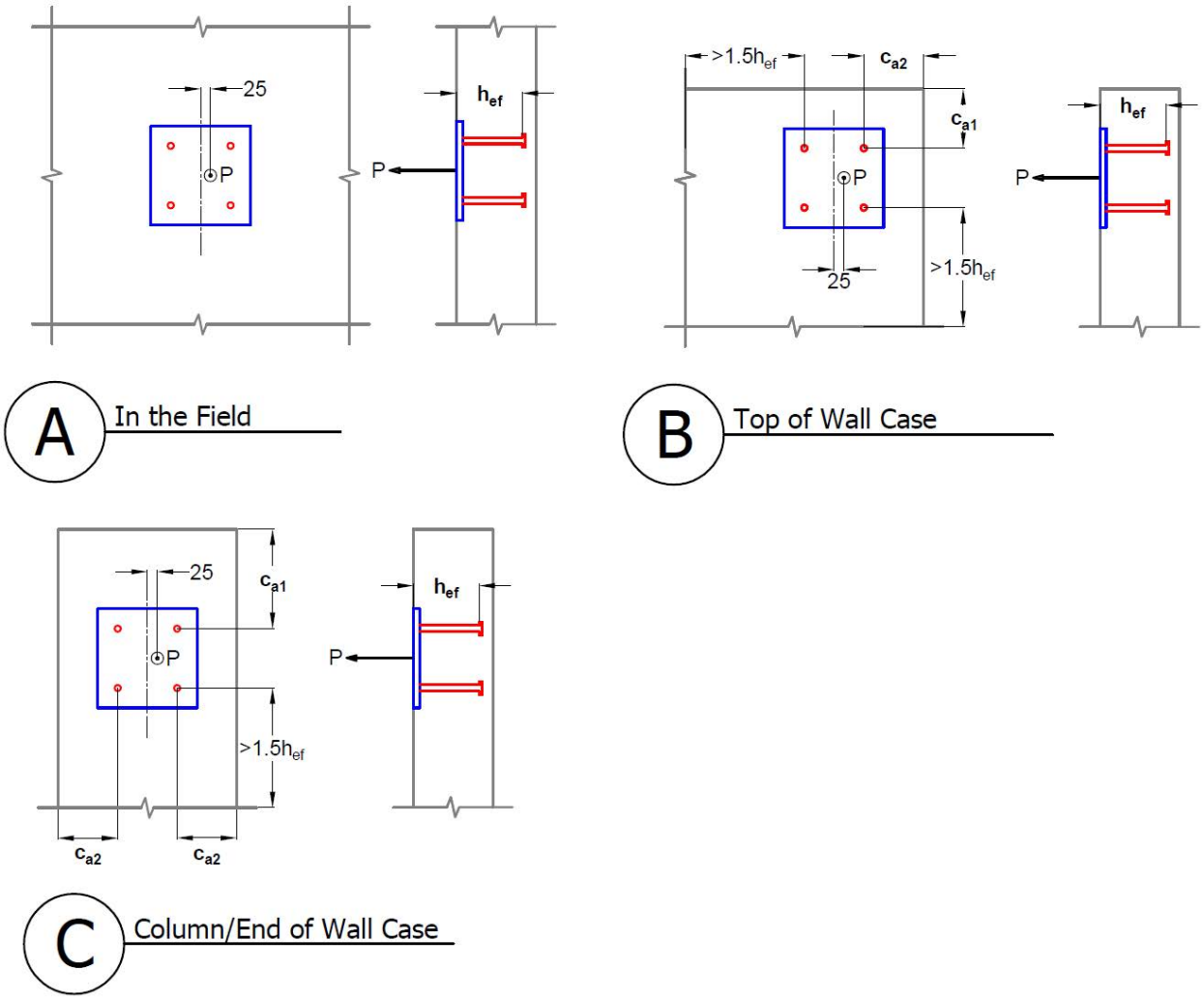

Figure 3.3 Embedded plate design cases for tensile load

The number of anchors in the proposed standard embedded plates was chosen to be noticeably different from each other, both visually and in capacity, to prevent confusion on site and overlapping use cases. Additionally, 16 mm diameter anchors were chosen since they were the smallest commonly available anchors where the capacity of the embedded plates were not typically governed by the anchor capacity within the boundaries of the design tables; if such were the case, increasing the capacity of the concrete failure mode (such as by moving the embedded plate away from the concrete edge) would provide no apparent benefit. Embedment depths available in the design tables are 100, 150, and 200 mm (4, 6, and 8 in.), which are consistent with anchor lengths commonly available from manufacturers used in industry (also 100, 150, and 200 mm, as the sum

of the stud head thickness and shortening of the stud during welding is approximately equal to the embedded plate thickness). The centre-to-centre spacing between anchors is a consistent 150 mm in both directions for all proposed standard embedded plates to keep designs simple and lessen the difficulty of installing embedded plates where reinforcement is dense. A 150 mm anchor spacing was also very commonly used in the embedded plate designs provided by the designer.

3.3 Capacity Calculations of Standard Embedded Plates

Annex D of CSA A23.3:19 is used to calculate all the design capacities presented in the proposed standard embedded plate design tables. This section describes the assumptions and their justifications.

3.3.1 General Assumptions

3.3.1.1 Material Properties

The following lists the assumed material properties used to calculate the standard embedded plate capacities in the design tables.

Steel Plate:

- CSA G40.21 Grade 300W

Welded Headed Steel Anchor:

- Minimum specified tensile strength (f_{uta}) of 420 MPa
- Elastic modulus (E_s) of 200 000 MPa
- Minimum elongation of 14% and a reduction in area of at least 30% at failure
- Weld is sufficient to fully develop tensile strength of the anchor

Concrete:

- Minimum 28-day cylinder compressive strength (f_c') of 30 MPa
- Elastic modulus (E_c) calculated using CSA A23.3:19 Equation 8.2
- Normal density (2400 kg/m^3)
- Unreinforced

Required material properties were chosen based on their prevalence in the industry and to encompass a wide variety of realistic conditions. For example, the steel plate chosen is CSA

G40.21 Grade 300W steel, since this grade is common for plate stock and the minimum strength used for steel plates in the construction industry. Although many different welded headed anchors can be used for embedded plates, the specified tensile strength (f_{uta}) of 420 MPa is typically the minimum; thus, 420 MPa is assumed. The elastic modulus is assumed as 200 000 MPa. Furthermore, the anchor must be ductile, meaning it has a tensile test elongation of at least 14% and a reduction in area of at least 30% at failure, determined using ASTM Standard A370. Finally, the concrete has a compressive strength (f_c') of 30 MPa, since from the industry meeting this was found to be the typical minimum strength of concrete used in buildings. Only one minimum compressive strength (f_c') was chosen to reduce the number of tables.

3.3.1.2 Resistance Modification, Concrete Cracking and Reinforcement Factors

First, the material resistance factors for the structural steel plate (ϕ_a), steel anchors (ϕ_s), and concrete (ϕ_c) are 0.9, 0.85, and 0.65, respectively, as stated in CSA A23.3:19. Furthermore, as discussed in Section 2.5, the resistance modification (R) depends on the failure mode and supplementary reinforcement assumptions. In order to balance conservatism (to allow the design table to be used as often as possible) and economy, the concrete is assumed to have no supplementary reinforcement (Condition B), and the steel anchors are assumed to be ductile. Consequently, the resulting resistance modification factor (R) is taken as 0.80 for steel failure in tension, 0.75 for steel failure in shear, and 1.00 for concrete failure in shear or tension. Furthermore, concrete is assumed to be cracked and unreinforced to improve the range of applicability of the design tables. Since cracking in concrete is determined by a variety of factors, and although reinforcement is ubiquitous for concrete used in structures, it is difficult to predict the reinforcement layout and thus the reinforcement's capacity contribution. Specific factors used for cracked concrete are as given in Section 2.5. For steel anchors, it is a common industry standard to specify ductile studs, and most cast-in concrete anchors will satisfy the ductility requirements.

3.3.1.3 Rigid Plate Assumption

In all cases, a rigid steel plate is assumed when distributing loads to anchors. Although this assumption is difficult to confirm without detailed models and experimental testing, distributing moments elastically to the anchors in most practical cases delivers sufficiently accurate results (Eligehausen et al. 2006). Even if the selected plate is not fully rigid, resulting in a shortened

resisting moment arm under an eccentrically applied shear force, the assumptions of negligible anchor displacement and triangular compressive stress block under the plate is conservative. In practice, when a moment is applied to an embedded plate, the plate will rotate, causing a reduction in the depth of the compressive block, leading to an increase in the resisting moment arm (Mallee and Burkhardt 1999). Therefore, for standard embedded plates loaded in shear, the plate thicknesses were chosen based on hand calculations using the Handbook of Steel Construction (CISC 2017) to prevent prying of the anchors and yielding of the plate at the maximum capacity of each standard embedded plate; a shear tab welded onto the embedded plate would further increase the effective plate stiffness, and a more flexible connection type would reduce the load eccentricity and, therefore, the applied moment.

For embedded plates loaded in tension, because of the wide variety of connection types that may be used, such as shear tabs or angles, assuming the worst-case connection would result in significantly thicker plates to prevent yielding, reducing economy. Thus, to use the tension design tables, the rigid plate assumption should be checked since the flexibility of the connection and plate may increase forces on the anchors due to prying.

3.3.2 Shear

3.3.2.1 Connection Eccentricity

A designer has many options for connecting a steel member to the exposed surface of an embedded plate; connections such as shear tabs are common, but single and double angles and others are possible. However, since in most cases the applied load (P) is through the centroid of the bolt group, the embedded plate will have to resist an eccentric (away from the face of the plate) shear force or, equivalently, an in-plane shear force (V) and a moment (M), shown in Figure 3.4 for an embedded plate with three rows of anchors. Although connections can be specified by the designer to prevent moment transfer, by including this connection eccentricity the range of applicability of the shear design tables increases. Thus, for the shear load design tables, a connection eccentricity of 75 mm away from the face of the plate is assumed. This distance was chosen since the maximum pure shear capacity of the standard embedded plates can be resisted by a single line of bolts, and the bolt line is typically less than 75 mm from the plate.

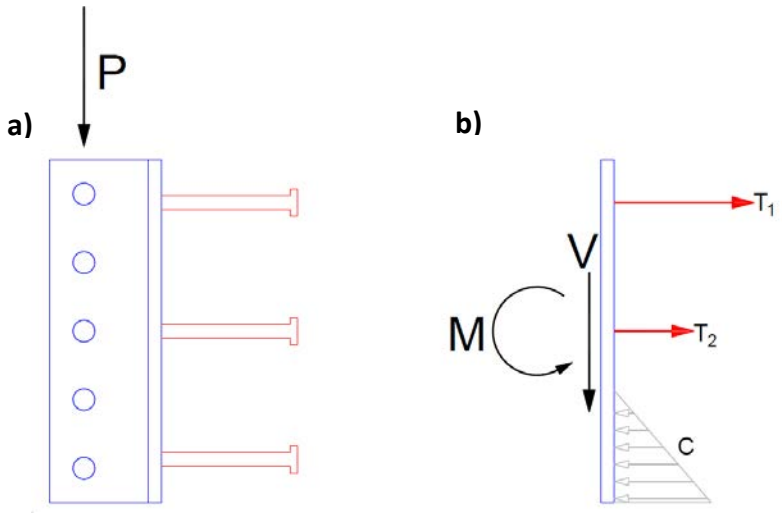

Figure 3.4 Assumed (a) shear load application and (b) resulting load distribution to anchors and concrete

The moment (M) is distributed to the steel anchors using an elastic analysis, as recommended by Annex D, since the standard embedded plates' failure modes are often not in the ductile steel anchors. In the case of an embedded plate with three rows of anchors, shown in Figure 3.4, the moment (M) creates a tensile force on the top and middle rows of anchors (T_1 and T_2), and a compressive force by the bearing of the plate against the concrete (C). If an anchor is in compression, its contribution to the resistance of the compressive force is neglected to remain conservative, since little research exists quantifying their compressive capacity.

3.3.2.2 Steel Anchor Resistance

To distribute the in-plane shear force into the anchors, all anchors are assumed to be welded to the plate and have the same stiffness. The load is first resolved into a shear force (V) and a torque (T) acting at the centroid of the anchor group, as shown in Figure 3.5. The shear force is distributed equally among the anchors ($V_{V,a}$), while the torque is distributed into each anchor in proportion to its distances from the centroid of the anchor group ($V_{T,a}$). The most highly loaded anchor is used to determine the steel anchor group resistance using Equation 2.16. Also, in all the shear cases described in the design tables, all anchors are assumed to contribute to the embedded plates' steel anchor resistance. This is important to note since if the embedded plate fails in the concrete first, the cracked concrete can change the distribution of the load to the anchors. This effect is evident in unreinforced concrete (Grosser 2012); however, reinforcement of appropriate size and orientation can limit crack width, allowing more anchors to participate in carrying the load. In the

concrete breakout failure mode for Cases B, C, and D, different assumptions of the controlling breakout surface can reduce the number of steel anchors carrying the load. However, the assumed failure surface of the concrete breakout failures, detailed in Section 3.3.2.4, allows all anchors to participate in load resistance. For concrete pryout failures, the failure mode is always assumed to engage all the anchors. Thus, all the steel anchors are considered when calculating the anchor steel shear resistance for all the standard embedded plates.

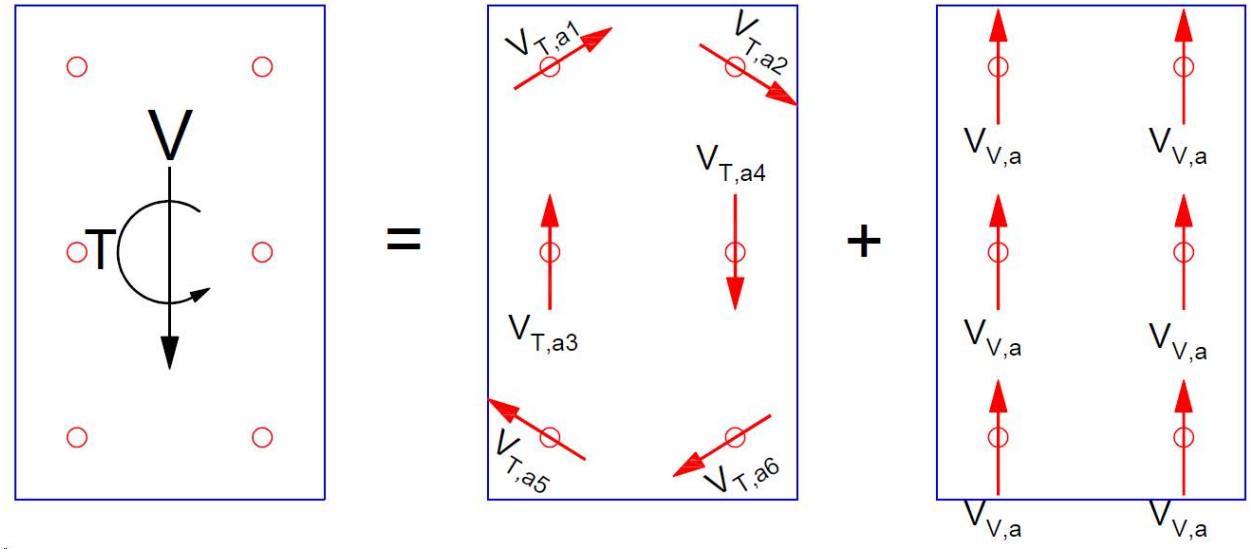

Figure 3.5 Distribution of torque ($V_{T,a}$) and in-plane shear ($V_{V,a}$) to anchors

3.3.2.3 Steel Plate Friction and Bearing Strength

The contribution of friction and bearing of the steel plate against concrete to the capacities of the embedded plates is ignored to remain conservative, as little research exists about these factors regarding embedded plates.

3.3.2.4 Concrete Breakout Resistance in Shear

Using Annex D to calculate concrete breakout resistance for large anchors groups, with four or more anchors, requires assumptions regarding the critical breakout surface, since that surface will determine the capacity of the anchor group. Smaller anchor groups typically have a more obvious breakout surface, while larger anchor groups may be able to redistribute loads after an initial concrete breakout failure of anchors closer to an edge. For embedded plates "In the Field" (Case A), concrete breakout is not possible since it is too far from an edge. Thus, this section focuses on embedded plates in corners of walls, columns, and beams (Cases B, C, and D, respectively).

For Case D, V_{br} was calculated as the minimum of Equations 2.23 and 2.24. For Cases B and C for all of the standard embedded plate tables, the factored concrete breakout resistance in shear of a single anchor (V_{br}) is calculated as the minimum of Equations 2.22 and 2.23. Although Annex D does allow a slight increase in capacity for welded headed studs, the required conditions for the increase is not met. Specifically, their concrete breakout resistance is not calculated based on a row of anchors farthest from the edge.

The assumed concrete breakout failure surface for Case D is shown in Figure 3.6, it is based on the anchors farthest from the edge. That is, c_{a1} is taken as the distance from the centreline of the farthest row of anchors to the edge of concrete. This assumption is consistent with the recommendations in Annex D and has been verified experimentally (Grosser 2012). However, with that assumption, Annex D allows only the steel anchors at the back row to be considered for steel anchor shear resistance. However, this can be very conservative for anchor groups far from an edge (with a ratio of spacing (s) to distance between the concrete edge and the centreline of the closest anchor row ($c_{a1,1}$) less than 0.6 or in equation form ($\frac{s}{c_{a1,1}} < 0.6$)), since the concrete will not crack at the front anchors because of the compression stress field caused by the back anchors (ACI 2014). For anchor groups close to an edge ($\frac{s}{c_{a1,1}} > 0.6$) in unreinforced concrete, once the anchors closer to the edge break out, very little load can be carried by those anchors, and the load will be transferred to the anchors farther from the edge. Although this has been shown to be the case in unreinforced concrete (Grosser 2012), there is evidence that it may not be the case for reinforced concrete as studies by Sharma et al. (2016) and Bui et al. (2018) have shown that the concrete breakout resistance of an anchor group exceeds the predicted resistance considering only the back row of anchors. It is possible that a small amount of reinforcement can control crack width sufficiently, allowing the anchors closer to the edge to share the load after initial concrete breakout. Furthermore, capacity calculated assuming the critical anchor group failure surface is initiated by the anchors closest to the edge is not consistent with experimental test results since ultimate breakout capacity is reached when the anchors farthest from the edge break out (Grosser 2012).

Therefore, in the embedded plate design tables, all steel anchors are considered when determining steel anchor resistance to shear. More research is required regarding the amount and orientation

of this reinforcement and the experimental program section of this report describes this topic in more detail.

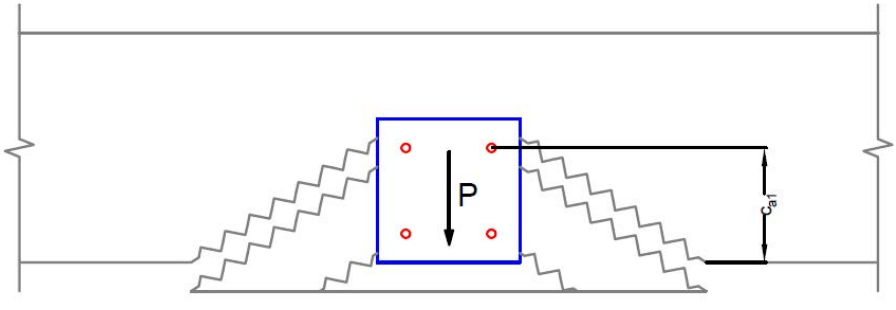

Figure 3.6 Assumed ultimate concrete breakout surface for shear Case D

The concrete breakout equations developed for Annex D are based on anchors loaded towards the edge. (Eligehausen et al. 2006), but when anchors are loaded in shear parallel to an edge they can also experience concrete breakout failure. For Cases B and C, the ultimate breakout resistance is assumed to be reached, shown in Figure 3.7, when the anchors closest to the edge break out of the concrete. Unlike Case D (Figure 3.6), the possibility of redistributing the loads to the anchors farther from the edge is neglected. All anchors are considered when determining steel anchor shear resistance.

For Case C, experimental tests conducted by Grosser (2012) have shown that the anchors' breakout crack only goes towards the closer edge; it does not travel to the opposite side of the column, meaning the load is not redistributed, illustrated in Figure 3.7. Thus, concrete breakout capacity is calculated using anchors closest to the edge. For Case B, redistribution of loads is possible. However, the redistribution is not well understood and may depend on many factors such as whether the member connected to the embedded plate is torsionally restrained (Grosser 2012). As a result, the concrete breakout capacity is also calculated using the anchor column closest to the edge. Furthermore, the anchor group must be very close to an edge to have a higher capacity after the initial breakout. For larger edge distances, the breakout capacity of close-edge anchors in an embedded plate is larger than the redistributed breakout capacity of far-edge anchors in an embedded plate. This is because, initially, there is only approximately half of the total shear load on the column of anchors closer to the edge for the standard embedded plates with 2 columns of anchors. After initial breakout of the close-edge anchors, it is assumed that the close-edge anchors

are no longer carrying a significant amount of force. Thus, the far-edge anchors carry the entire shear load. Furthermore, it may also be undesirable to have cracking under service loads; this is prevented if the failure surface is assumed to be at the close-edge anchors.

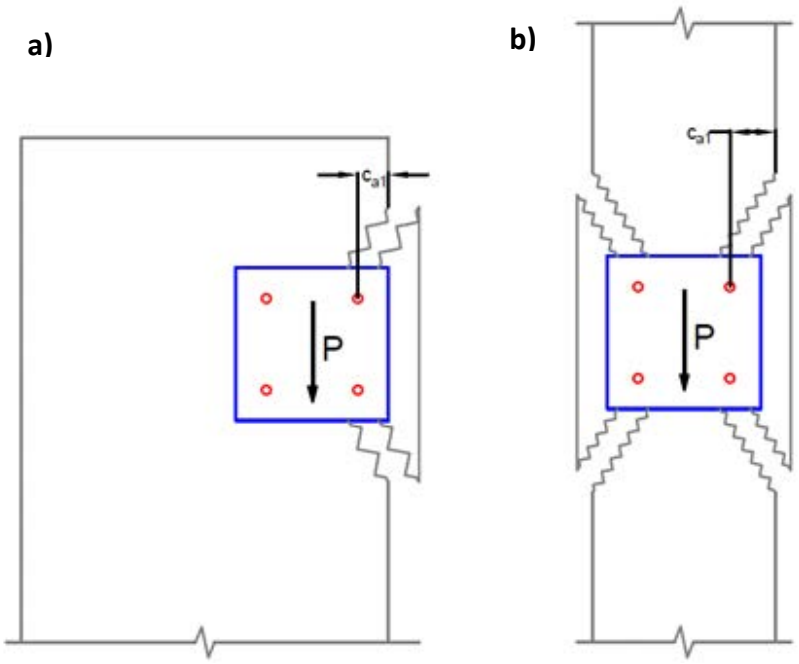

Figure 3.7 Assumed ultimate concrete breakout surface for (a) shear Case B and (b) shear Case C

3.3.2.5 Concrete Pryout Resistance

In all cases, all anchors are assumed to participate in concrete pryout resistance.

3.3.3 Tension

3.3.3.1 Resistance of Steel Anchor

Similar to the resistance of steel anchors in shear, all of the anchors are assumed to have the same stiffness and the tensile load is distributed elastically to each anchor. The most highly loaded anchor is then used to determine the capacity of the embedded plate.

3.3.3.2 Concrete Breakout Resistance in Tension

With the rigid plate assumption, the effects of prying due to the bending of the plate are not considered.

3.3.3.3 Pullout Resistance

The diameter of the anchor head is assumed to be 32 mm for the 16 mm diameter anchor used for the standard embedded plates. This anchor head diameter is consistent with anchors commonly available in industry.

3.3.3.4 Concrete Side-face Blowout Resistance

Like with pullout resistance, the diameter of the anchor head is assumed to be 32 mm.

3.3.4 Shear and Tension Interaction

As mentioned in Section 2.5.4, a trilinear interaction approach is used in Annex D to determine combined shear and tension resistance of anchors. However, an elliptical interaction approach is used to determine the combined shear and tension resistance of the anchors. That is, the exponent, k, in Equation 2.29 is taken as 5/3, since the trilinear approach in A23.3 is based on simplifying the interaction relationship when k is taken as 5/3.

3.4 Previous Experimental Testing Compared to Annex D Calculations

Figure 3.8 shows the test-to-predicted ratios from Grosser (2012) and Sharma et al. (2016) of anchor groups close to an edge loaded in shear towards the edge. Predicted capacities are calculated using the mean equations found in Fuchs et al. (1995), on which the equations in Annex D are based. The mean equations are used since the design equation in Annex D are the 5% fractile equations. Importantly, both studies attempt to reduce connection eccentricity to apply a pure shear load by applying the shear load very close to the surface (Grosser 2012) or restricting the rotation of the loading system (Sharma et al. 2016).

For the steel failures from the tests by Grosser (2012), which were conducted in unreinforced concrete, only the back anchor was found to significantly contribute to the anchor group's steel shear capacity, shown by the ruptured back anchor, and the calculated test-to-predicted ratio is 0.92 when considering only the back anchors in the anchor group's steel shear capacity. However, in all reinforced concrete tests by Sharma et al. (2016), test capacities were significantly greater than those when considering only the back row of anchors when predicting steel strength, suggesting more anchors may be participating in resisting load.

Additionally, very large test-to-predicted ratios were found for anchor groups installed in reinforced concrete. The test-to-predicted ratios calculated using test data of Sharma et al. (2016)

had an average value of 1.92, showing that the mean equations that Annex D is based on for concrete breakout in shear can be very conservative for reinforced concrete, as test capacities increase with increasing reinforcement while the predictions remain the same, since the effect of varying the amounts of reinforcement, is not considered in the current design method in Annex D.

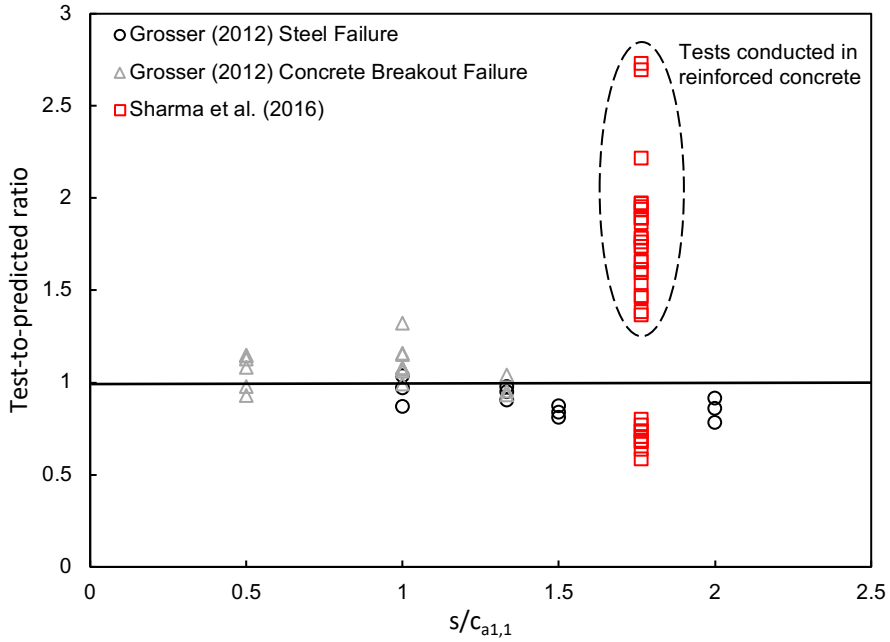

Figure 3.8 Anchor groups close to an edge tested in shear towards the edge by other researchers

From the comparisons of the test results from the two studies to the mean prediction equations upon which Annex D is based, reinforcement is shown to be not well considered for the current design method in Annex D for anchor groups loaded in shear towards an edge. As noted in Section 2.5.3.2, the effects of reinforcement are not considered for uncracked concrete, resulting in increased test-to-predicted ratios when reinforcement is present in the concrete. Additionally, the shear load distribution in the anchors, after initial cracking at the front anchors occurs, may be influenced by the presence of reinforcement.

3.5 Summary

Standard embedded plates, complete with design tables (presented in Appendix A) calculated using Annex D in CSA A23.3:19, are proposed considering feedback from industry members involved in the design, fabrication, and installation of embedded plates. Also, important assumptions made in the calculations of the capacities in the design tables are highlighted.

Experimental results from other studies regarding anchor groups loaded in shear towards an edge are compared with capacities predicted using the mean prediction equations upon which Annex D is based, highlighting gaps in the current design standard for embedded plates. For example, reinforcement is ubiquitous in concrete used for construction, but it is still not well incorporated into the design equations in Annex D for anchor groups loaded in shear towards an edge. Additionally, the embedded plate system, consisting of the anchor group, steel plate and connection are not often tested as an integral assembly, especially in shear towards an edge.

Many assumptions are required to use Annex D to design embedded plates in practical applications. For example, the location and size of the ultimate concrete breakout cone when there are multiple anchors, and the redistribution of shear load to the back anchors when an anchor group is loaded in shear towards an edge are assumptions based on previous studies, and the assumed distribution of moment due to connection eccentricity is accounted for in the steel plate design. Thus, in Chapter 4, the testing program conducted to verify selected calculated design table capacities is described, and selected assumptions are examined to ensure that the proposed standard embedded plates' design tables not only improve the design, fabrication and installation process of embedded plates, but are also safe.

4 Experimental Program

4.1 Introduction

Embedded plates, typically made of anchors that are welded or bolted to a steel plate, are commonly used to connect steel to concrete members. The anchors are embedded in concrete, and the exposed steel plate provides a surface onto which steel members can be connected. Depending on the location of the embedded plate in the concrete, concrete member dimensions, and reinforcement arrangement in the concrete, the load capacity of embedded plates can vary significantly. One situation where embedded plates are used is in a concrete beam or above an opening in a concrete wall, when they are close to an edge with a shear load applied towards the edge (Figure 4.1). In that case, the distance that the embedded plate is from the edge (i.e., edge distance) has a significant effect on the load bearing capacity.

Figure 4.1 Embedded plates located close to the edge of a concrete beam

Anchors used for embedded plates can be designed using provisions from CSA A23.3:19 Annex D (CSA 2019). However, in many situations designers need to make assumptions about how the load is transferred from the steel plate to the anchors that may not be clearly stated in the design standard. Furthermore, most research studies on concrete anchorage have focused on the load resisting behaviour of anchors only; there are few studies regarding full embedded plates with typical connections attached. For example, Sharma et al. (2016) ensured pure shear loading on the tested anchor groups by preventing rotation of the loading apparatus. Teflon sheets were also used in studies such as those of Sharma et al. (2016) and Grosser (2012) to further isolate the behaviour of the embedded anchors.

The main objective of the full-scale tests is to study the behaviour of the proposed standard embedded plates from Chapter 3 loaded in shear towards an edge with varying edge distances. The embedded plates were loaded in shear towards an edge, like Case D in the design tables found in Appendix A, with eccentricities that simulate loading conditions that occur in typical construction scenarios. Rather than focusing on the behaviour of the anchors only, the embedded plate behaviour (i.e. anchors, steel plate, and steel connection) are observed as a whole. Eccentricity away from the face of the plate, referred to as connection eccentricity, is included in the tests via a shear tab, a common method used to connect steel members to embedded plates. The effect of the connection eccentricity is also described. In accordance with CSA A23.3:19, only the row of anchors farthest from the edge can be used to calculate steel anchor capacity for welded anchors, as the ultimate failure crack is assumed to initiate at the back anchors (CSA 2019). This assumption has been shown to be adequate for welded headed anchors in unreinforced concrete, but may be conservative for even lightly reinforced concrete.

Two lightly reinforced concrete specimens with four full-scale embedded plates each, with varying distances from the free edge, were constructed to evaluate the behaviour of two standard embedded plates loaded in shear towards the free edge. A test frame was constructed (described in Section 4.2.3) to load the embedded plates under eccentric shear—with eccentricities from both the shear tab connection away from the embedded plate face and "accidental" lateral eccentricities commonly found during construction—to failure. Additionally, the full-scale test results are compared with the predicted capacities of CSA A23.3:19 Annex D (CSA 2019) to determine the effectiveness of the current Canadian design standard used to design embedded plates with multiple anchor rows close to an edge that are loaded towards the edge.

4.2 Test Program

Two sizes of embedded plates, each placed at four different edge distances, were loaded in shear towards the edge. Each embedded plate included anchors, a steel plate, and a shear tab, to represent a common use case in buildings. Notably, the inclusion of the shear tab causes the shear load to be applied eccentrically at 75 mm away from the face of the plate, and the lateral eccentricity simulates a misplacement of the embedded plate by 10% of the plate width.

Four-anchor (SEP4) and six-anchor (SEP6) standard embedded plates were tested. Drawings and photos of these plates are shown in Figure 4.2. Both embedded plates used 150 mm (nominal)

long, 16 mm (5/8 in.) diameter welded headed studs, and shear tabs with a single bolt line. The 16 mm thick shear tabs, running the full length of the embedded plates, were designed to ensure that failure occurred in the anchors or concrete block first. The headed studs for the four-anchor embedded plate were welded onto a 16 mm thick steel plate, and those for the six-anchor embedded plate were welded onto a 19 mm thick steel plate, as presented in Chapter 3.

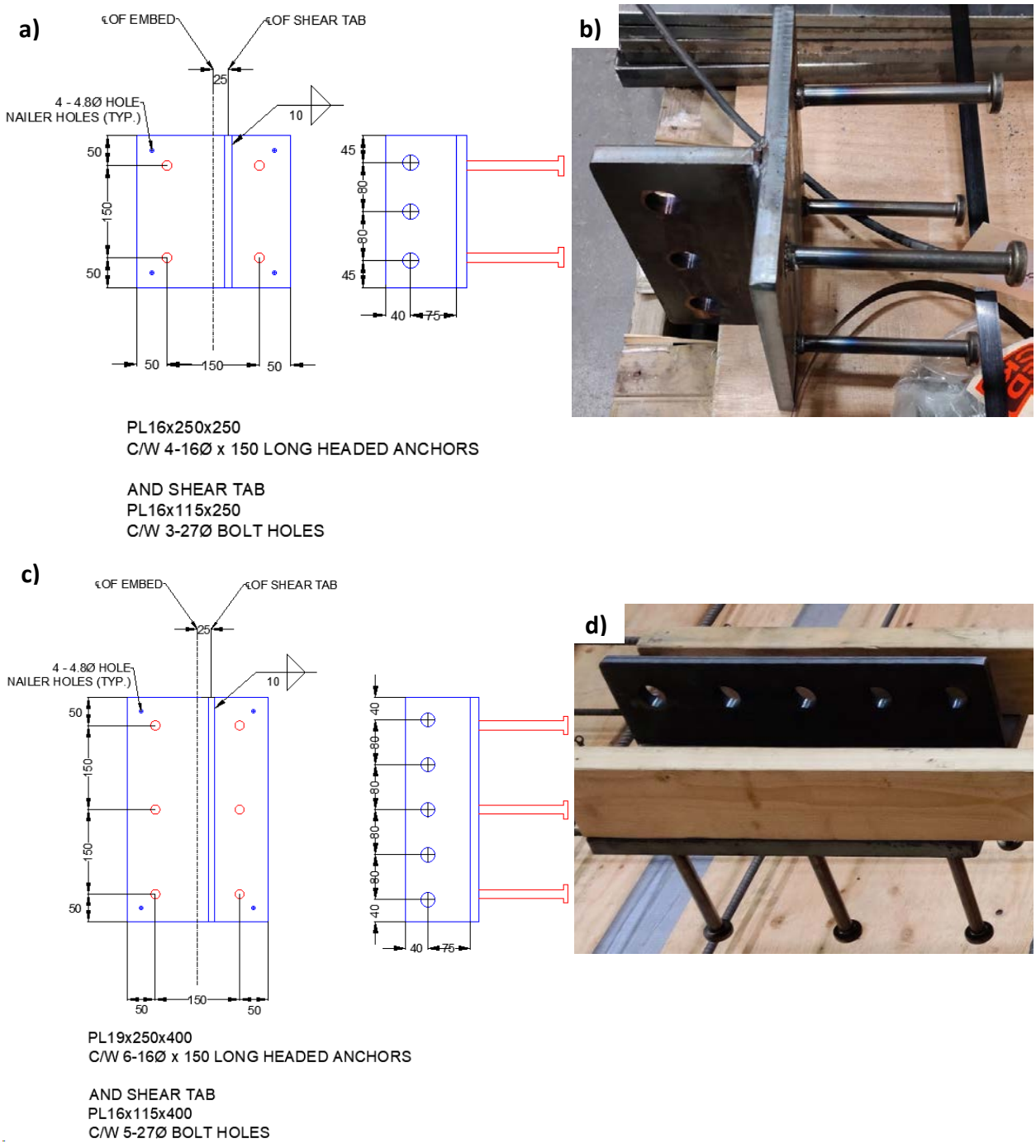

Figure 4.2 Standardized embedded plates in test program (a) drawing of SEP-04, (b) photo of SEP-04, (c) drawing of SEP-06, (d) photo of SEP-06 suspended in position prior to casting concrete. (All dimensions in mm.)

Two concrete blocks were constructed, each with four embedded plates placed at different distances from the edge, as shown in Figure 4.3. The two concrete blocks were 1950 × 1950 × 400 mm and 2400 × 2400 × 400 mm in size. The longer dimensions were chosen for the SEP6 specimens such that the expected concrete breakout failure cone could develop without interference from the supports during testing; a lateral distance of at least three times the distance of the farthest anchor from the edge was maintained between the anchors and the face of the closest supports. Multiple plates were tested on the same concrete block to streamline the construction and testing process, similar to studies such as Sharma et al. (2016) and Anderson and Meinheit (2005). Care was taken in the concrete block design to prevent the embedded plates from affecting each other. The thickness of the block (400 mm) was chosen to be representative of the thickness of a concrete beam that could likely be found in buildings. Similarly, the design concrete strength is 30 MPa, representing concrete strengths used in typical building construction. Reinforcement in the concrete block consisted of 10M stirrups spaced at 250 mm or 300 mm in the smaller and larger blocks, respectively, and 15M boundary steel placed at the perimeter of each concrete blocks. The minimum concrete cover was 30 mm. This plan was chosen so that the concrete was reinforced as lightly as possible, while still being representative of a reinforced concrete beam, as unreinforced concrete, while conservative, is not commonly used in this application.

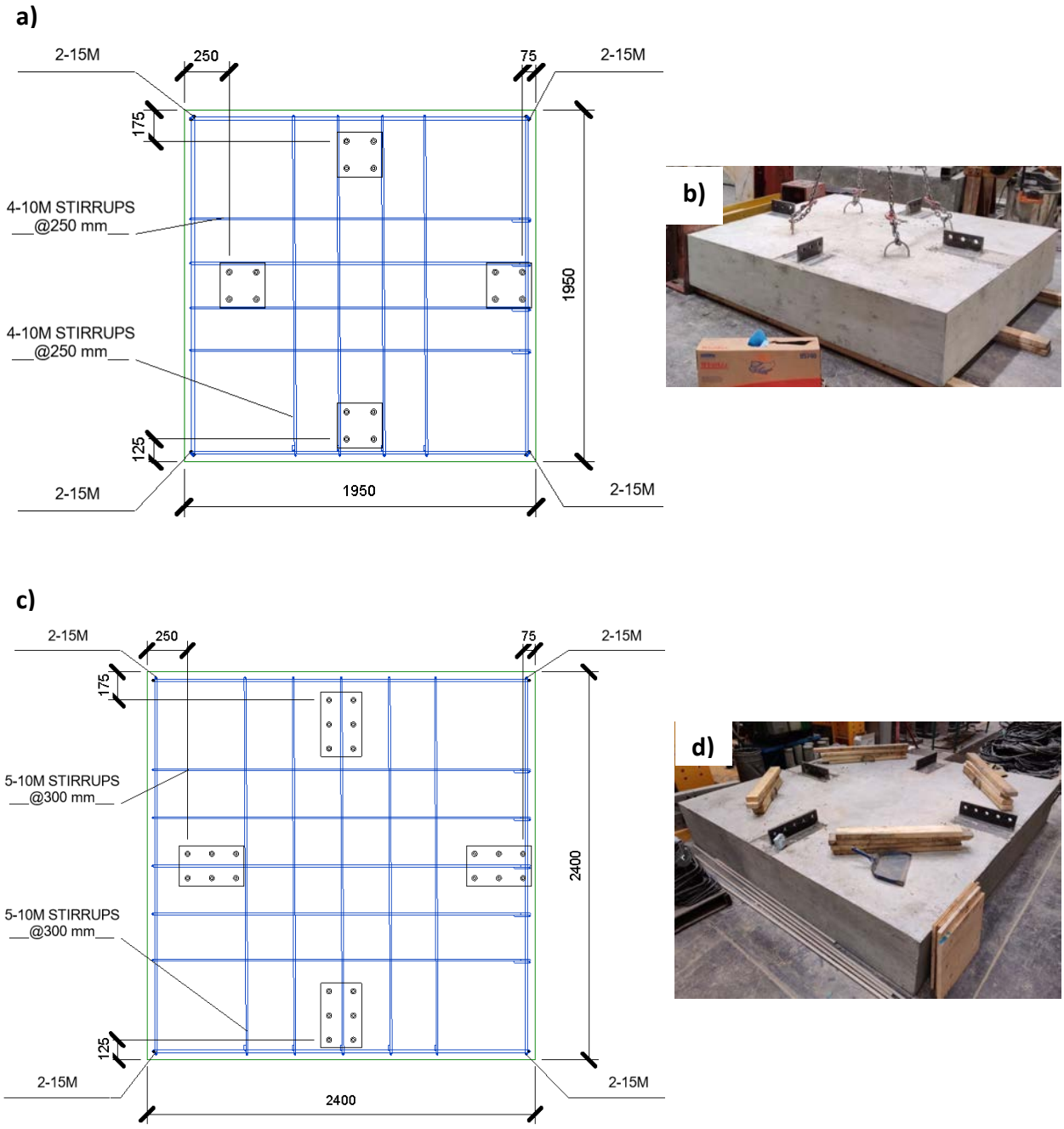

Figure 4.3 Assemblies used in test program (a) drawing of concrete specimen for SEP4 tests (b) photo of concrete specimen for SEP4 tests (c) drawing of concrete specimen for SEP6 tests (d) photo of concrete specimen for SEP6 tests. (All dimensions in mm.)

Table 4.1 shows the experimental test matrix. The tests are identified using a three-term description based on the embedded plate type, stud length in millimetres, and edge distance of the anchor closest to the edge in millimetres, with each description separated by dashes. "SEP4" refers to the proposed standard embedded plate with four anchors, and "SEP6" refers to the proposed standard embedded plate with six anchors.

The plates were placed at 75, 125, 175, and 250 mm from the edge of concrete to the centre of the closest anchor of the embedded plate. Due to the 30 mm concrete cover, reinforcing bars and bend radius of the stirrups, the shortest possible distance that anchors could be placed to the edge of the concrete was 75 mm. The maximum edge distance of 250 mm was chosen since the ACI 318-14 Commentary (ACI 2014) states that for an anchor spacing to front edge distance ratio ($\frac{s}{c_{a1,1}}$) of less than 0.6, the load can be assumed to be resisted by all anchor rows. For both embedded plates, the spacing between studs in both directions is 150 mm, and the resulting maximum front edge distance such that the $\frac{s}{c_{a1,1}}$ ratio is less than 0.6 is 250 mm.

Table 4.1 Test Matrix

Test ID	Number of Anchors	Nominal Stud Length (mm)	Edge distance to centre of front anchor (mm)	Edge distance to centre of back anchor (mm)
SEP4-150-75	4	150	75	225
SEP4-150-125	4	150	125	275
SEP4-150-175	4	150	175	325
SEP4-150-250	4	150	250	400
SEP6-150-75	6	150	75	375
SEP6-150-125	6	150	125	425
SEP6-150-175	6	150	175	475
SEP6-150-250	6	150	250	550

4.2.1 Fabrication Process

Both concrete blocks were cast in wooden forms; the process is outlined in Figure 4.4 for the concrete blocks with SEP6 embedded plates (the same process was used for the concrete block with SEP4 plates). The forms had an approximately 2.4 m × 2.4m, and 3.0 m × 3.0 m footprint to accommodate the plywood forms and diagonal braces (Figure 4.4b). The braces were spaced at 300 mm to support the plywood walls and used to resist lateral pressure from the concrete during casting. Next, the reinforcement cage was assembled with wire ties and placed into the formwork

with reinforcement chairs to ensure 30 mm cover (Figure 4.4c). Perimeter reinforcement was hooked for anchorage and tied as shown in Figure 4.4a. Lifting hooks made from 10M reinforcement bars were tied to the cage so that the cured concrete blocks could be lifted with the lab's overhead crane. To install the embedded plates into the formwork, the plates were first screwed onto two pieces of lumber, then cantilevered over the edge of the forms and fixed to the formwork with additional lumber and screws (Figure 4.4c). Concrete was then placed and vibrated to ensure the concrete flowed under the plates and between the anchors (Figure 4.4d). Finally, the concrete was troweled for a smooth finish. The forms were stripped 7 days after the concrete was poured and cured for a minimum of 28 days before testing (Figure 4.4e).

Figure 4.4 Specimen fabrication process (a) reinforcement cage, (b) formwork, (c) formwork (immediately before pouring), (d) casting/finishing concrete, (e) finished concrete specimens

4.2.2 Materials

The stress–strain curves of the concrete, reinforcement (10M and 15M) and headed anchors used to construct the specimens are shown in Figure 4.5. The full materials test results are presented in Appendix C.

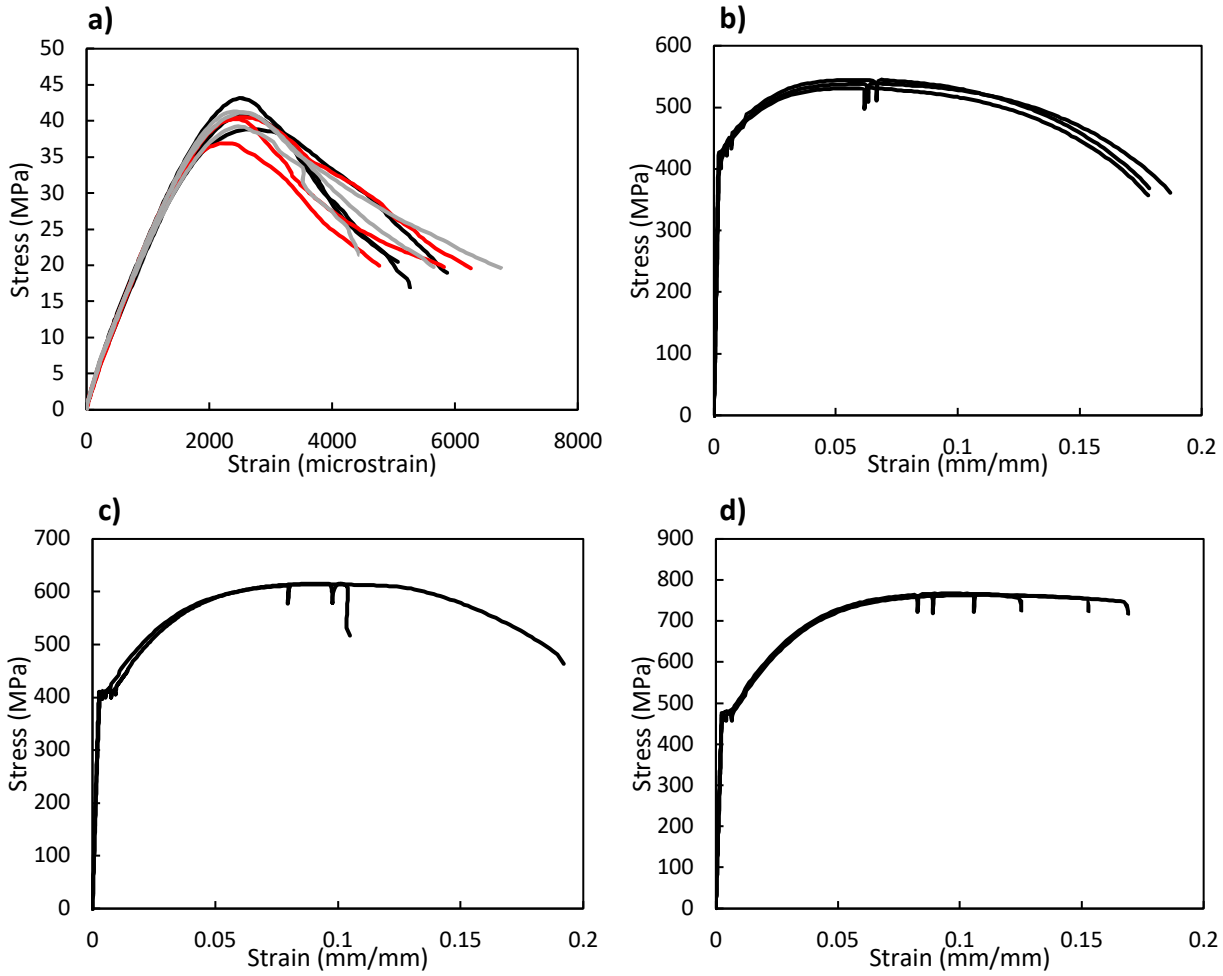

Figure 4.5 Stress–strain curves of (a) concrete cylinders (black) right before first full-scale test, (red) after 4 full-scale tests, (grey) after all 8 full-scale tests (b) headed studs (c) 10M rebar (d) 15M rebar

4.2.2.1 Concrete

Normal-weight concrete with a maximum nominal aggregate size of 19 mm and slump of 100 mm from Lafarge was used to construct the two concrete specimens. For the small concrete specimen with embedded plates with four anchors, the concrete had an average test day strength of 40.1 MPa with a standard deviation of 2.1 MPa. For the larger concrete specimen with embedded plates with 6 anchors, the concrete had an average test day strength of 39.9 MPa with a standard deviation of

1.6 MPa. The strength was determined using ASTM Standard C39 with 100 mm × 150 mm cylinders cast at the same time as the full-scale concrete specimens. The average modulus of elasticity, determined using ASTM C39, is 20.7 GPa with a standard deviation of 1.01 GPa, and 21.0 GPa with a standard deviation of 1.07 GPa, for the small and large concrete specimens, respectively. The modulus of rupture tested according to ASTM C78 is 5.9 MPa with a standard deviation of 0.6 MPa.

4.2.2.2 Rebar

The steel reinforcement used in the concrete specimens consists of 10M and 15M rebars. For the 10M rebar, the average yield and peak tensile loads are 40.0 kN with a standard deviation of 0.1 kN and 58.0 kN with a standard deviation of 0.2 kN, respectively. For the 15M rebar, the yield strength was 460 MPa with a standard deviation of 3.1 MPa, the ultimate strength was 720 MPa with a standard deviation of 0.6 MPa, and the modulus of elasticity was 197 MPa with a standard deviation of 5.8 MPa.

4.2.2.3 Headed Anchors

The headed anchors used in the embedded plates are made of AWS Type B steel and were machined to have a reduced section in the centre of the stud and threaded at the ends to allow for them to be gripped by the testing machine in the lab. The nominal ultimate strength is 450 MPa. The measured ultimate strength was 504 MPa with a standard deviation of 6.2 MPa, and the modulus of elasticity was 208 GPa with a standard deviation of 7.2 GPa. The percent elongation was 18.9% with a standard deviation of 0.7%, using a gauge length of 50.8 mm. The percent area reduction was 61.6% with a standard deviation of 0.8%. From the material properties, the headed anchors used in the tests meet the minimum required percent elongation and percent area reduction to be considered ductile according to Annex D.

4.2.3 Test Setup and Instrumentation

The embedded plates were tested in shear using the test setup shown in Figure 4.6. The concrete block reacted against steel support blocks at each edge, and the embedded plate was loaded horizontally towards the hydraulic jack. The clear spans between the support pedestals are 1450 mm and 1900 mm for the SEP4 and SEP6 concrete specimens, respectively. The spacing between the support pedestals was selected to ensure that the expected full concrete breakout cone can form without restriction. The steel support blocks react on a support beam so that the location of the

pedestals can accommodate the different concrete specimen sizes. A loading arm, consisting of 32 mm steel plates sandwiched between two 16 mm steel plates, was designed to resist a load of 700 kN without failing, and fabricated to attach the shear tab, welded to the embedded plate, to the actuator. The loading arm was connected to the actuator with a 51 mm diameter (two-inch) pin, and to the shear tabs on the SEP4 and SEP6 embedded plates, with three and five 25 mm (one-inch) diameter bolts, respectively. To provide a strong and stiff frame for the hydraulic actuator and concrete specimen to react on, a braced frame was constructed using steel braces and columns available in the lab. Tie-downs consisting of an HSS section and a steel support block were used to tie the concrete specimen down to the strong floor in the lab during testing to prevent potential uplift of the concrete block.

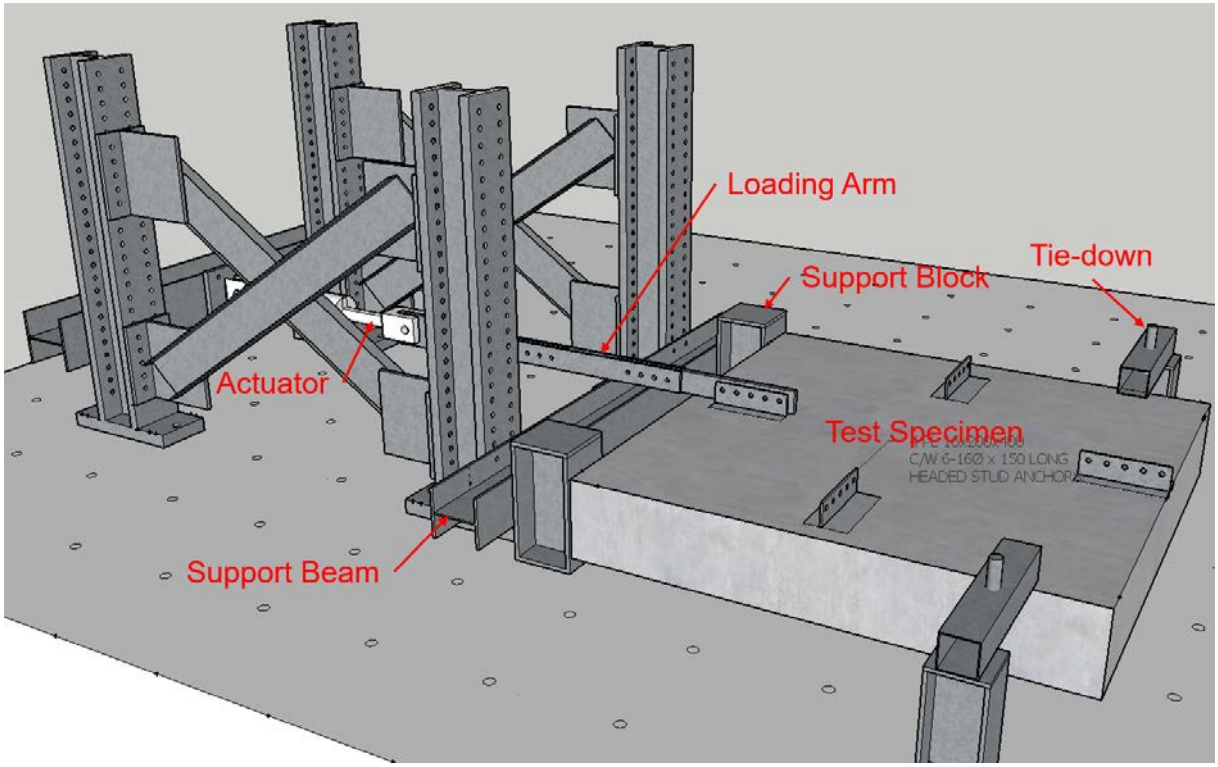

Figure 4.6 Test setup

To test the embedded plates, the concrete specimen was first centred and set into place using an overhead crane. Lifting hooks embedded into the concrete specimens allowed them to be lifted by the crane. The loading arm was bolted to the shear tab, then a small load was applied with the hydraulic actuator (typically less than 15% of the anticipated test failure load) to settle the concrete specimen onto the supports. This load was then released, and instruments were installed and zeroed before running the tests to failure. Note that the initial settlement load procedure was

developed after completing the first test (SEP4-150-75) and noticing that the block slid until it made contact with the support, giving an initial response different than the other tests, which is discussed more in Section 4.3.1.

During testing, the loading rate was controlled manually with a typical loading rate of 0.25 to 1 kN/s, resulting in typical displacement rates of 0.6 to 2.4 mm/s. Peak load was reached in 17 minutes on average. For the first embedded plate tested (SEP4-150-75) loading proceeded until there was a sudden significant (i.e., 70%) drop in load. For subsequent tests, significant embedded plate displacement relative to the concrete specimen (at least 20 mm) was achieved, well past the displacement at peak load. After each test, the concrete block was rotated, and the testing process repeated for the next embedded plate. After all tests in the first concrete block were completed, the second concrete block was set in place and tested following the same procedure.

As shown in Figure 4.7, a variety of instruments were used to evaluate the response of the embedded plates. A load cell mounted on the hydraulic actuator was used to measure the load applied to the embedded plate. Two LVDTs were mounted on a piece of lumber to measure the vertical displacement used to calculate the rotation of the embedded plate. They were placed 200 mm and 338 mm apart for SEP4-150, and SEP6-150 embedded plates, respectively. Furthermore, two cable transducers were used to measure the horizontal displacement of the embedded plate.

Two additional LVDTs were mounted on the sides of the concrete block to measure the horizontal displacement of the concrete block so that the relative plate movement with respect to the concrete block could be determined. Data was collected from the 1000 kN load cell connected to the actuator, LVDTs and cable transducers at 1 second intervals during each test. Two instruments were used to measure each of the horizontal and vertical displacements to account for any rotation of the embedded plate relative to the concrete block to be calculated, as well as to provide some redundancy in case one sensor dislodged during the test.

Two cameras (Canon EOS Rebel T6, and Canon EOS Rebel T7i) mounted 1.2 m above the concrete specimens (shown in Figure 4.7) were used to capture images at ten-second intervals during testing for digital image correlation (DIC). The photos captured were 3456 × 5184 pixels resulting in a scale of 3.4 pixels/mm, and 4000 × 6000 pixels resulting in a scale of 4.2 pixels/mm for the T6 and T7i cameras, respectively.

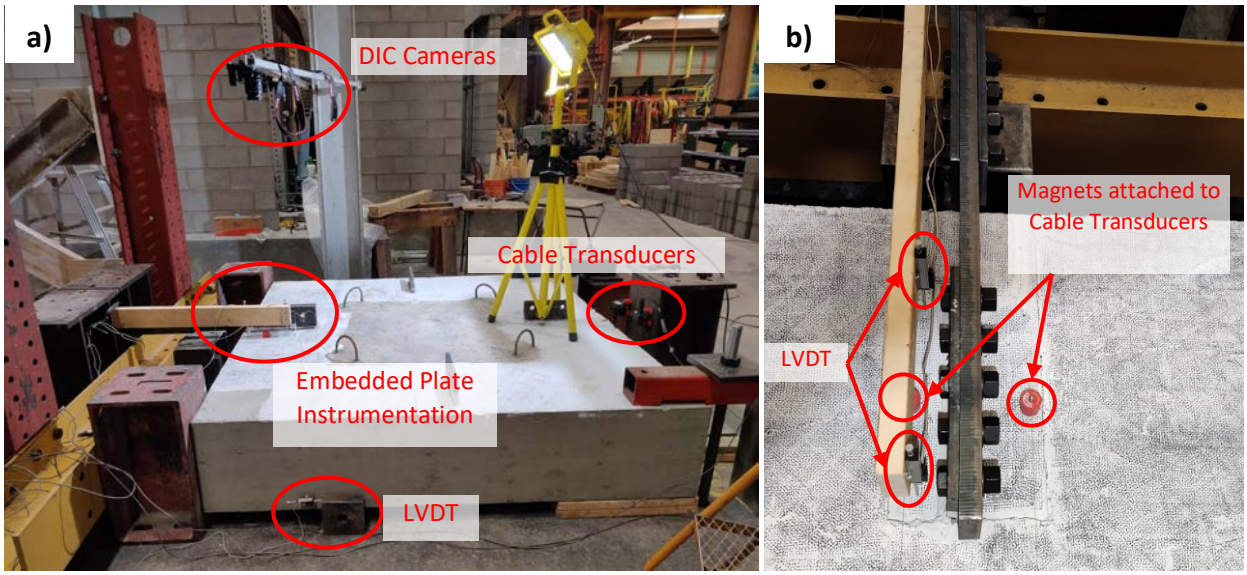

Figure 4.7 Instrumentation layout (a) of the concrete specimen and, (b) closeup at the embedded plate

4.3 Test Results and Discussion

4.3.1 Load–Displacement and Load–Rotation Results

A summary of the test results is shown in Table 4.2, and the load–displacement curves for all eight tests are shown in Figure 4.8. Cracking loads are defined as the point where a crack first propagates to the edge of the concrete and was determined using the DIC images and loading data. The reported net embedded plate displacement is the average concrete block displacement measured using the LVDTs subtracted from the average plate displacement obtained from the cable transducers to account for the movement of the supports and concrete block as load is applied. For the first test, SEP4-150-75, the concrete specimen moved approximately 3 mm before it made contact with the support. This movement affected the load-displacement curve. Thus, for the following tests, a small load was applied (less than 15% of the maximum load) after the loading arm was connected to the embedded plate to ensure the concrete specimen was flush with the supports to prevent excessive movement of the concrete specimen. The curve for SEP4-150-75 in Figure 4.8 was shifted 1.3 mm to the left to align the response of the embedded plate after the concrete specimen has settled with the remaining SEP4 tests. The load–displacement curves for SEP4-150-75 and SEP4-150-125 were truncated when a sudden failure of the specimen, immediately after the peak load was achieved, caused a sudden decrease in load and corresponding

sudden displacement of the plate caused the magnets attached to the cable transducers on the embedded plate, to detach or shift. SEP6-150-175 also failed suddenly, as shown in Figure 4.8, by two steep declines in load. However, the magnets did not detach, and the load–displacement curve was not truncated.

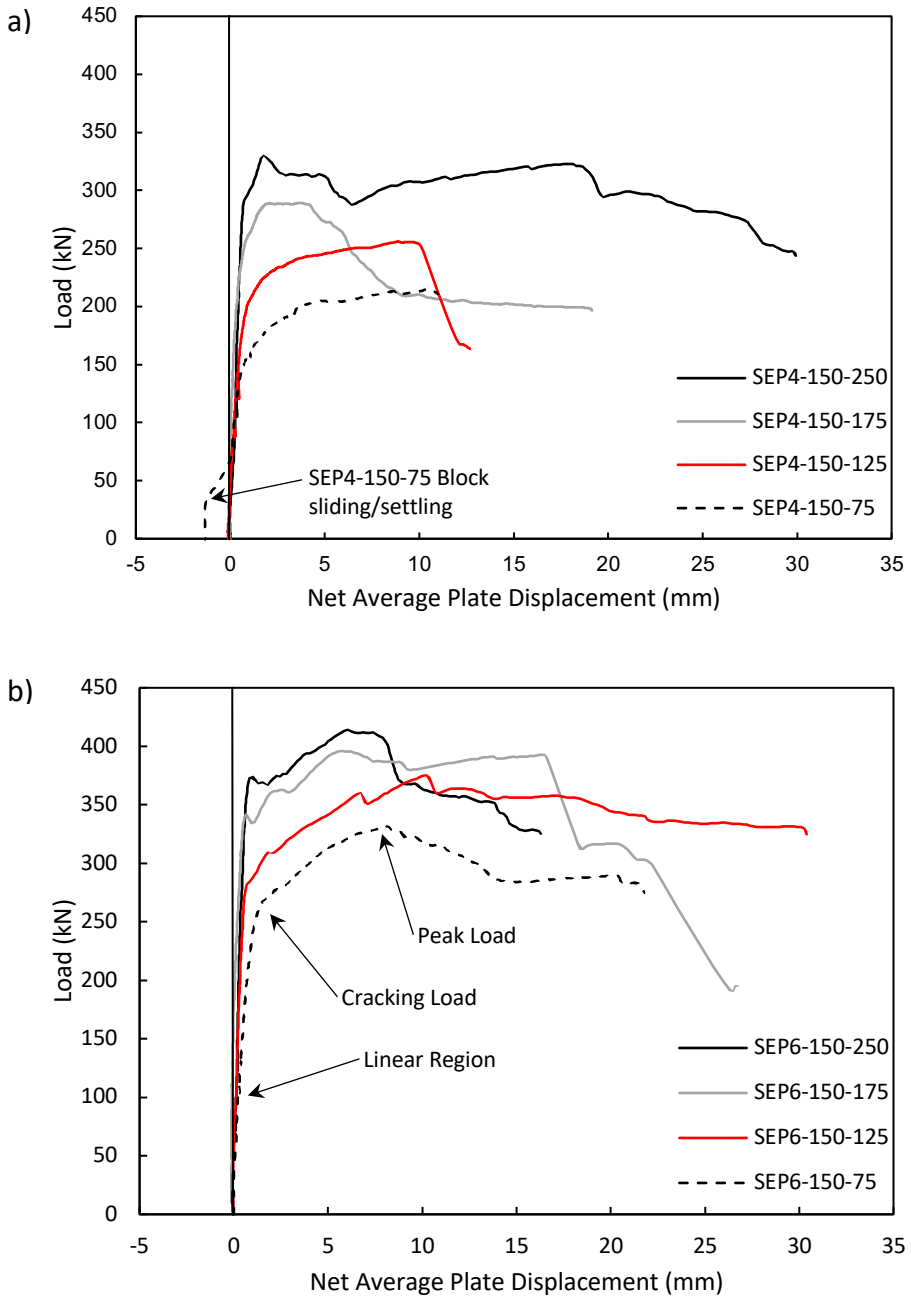

Figure 4.8 Load–displacement curves (a) SEP4 tests (b) SEP6 tests

Table 4.2 Test Results

Test ID	Cracking Load (kN)	Net Displacement at Cracking (mm)	Peak Load (kN)	Net Displacement at Peak (mm)	Rotation at Peak (rad)	Failure mode
SEP4-150-75	130.2	0.408[(1)]	215.2	10.4	0.0260	C
SEP4-150-125	197.3	0.844	256.2	8.9	0.0209	S[(2)]
SEP4-150-175	237.5	0.583	289.2	3.59	0.0127	C
SEP4-150-250	329.5	1.69	330.3	1.76	0.00901	C
SEP6-150-75	266.9	1.52	331.8	8.15	0.0161	C
SEP6-150-125	288.8	1.03	375.4	10.24	0.0213	C
SEP6-150-175	342.9	0.628	395.9	5.67	0.0122	C
SEP6-150-250	373.5	1.08	414.3	6.03	0.0152	C

Notes: Failure mode 'C' refers to the concrete breakout failure mode. Failure mode 'S' refers to the steel anchor failure

[(1)] Net displacement measured is 1.708 mm, from which 1.3 mm was subtracted to account for concrete block movement

[(2)] Back row of anchors failed

Shown in Figure 4.8, generally, the load–displacement response of the embedded plates is linear initially, then stiffness decreases past the initial cracking load and the response becomes non-linear until the peak load is reached. After peak load, the load either decreased gradually until the test was stopped or decreased suddenly due to a sudden failure of the specimen, which was the case for the SEP4-150-75, SEP4-150-125 and SEP6-150-175 tests.

For SEP4-150-250, the reported cracking load is much greater than the load at which the stiffness of the specimen first starts to decrease. The initial formation of cracks happened earlier than the reported cracking load, and for this test, the first breakout crack closest to the edge, initially propagates at approximately 35 degrees to the edge of the concrete, but then changes direction and travels nearly parallel to the edge of the concrete before finally reaching the edge. This contrasts to the crack propagation found in the other tests, which typically traveled at 35 degrees to the edge of the concrete throughout its length. The large edge distance of this specimen may have affected the crack formation, as the propagation of the first breakout cone cracks formed by the row of anchors closest to the edge may be impeded by stresses caused by the back row of anchors, as it is at the limit at which all anchor rows may be assumed to carry load in ACI 318-14, as discussed in Section 4.2 (ACI 2014).

The failure mode of all specimens except for SEP4-150-125 was in the concrete. Using the DIC images and images taken after the test, shown in Figure 4.9, SEP4-150-125 is shown to have failed in the back row of anchors; one of the back anchors failed first, then the remaining back anchor failed soon after. For this test, the predicted failure load of the concrete (241.9 kN) and steel anchors (263.3 kN) were similar, thus with material variability the specimen could have failed in either failure mode. Also, the load bearing behaviour of the edge reinforcement due to dowel action, may have reduced the stiffness at the front anchors, resulting in the anchors farther from the edge carrying more load.

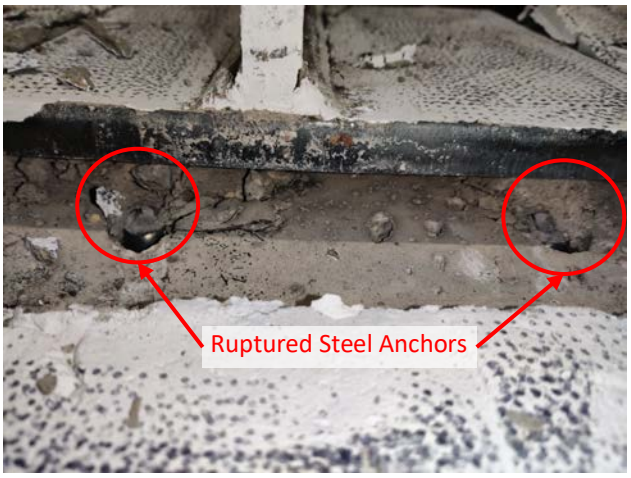

Figure 4.9 Steel anchor failure of SEP4-150-125

As expected, increasing edge distance also increased peak load. The responses of each of the SEP6 embedded plates were similar even after the peak load. However, of the SEP4 embedded plates, the load–displacement response for the SEP4-150-75 and SEP4-150-125 tests were very similar, but differed from the SEP4-150-175 and SEP4-150-250 tests. Specifically, the SEP4-150-75 and SEP4-150-125 load–displacement curves show a nearly identical steady decrease in stiffness after the cracking load and plateau up to the peak load. Also, compared to the SEP4-150-175 and SEP4-150-250 tests, the SEP4-150-75 and SEP4-150-125 tests reached peak load at a greater net average plate displacement (10.4 and 8.9 mm compared to 3.59 and 1.76 mm). Additionally, shown in Figure 4.10, the yielded edge reinforcement of SEP4-150-125 compared to the less deformed edge reinforcement of SEP4-150-175 suggest that edge reinforcement for embedded plates can significantly affect the response of embedded plates located close to the concrete edge. Anchors

that are too close to an edge may not be able to engage the stirrups sufficiently, resulting in the bearing of the anchors against the longitudinal reinforcement.

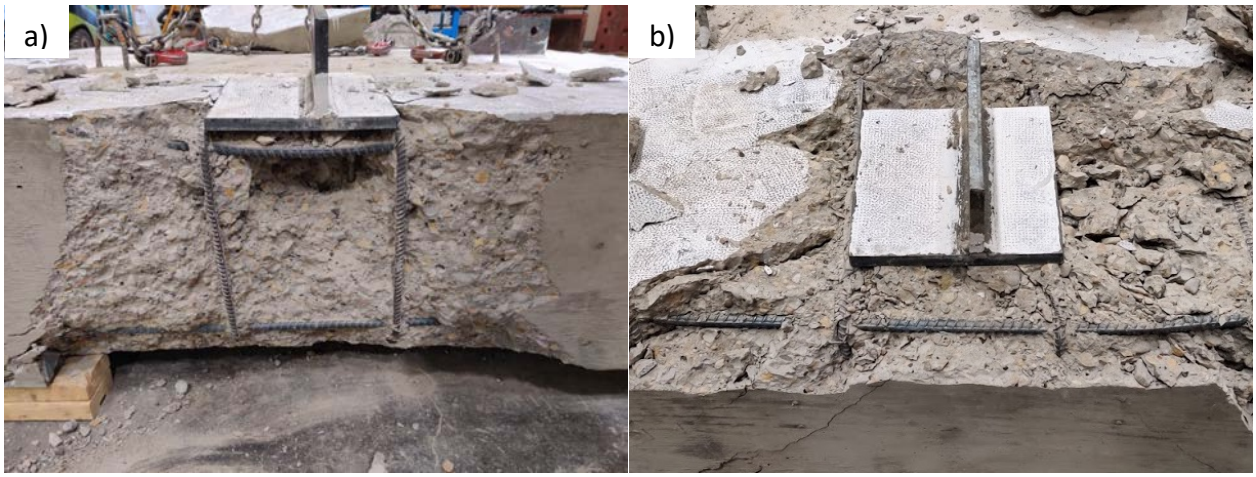

Figure 4.10 Edge reinforcement after testing of (a) SEP4-150-125 and (b) SEP4-150-175

The load–rotation curves for the tests, shown in Figure 4.11, show the rotation of the embedded plate out of its plane, as illustrated in Figure 4.12. The difference in the measurements of the two LVDTs mounted on the piece of lumber, along with the spacing of the LVDTs, were used to calculate the angle of the embedded plate. The LVDTs were spaced at 200 mm and 338 mm for the SEP4 and SEP6 embedded plates, respectively. Out-of-plane rotation (θ) was calculated using Equation 4.1, assuming the plate remained rigid throughout the test, since the plate was not expected to deform significantly based on the design calculations, and visual inspection of the embedded plate after each test showed no yielding had occurred in the steel plate. Additionally, in Figure 4.11, the curves were truncated at a similar location as the load–displacement curves or when the embedded plate moved horizontally past the static LVDTs such that the LVDTs were no longer in contact with the plate. Generally, the load–rotation responses of the embedded plates, shown in Figure 4.11, were similar to the load–displacement response. The response was linear initially, then stiffness decreased, and the response becomes non-linear until the peak load was reached.

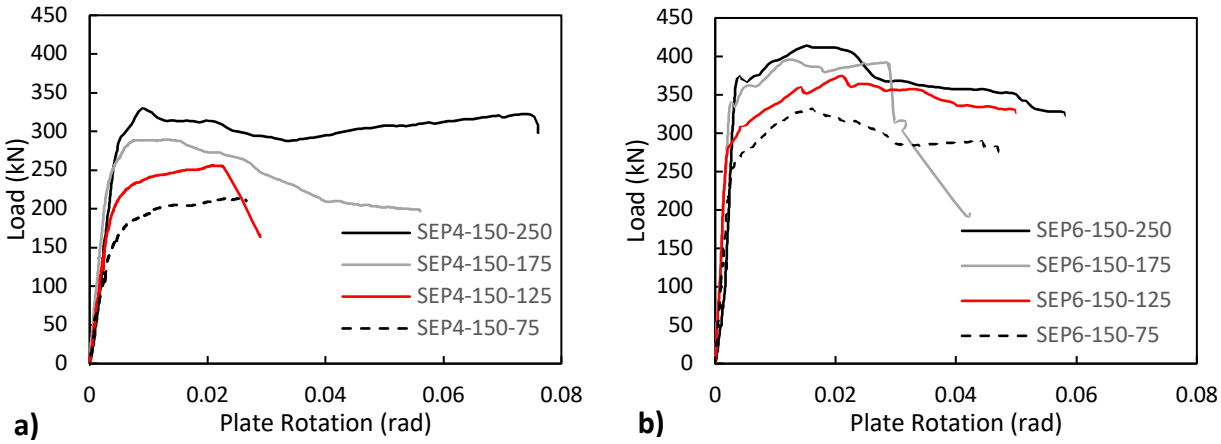

Figure 4.11 Out-of-plane load–rotation curves for (a) SEP4 tests (b) SEP6 tests

$$\theta = \tan^{-1}\frac{\delta_2 - \delta_1}{s_{LVDT}} \qquad \textbf{4.1}$$

where: δ_2 = measurement at vertical LVDT 2 (see Figure 4.12)

δ_1 = measurement at vertical LVDT 1 (see Figure 4.12)

s_{LVDT} = LVDT spacing

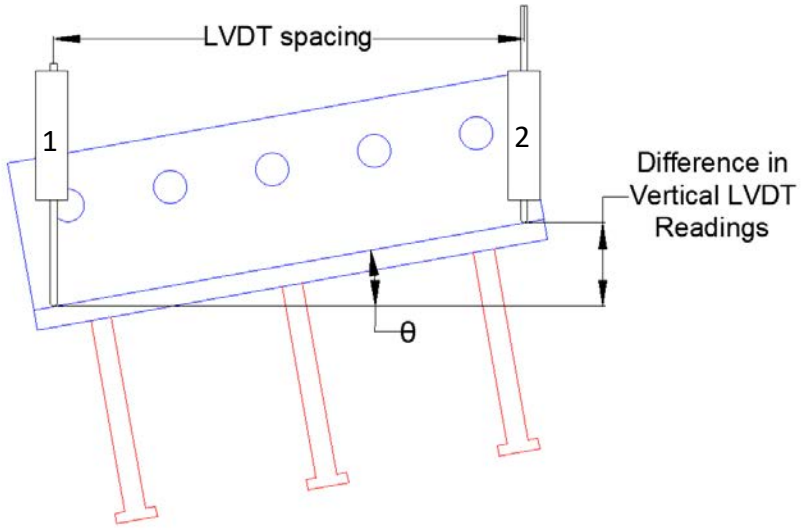

Figure 4.12 Embedded plate out-of-plane rotation diagram

4.3.2 Digital Image Correlation Results

Images captured by the two cameras mounted above the concrete specimen were analyzed with GOM Correlate to produce the DIC results. These results allow displacement to be measured

across the top surface of the concrete specimen, showing clearly when the concrete specimen cracks initially, and the crack's propagation. However, only the displacement of the surface horizontally (across the top surface of the concrete specimen) can be determined, as the images were processed using two-dimensional DIC analysis. The main points at which DIC results are presented, shown in Figure 4.13 for SEP4-150-125 and in Figure 4.14 for SEP6-150-250, are at initial cracking (when a crack first reaches the edge of the concrete), at peak load, and at a net plate displacement of 15 mm to capture some post-peak behaviour. Using DIC, the processed images clearly show the crack patterns, and when synchronized with the loading data, were used to determine initial cracking loads for each test. In Figure 4.13 and Figure 4.14, the displacement of the top surface of the concrete and embedded plate are shown visually. For Figure 4.13, a changing scale was used for each image, as a static scale would not allow any observations to be made at peak load and initial cracking.

All test specimens failed in concrete breakout except for SEP4-150-125, which failed in the back row of steel anchors. DIC images at initial cracking, peak load, and at 15 mm of net plate displacement for SEP4-150-125 and SEP6-150-250, shown in Figure 4.13 and Figure 4.14, were chosen as representative of the responses observed in the tests. Additionally, only one camera's DIC analysis is shown in Figure 4.13 and Figure 4.14 for clarity, and similar results are found in the other camera's images. Generally, the concrete breakout cracks formed at approximately 35 degrees, which agrees with the assumed concrete breakout cone angle in CSA A23.3:19 (CSA 2019). Each breakout cone typically initiated at a row of anchors and propagated towards the edge of the concrete. The smaller breakout cone formed by the anchor row closer to the edge generally forms first, followed by larger cones formed by anchor rows farther from the edge. Additionally, once the first breakout cone crack reaches the edge of the concrete, a significant decrease of stiffness of the specimen is typically measured (Figure 4.8). Based on the DIC images, edge distance and the number of rows of anchors generally did not affect this behaviour. As edge distance increased, the size of the concrete breakout cones increased as well, resulting in an increased capacity. Since a larger surface of the concrete is required to fail, a larger breakout cone is intercepted by more stirrups and the stirrups are more sufficiently embedded into the cone. Sudden failure after peak load is also shown in Figure 4.13c by the concrete debris, and displaced magnet caused by the sudden movement.

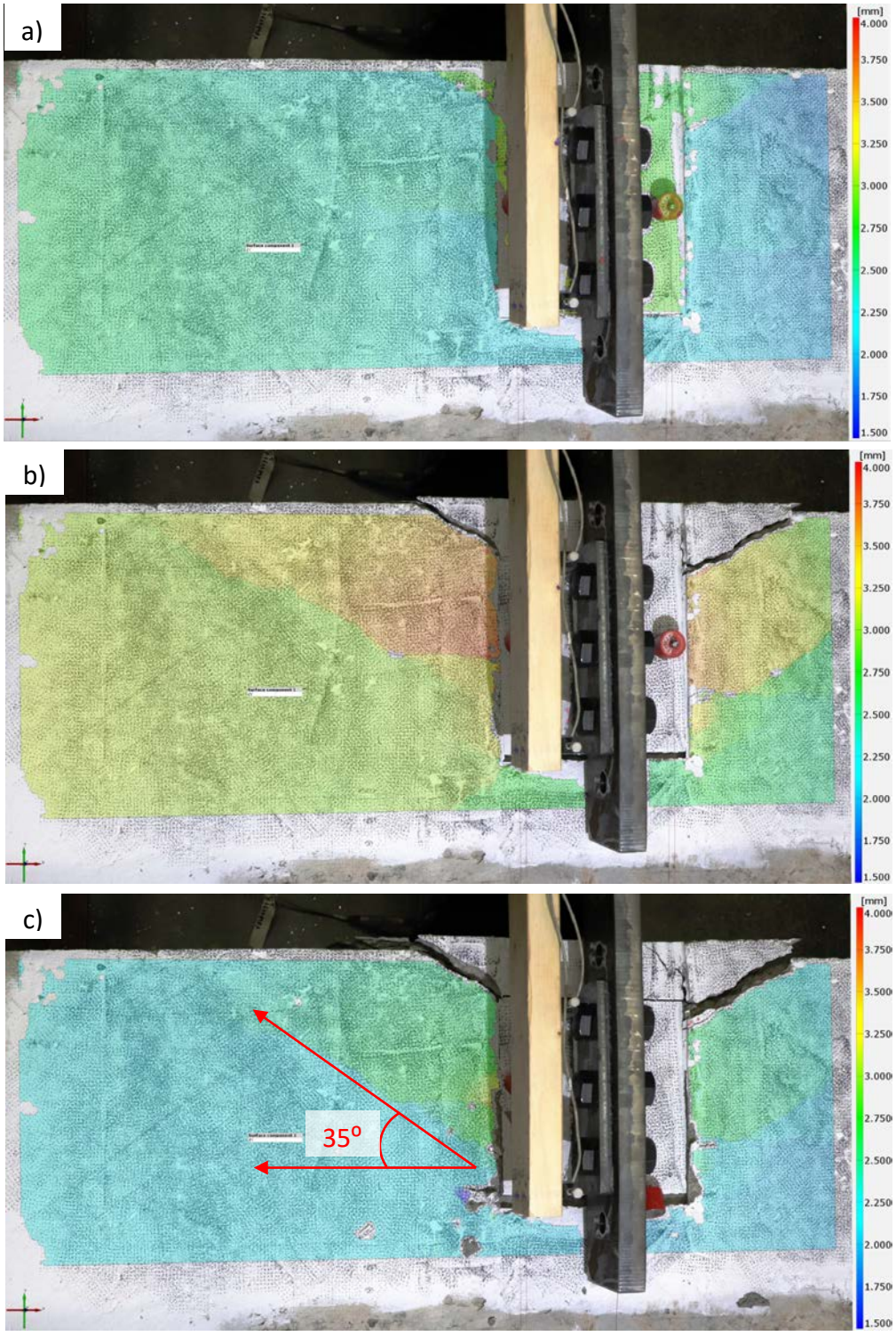

Figure 4.13 DIC images of SEP4-150-125 at (a) initial cracking, (b) peak load, (c) net plate displacement of 15 mm, with static scales

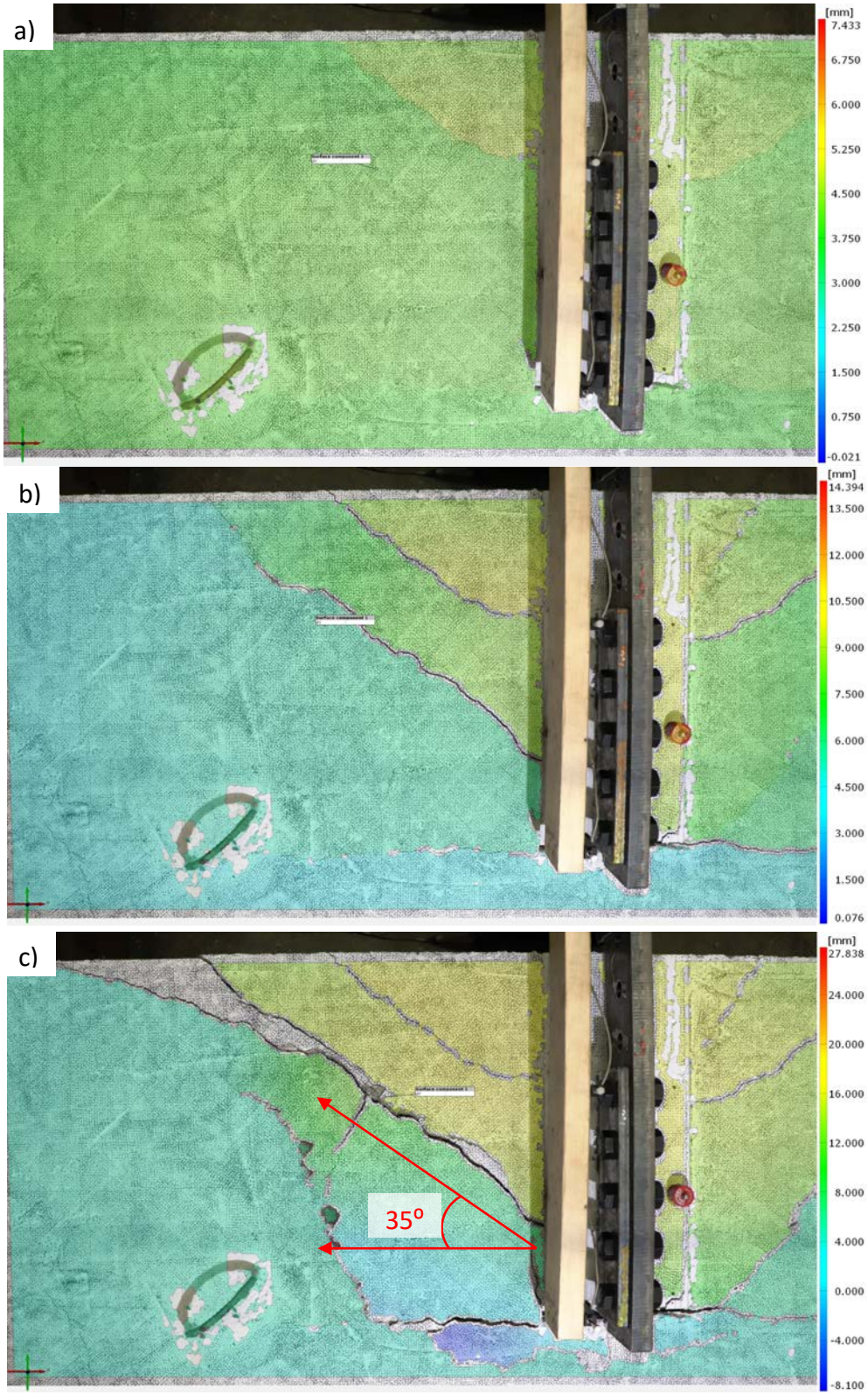

Figure 4.14 DIC images of SEP6-150-250 at (a) initial cracking, (b) peak load, (c) net plate displacement of 15 mm, with a changing scale

Using DIC, crack widths were measured for SEP6-150-175, shown in Figure 4.15, which is representative of the response observed in the tests, near the edge (Crack Widths 1 and 4), between stirrups (Crack Width 2), and close to the embedded plate (Crack Widths 3 and 5). The crack widths throughout the test are then plotted against the net average plate displacement shown in Figure 4.16. After the initial cracking of the concrete, (a) in Figure 4.16, Crack Width 2, 3 and 5 increase rapidly, corresponding to a rapid decrease in stiffness shown in Figure 4.8b). As the test progresses, after (b) in Figure 4.16, Crack Width 1, 2 and 4 begin to increase rapidly, again, corresponding with a decrease in stiffness shown in Figure 4.8b) before the peak load at approximately 2 mm of net average plate displacement. After the peak load, (c) in Figure 4.16, growth of Crack Widths 1, 2 and 3 slow, while Crack Widths 4 and 5 accelerate slightly, possibly due to a loss of resistance of the front anchors due to the smaller and thus more fully formed breakout crack. After the first sudden failure of the test occurs at (d) in Figure 4.16, Crack Widths 1, 2 and 3 decrease slightly as the concrete rebounds. Similarly, crack widths decrease around the point where the second sudden failure of the test occurs at (e) in Figure 4.16. No measurement of Crack Width 3, 4 and 5 are made after the second sudden failure, as the surface of the concrete was too damaged and rotation out-of-plane was too large for DIC to properly track.

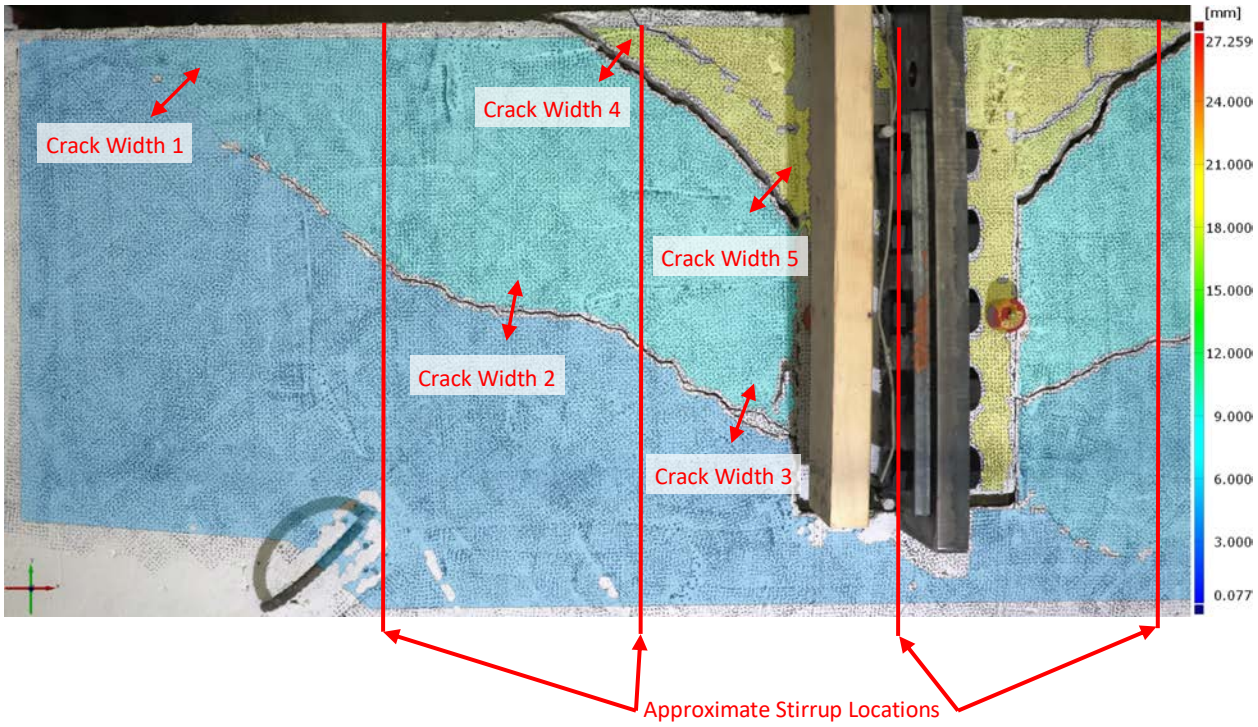

Figure 4.15 DIC image of SEP6-150-175 before first sudden failure

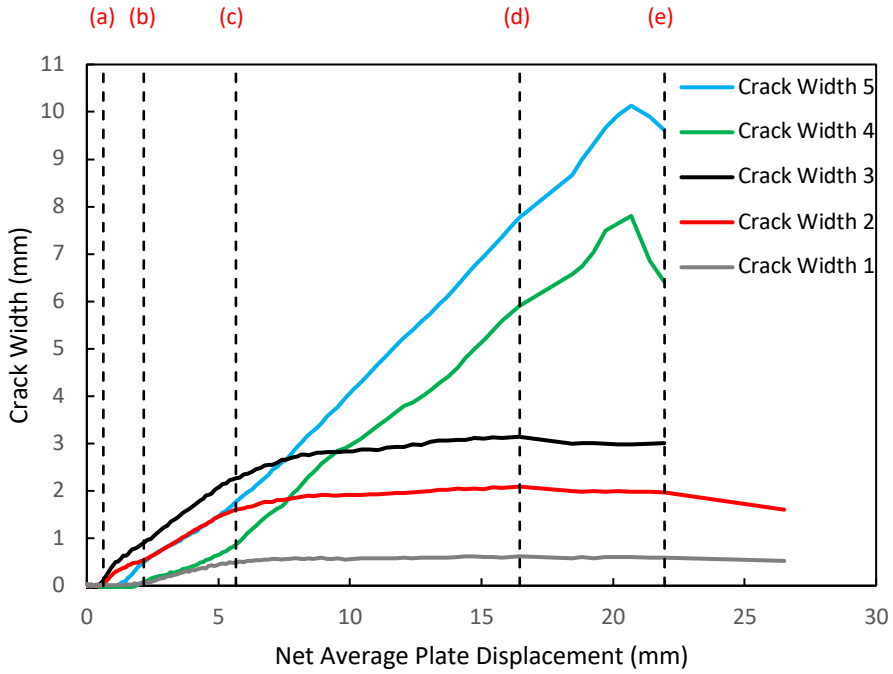

Figure 4.16 Crack width vs net average plate displacement of SEP6-150-175

Crack widths were also measured for a test with a plate closer to the edge, SEP6-150-75, shown in Figure 4.17, near the edge (Crack Width 6), between stirrups (Crack Width 7), and close to the embedded plate (Crack Widths 8 and 9). No sudden failures were observed for SEP6-150-75, unlike SEP6-150-175 where two sudden failures occurred. Similar to Figure 4.16, the crack widths were then plotted against the net average plate displacement in Figure 4.18. Similar to the response of SEP6-150-175, the cracks near the embedded plate (Crack Widths 8 and 9) in SEP6-150-75 rapidly increase after the initial cracking of the concrete, (a) in Figure 4.18, corresponding to the stiffness decrease found in Figure 4.8b). After peak load, (b) in Figure 4.18, the crack closer to the edge (Crack Width 9) plateaus, while the cracks farther from the edge (Crack Widths 6,7, and 8) rapidly increase. This differs from the response found in SEP6-150-175, where the deformation was concentrated in the crack closer to the edge. However, no clear trend was found regarding which crack the deformation was concentrated in after peak load.

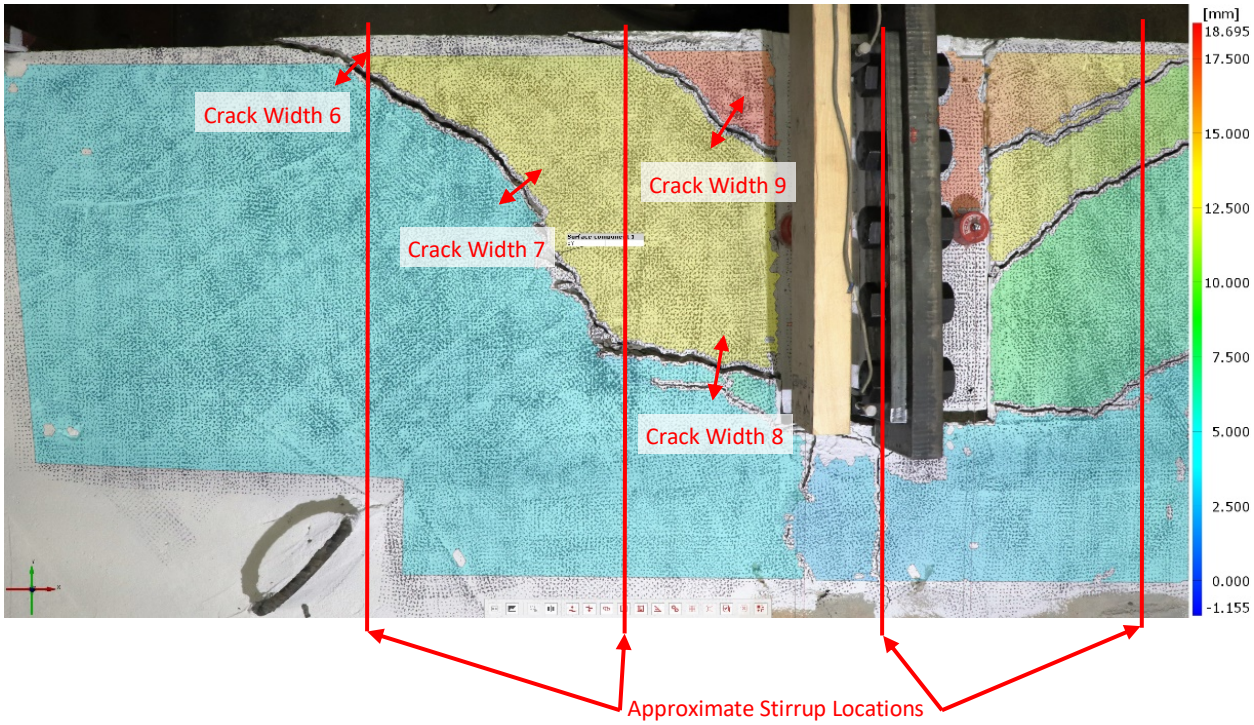

Figure 4.17 DIC image of SEP6-150-75 at 15 mm of net plate displacement

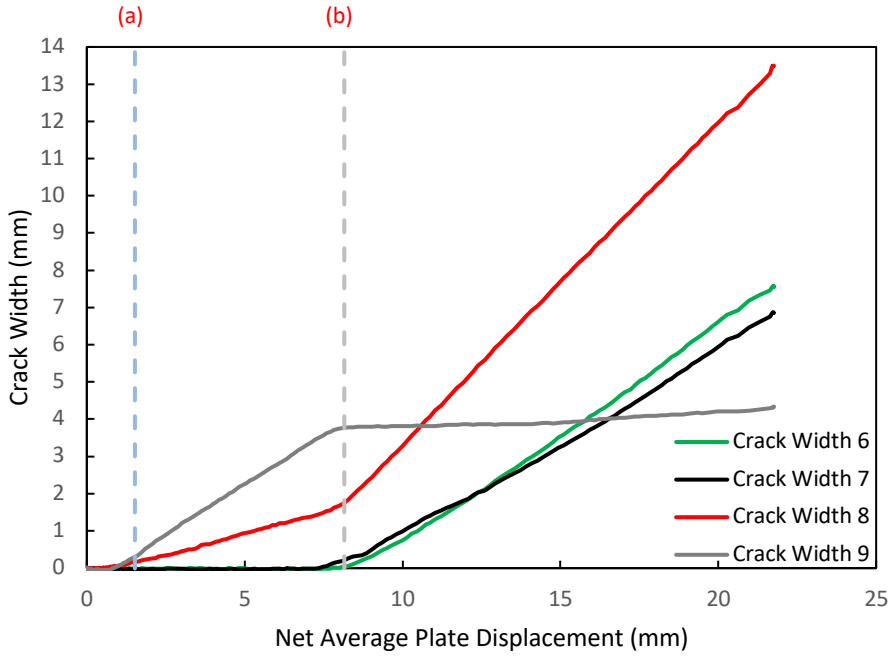

Figure 4.18 Crack width vs net average plate displacement graph for SEP6-150-75

4.3.3 Comparison to Design Code Predictions

Predictions calculated using Annex D of A23.3:19, as discussed in Section 2.5, and using their respective mean prediction equations were compared with the test results (Table 4.3 and Table 4.4). Both the mean and code predictions were calculated since the methods provided in Annex D predict the 5% fractile resistance of the anchors; therefore, calculated predictions using the mean equations found in Fuchs et al. (1995), on which the design equations in Annex D are based, were also compared with the test results. For all predictions, material resistance factors (ϕ_c and ϕ_s), resistance modification factors (R), and edge distance modification factors ($\psi_{ed,V}$ and $\psi_{ed,N}$) are set equal to 1.0. The eccentricity modification factors ($\psi_{ec,V}$ and $\psi_{ec,N}$) are calculated as shown in Equations 2.19 and 2.20, respectively. The concrete cracking modification factors ($\psi_{c,V}$ and $\psi_{c,N}$) are taken as 1.4 for the uncracked concrete used. Additionally, two assumptions were made about the loading condition of the embedded plate: Assumption 1, where only shear is assumed to act on the embedded plate, and Assumption 2, which accounts explicitly for the 75 mm connection eccentricity from the plate surface resulting in both shear and moment acting on the embedded plate. The moment is distributed to the anchors and concrete as tension and compression forces, respectively, using a rigid plate assumption. Then, using the combined shear tension interaction equation with k=5/3 (Equation 2.29), the capacity of the embedded plate is calculated.

From Table 4.4, the predictions using the Annex D provisions, regardless of the assumed loading condition, are very conservative, with mean test-to-predicted ratios of 1.39 and 1.74 for Assumption 1 and Assumption 2, respectively. Thus, the code is conservative at predicting anchor capacities. The mean test-to-predicted ratios, on the other hand, are 0.92 and 1.11 for Assumptions 1 and 2, respectively. Importantly, with Assumption 1, the predictions are generally unconservative, while with Assumption 2, the predictions are generally slightly conservative. This suggests that the moment caused by applying the load at the bolt line of a shear tab 75 mm away from the face of the embedded plate significantly affects the load carrying capacity of the embedded plate. Specifically, the moment transferred by shear tab connections should be considered when designing embedded plates. Additionally, the SEP4-150 tests had a slightly greater mean test-to-predicted ratio of 1.20 compared to 1.02 for the SEP6-150 tests. This was possibly influenced by more closely spaced stirrups in the SEP4-150 concrete block, which were also very close to the anchors, improving the concrete breakout strength compared to the stirrups

in the SEP6-150 concrete block. Nevertheless, the ratio for the less favourable case is still greater than 1.0.

Table 4.3 Test Capacity vs Calculated Capacity

Test ID	Test Load Capacity (kN)	Code Prediction[1] (Assumption 1) (kN)	Code Prediction[1] (Assumption 2) (kN)	Mean Prediction (Assumption 1) (kN)	Mean Prediction (Assumption 2) (kN)
SEP4-150-75	215	136	113	206	181
SEP4-150-125	256	178	142	269	221
SEP4-150-175	289	207	162	313	246
SEP4-150-250	330	250	188	379	261
SEP6-150-75	332	235	195	356	324
SEP6-150-125	375	264	216	400	357
SEP6-150-175	396	293	237	444	388
SEP6-150-250	414	337	267	510	433

[1] *Code Prediction refers to the 5% fractile resistance design equations in Annex D of A23.3:19*

Table 4.4 Test-to-predicted Ratios

Test ID	Code Prediction[1] (Assumption 1)	Code Prediction[1] (Assumption 2)	Mean Prediction (Assumption 1)	Mean Prediction (Assumption 2)
SEP4-150-75	1.58	1.91	1.04	1.19
SEP4-150-125	1.44	1.80	0.95	1.16
SEP4-150-175	1.40	1.79	0.92	1.18
SEP4-150-250	1.32	1.76	0.87	1.26
SEP6-150-75	1.41	1.70	0.93	1.03
SEP6-150-125	1.42	1.74	0.94	1.05
SEP6-150-175	1.35	1.67	0.89	1.02
SEP6-150-250	1.23	1.55	0.81	0.96
Mean	1.39	1.74	0.92	1.11
Standard Dev.	0.101	0.106	0.067	0.105

[1] *Code Prediction refers to the 5% fractile resistance design equations in Annex D of A23.3:19*

Additionally, all tested embedded plates had an ultimate capacity greater than the shear capacity of only the back row of steel anchors, at 200 kN. In other words, in all the full-scale tests, the steel anchor capacity of the embedded plate may not be limited to only considering the back row of anchors. However, if there is insufficient support from reinforcement, specifically from the stirrups, a significant loss in stiffness of the front anchors may occur, as shown in Figure 4.10a) by the large deformation of the edge reinforcement, transferring a significant portion of the load to the back anchors. Thus, to reliably consider all anchors when calculating steel anchor capacity, sufficient reinforcement must be present, especially for anchor groups close to the edge.

4.3.4 Comparison with Other Test Programs

Few studies have investigated the concrete breakout capacity of anchor groups with multiple anchor rows, even though the use of the design code to predict their capacity still requires assumptions about the ultimate failure mode and the effects of reinforcement. Recent studies attempt to close the gap in the design code, such as those of Grosser (2012) and Sharma et al. (2016), where assumptions about how many rows of anchors can be used when calculating steel anchor shear capacity, and how varying amounts of reinforcement affects concrete breakout capacity, respectively, are investigated.

Often in research, as was done by Grosser (2012) and Sharma et al. (2016), the distance between the line of load application and the face of the embedded plate is minimized, and unique test setups are used to prevent the anchor group from rotating above the surface of the concrete to isolate the shear behaviour of the anchor group. In the current study, the eccentricity is included to study a more typical case found in industry. Although the test setups from this study and that of Sharma et al. (2016) differ, both show that even a small amount of reinforcement affects load bearing behaviour. Specifically, anchor rows too close to the edge could not reliably activate the stirrups and instead relied on the dowel action of the edge reinforcement. The anchor groups tested by Grosser (2012) showed that, with no reinforcement, only the back row of anchors should be used when predicting steel anchor shear capacity of an anchor group close to an edge. However, as shown in this study, even a small amount of reinforcement can significantly affect the load bearing behaviour of an anchor group.

4.3.5 Limitations of Findings

In this study, embedded plates were loaded in shear with a loading arm, connected using a shear tab. However, in many common applications, embedded plates are loaded with beams connected using a wide variety of steel connections, resulting in a wide range of degrees of fixity and moment transferred to the face of the embedded plate. For example, shear tabs are typically considered fairly rigid in their plane, transferring a significant amount of moment to the embedded plate, and beams when connected with multiple rows of bolts can also transfer a significant amount of moment. Furthermore, the shear tabs used in the full-scale tests were somewhat thicker and longer than what would typically be designed for these particular embedded plates to prevent premature failure, resulting in a stiffer embedded plate.

Since test conditions are not exactly 'Case D' as described in Section 3.2, test capacities cannot be directly compared to the design capacities found in the design tables. However, important assumptions such as the inclusion of moment in the design loads are validated.

4.3.6 Summary

This chapter presented a discussion of the behaviour of two embedded plates at varying distances from the edge of a concrete element, detailed as a lightly reinforced beam, loaded in shear towards the edge. An embedded plate with four anchors and one with six anchors were each tested at four different edge distances, resulting in a total of eight full-scale tests. The tests investigate the full embedded plate system as how it is typically used in the industry, including the connection, steel plate and anchors. Additionally, DIC was used to investigate possible causes of change in load-displacement behaviour. A test frame was constructed to load the embedded plates in eccentric shear towards the concrete edge. A load cell, LVDTs, cable transducers and cameras were used to investigate the behaviour of embedded plates loaded towards a free edge, including cracking load, peak load, failure mode, and crack widths.

The following is concluded from the research results:

1. Predicting capacities of embedded plates near an edge, loaded in shear towards the edge using Annex D in CSA A23.3:19, is very conservative. Mean test-to-predicted ratios are 1.39 for Assumption 1, and 1.74 for Assumption 2.
2. Although the code design equations are conservative, since they are based on the 5% fractile resistance, the underlying mean equations upon which the code equations are based are effective in determining the capacity of the embedded plates. The moment caused by the application of load away from the face of the embedded plate—in this case the 75 mm distance between the bolt line of the shear tab and face of the embedded plate—can be significant, as seen by the out-of-plane rotation during testing, and should be considered when designing embedded plates. Using the mean design equations, when assuming shear is the only force acting on the embedded plate, test-to-predicted ratios were not conservative, at 0.92, and when assuming shear and moment act on the embedded plate, test-to-predicted ratios were conservative at 1.11.
3. More than just the back row of anchors in an anchor group may be used when determining steel anchor shear capacity of an anchor group loaded in shear towards the concrete edge

if there is sufficient reinforcement to prevent significant loss of stiffness at the front anchor rows after initial concrete breakout.

4.3.7 Recommendations for Future Research

Based on the results of this chapter, the following recommendations are given:

1. Different connections should be tested to determine how the fixities affect the transfer of moment to the embedded plate. In the full-scale tests, only a shear tab was used to connect the loading arm to the embedded plate. Since different connections may have different moment fixities, the amount of moment transferred to the anchors may differ.
2. The effect of reducing the thickness of the steel plate on the capacity of the assembly could be investigated to improve the economy of the proposed standard embedded plates. Currently, a rigid plate assumption is used to calculate the forces in the anchors due to the moment, consequently requiring a relatively thick steel plate. Different connections may also affect the required plate stiffness.
3. The effect of different reinforcement layouts should be further investigated to determine how it can affect the stiffness of the front row of anchors after the initial concrete breakout occurs, to determine more precisely when all anchors in an anchor group may be used when determining steel anchor shear capacity.

5 Summary and Recommendations

5.1 Summary

Embedded plates are commonly used to connect steel members to concrete. However, there continues to be disagreements among design standards and different assumptions are made by different designers. Moreover, a lack of widely available standard designs leads to inefficiencies in the design, fabrication, and installation process of embedded plates. As industry members involved with embedded plates are increasingly required to carry out projects faster and cheaper than ever, easily accessible—and easy to use—design guides are needed.

A literature review of embedded plate research, focused on studies related to welded headed anchors and steel plates used for embedded plates, and the design of embedded plates using Canadian design standards CSA A23.3:19, is presented in Chapter 2. Chapter 3 proposes a set of three standard embedded plate configurations, and their design tables are shown in Appendix A, calculated using CSA A23.3:19. Additionally, assumptions required to calculate the design capacities of the standard embedded plates are described. To support the calculated capacities and confirm select assumptions used in the design tables, two standard embedded plate configurations are tested, detailed in Chapter 4. Each standard embedded plate was placed at four different edge distances, and loaded in shear towards the concrete edge, resulting in a total of eight full-scale tests.

5.2 Conclusions

The following conclusions were drawn from this research:

1. From the literature review on the state of embedded plate design methods detailed in Chapter 2, gaps in the current literature and ambiguities in Annex D in A23.3 were identified. Currently, only limited attempts have been made to standardize embedded plate designs, with the attempts having very limited application, such as the standard tilt-up connectors found in the Concrete Design Handbook (CAC 2019), or being inaccessible as confidential in-house standards. Additionally, Annex D does not consider the effects of reinforcement on anchor capacity rigorously. The effects of reinforcement are only considered when concrete is cracked, and studies such as that of Sharma et al. (2016) show that reinforcement can significantly affect anchor capacity even with uncracked concrete.

In addition to the complexity of using Annex D to design anchors, there are ambiguities in its usage for anchor groups, leading to confusion for designers.

2. In Chapter 3, standard embedded plates with four, six and eight anchors (welded headed studs) are proposed, along with their design tables in Appendix A, for shear and tension loading. In the design tables, four placement cases are provided for embedded plates loaded in shear (A: In the Field, B: Top of Wall, C: Column/ End of Wall, and D: Beam), and three placement cases (A: In the Field, B: Top of Wall, and C: Column/ End of Wall) are provided for embedded plates loaded in tension. Notably, connection and lateral eccentricities are considered when calculating the design capacities of the standard embedded plates to account for the effects of a common shear tab connection loaded in shear, and for accidental misplacements during installation, respectively. Additionally, some ambiguities in using Annex D for anchor groups are discussed with guidance from the literature review in Chapter 2. For example, for embedded plates loaded in shear parallel to an edge close to an edge, such as in the Column/ End of Wall and Top of Wall cases, the study by Grosser et al. (2012) determined that the ultimate concrete breakout crack occurs at the column of anchors closest to the edge. Therefore, the shear concrete breakout capacities of the standard embedded plates are calculated assuming the ultimate concrete breakout crack occurs at the column of anchors closest to the edge.
3. From the experimental program, described in Chapter 4, design methods found in A23.3 for anchor groups, near a concrete edge, and loaded in shear towards the edge are conservative. Mean test-to-predicted ratios of 1.39 for Assumption 1 (shear only), and 1.74 for Assumption 2 (shear plus induced moment) were calculated. The high test-to-predicted ratios are due to the fact that the design methods in A23.3 are based on the resistance of the 5% fractile of test results, meaning there is a 95% probability that the actual strength of the anchor will exceed the predicted capacity. However, when the underlying mean equations, upon which the design equations in A23.3 are based, are compared with the test results, a mean test-to-predicted ratio of 1.11 was found for Assumption 2, suggesting the design methods in A23.3 are adequate.

The embedded plates used in the experimental tests were loaded in shear through the shear tab, resulting in the line of load application being 75 mm away from the exposed surface of the plate. The resulting moment caused by this connection eccentricity may be

significant, as seen by the test-to-predicted ratio of 0.92 when only shear is assumed to act on the anchors (Assumption 1), and of 1.11 when shear and moment are assumed to act on the anchors (Assumption 2). The unconservative estimate of capacity when assuming only shear is acting on the anchors, in addition to the out-of-plane rotation caused by the connection eccentricity of 0.01 rad to 0.02 rad at peak load, and further rotation of the embedded plate post-peak show that the moment caused by the connection eccentricity is significant and should be considered when designing embedded plates with shear tabs.

Additionally, in all the full-scale tests conducted, the embedded plates had ultimate capacities greater than the predicted failure load of just the back row of anchors at 200 kN. This suggests that more than just the back row of anchors may be considered when determining steel anchor shear capacity if there is sufficient reinforcement to prevent a significant loss of stiffness at the front anchors after their initial concrete breakout.

5.3 Recommendations for Future Research

This report focused on creating a small set of standard embedded plates along with design tables for shear and tension loading situations to make them easy to use and integrate into the current design process. To expand the use of standard embedded plate designs in more situations, more standard embedded plates with different anchor types (such as post-installed) and anchor configurations), along with their design tables covering more design conditions, could be added. For example, design tables could be added to provide plate capacities under torsion, combined shear and tension loading, and seismic loading.

Additionally, based on the experimental results of Chapter 4, there are several recommendations for future research:

1. In the experimental program, the embedded plates were loaded with a loading arm attached to the shear tab welded onto the exposed surface of the steel plate. However, in typical use, embedded plates are loaded in a variety of different ways, with one of the most common being with a beam bolted to some steel connection and welded to the embedded plate. The use of a loading arm may restrain the rotation of the embedded plate, affecting its behaviour, so tests using a more conventional transfer of load through a beam are recommended. Additionally, different connections may have different moment fixities, resulting in differing amount of moment transferred. Thus, different connections and

loading systems could be used to determine how the fixities of the connection affect the transfer of moment to the embedded plate.

2. In this report, a rigid plate assumption is used to distribute the moment from shear load due to the connection eccentricity to the anchors, resulting in a need for a thick and stiff steel plate. Different connections may also affect the plate stiffness, changing the load distribution to the anchors. A finite element model could be created to investigate the load distribution to the anchors to verify and improve the accuracy of current design methods.
3. Only one reinforcement layout was chosen for each embedded plate configuration tested. The effects of different reinforcement layouts on embedded plate behaviour should be further investigated to more accurately describe their effects on the assembly capacity and the stiffness of the front row of anchors after initial concrete breakout of the front row of anchors (so that the number of anchors that may be considered for steel anchor capacity of an anchor group may be determined more accurately).

References

ACI. (2014). *ACI 318-14: Building Code Requirements for Structural Concrete and Commentary.* American Concrete Institute, Farmington Hills, MI.

Anderson, N.S., Meinheit, D.F. (2000). "Design Criteria for Headed Stud Groups in Shear: Part 1 – Steel Capacity and Back Edge Effects." *PCI Journal*, 5, 46-75.

Anderson, N.S., Meinheit, D.F. (2000). "Pryout Capacity of Cast-In Headed Stud Anchors." *PCI Journal*, 2, 90-112.

ASTM. (2018) *C39-18: Standard Test Method for Compressive Strength of Cylindrical Specimens. ASTM International*, West Conshohocken, PA.

ASTM. (2018) C78-18: *Standard Test Method for Flexural Strength of Concrete (Using Simple Beam with Third-Point Loading)*, West Conshohocken, PA.

ASTM. (2019) *A370-19: Standard Test Methods and Definitions for Mechanical Testing of Steel Products. ASTM international*, West Conshohocken, PA.

Bode, H., Roik, K. (1987). "Headed Studs – Embedded in Concrete and Loaded in Tension." *American Concrete Institute SP 103-4*, American Concrete Institute, Farmington Hills, MI, 61-88.

CAC. (2014). *Concrete Design Handbook – 4th Edition*. Ottawa, ON.

Cannon, R.W., Godfrey, D.A., Moreadith, F.L. (1981). "Guide to the Design of Anchor Bolts and Other Steel Embedments." *Concrete International*, 3 (7), 28-41.

CISC. (2016). *Handbook of Steel Construction, 11th Edition*. Markham, ON.

Cook, R.A., Kingner, R.E. (1989). "Behavior and Design of Ductile Multiple-Anchor Steel-to-Concrete Connections." *Research Report No. 1126-3*, Texas Stat Department of Highways and Public Transportation, Austin, TX.

CPCI. (2017). *CPCI Design Manual, 5th Edition*. Canadian Precast/Prestressed Concrete Institute, Ottawa, ON.

CSA. (2019). *A23.3:19 Design of Concrete Structures*. Canadian Standards Association, Mississauga, ON.

CSA. (2019). *S16:19 Design of Steel Structures*. Canadian Standards Association, Mississauga, ON.

Eligehausen, R. (2017) "Fastening in Concrete Construction Past, Present and Future." *In Proc., 3rd International Symposium on Connections between Steel and Concrete*, Stuttgart, Germany, 1311-1336.

Eligehausen, R., Fuchs, W., Ick, U., Mallée, R., Reuter, M., Schimmelpfennig, K., Schmal, B. (1992). "Tragverhalten von Kopfbolzenverankerungen bei zentrischer Zugbeanspruchung" (Behaviour of headed anchors under concentrical tension). (in German). *Bauingenieur* 67, 183-196.

Eligehausen, R., Mallée, R., Silva, J.F. (2006). *Anchorage in Concrete Construction, First Edition*. Ernst & Sohn, Berlin, Germany.

Eriksson, D., Gasch, T. (2011). "Load capacity of anchorage to concrete at nuclear facilities." M.S. Thesis, Stockholm, Sweden.

Fuchs, W., Eligehausen, R., Breen, J.E. (1995). "Concrete Capacity Design (CCD) Approach for Fastening to Concrete." *ACI Structural Journal*, 92 (1), 73-94.

Fuchs, W., Eligehausen, R. (1986). "Tragverhalten und Bemessung von Befestigungen ohne Randeinfluß unter Querzugbelastung (Load-bearing behaviour and design of fixings without edge influence under shear loading). Report No. 10/8-86/12, University of Stuttgart. (Not published)

Furche, J., Eligehausen, R. (1991). "Lateral Blow-Out Failure of Headed Studs Near a Free Edge." *Anchors in Concrete-Design and Behavior, American Concrete Institute SP-130-10.* Farmington Hills, MI: American Concrete Institute, 235-252.

Goble, G.G. (1968). "Shear Strength of Thin Flange Composite Specimens." *AISC Engineering Journal*, 5 (2), 62-65.

Grosser, P.R. (2012). "Load-bearing behavior and design of anchorages subjected to shear and torsion loading in uncracked concrete." Ph.D. thesis, Stuttgart, Germany.

Jebara, L., Ozbolt, J., Hofmann, J. (2015). "Pryout failure capacity of single headed stud anchors." *Materials and Structures*, 49, 1775-1792.

Lee, N.H., Park, K.R., Suh, Y.P. (2010). "Shear Behavior of Headed Anchors with Large Diameters and Deep Embedments." *ACI Structural Journal*, 107 (2), 146-156.

Lemieux, K., Sexsmith, R., Weiler, G. (1998). "Behavior of Embedded Steel Connectors in Concrete Tilt-up Panels." *ACI Structural Journal*, 95 (4), 400-411.

Lin, Z., Liu, Y., Jun, H. (2014). "Behavior of stud connectors under combined shear and tension loads." *Engineering Structures*, 81, 362-376.

Lotze, D., Klingner, R.E., Graves, H.L. (2001). "Static Behavior of Anchors Under Combinations of Tension and Shear Loading." *ACI Structural Journal*, 98 (4), 525-536.

Mallée, R., Burkhardt, F. (1999) Befestigungen von Ankerplatten mit Dübeln (Fixings of steel plates with anchors). (in German). *Beton- und Stahlbetonbau* 94, 502-511.

Nilforoush, R. (2017). "Anchorage in Concrete Structures: Numerical and Experimental Evaluations of Load-Carrying Capacity of Cast-in-Place Headed Anchors and Post-Installed Adhesive Anchors." Ph. D. thesis, Lulea, Sweden.

Nilforoush, R., Nilsson, M., Elfgren, L. (2018). "Experimental Evaluation of Influence of Member Thickness, Anchor-Head Size, and Orthogonal Surface Reinforcement on the Tensile Capacity of Headed Anchors in Uncracked Concrete." *Journal of Structural Engineering*, 144 (4), 04018012

Nilsson, M., Ohlsson, U., Elfgren, L. (2011). "Effects of Surface Reinforcement on Bearing Capacity of Concrete with Anchor Bolts." *Nordic Concrete Research*, 44, 161-174.

Ollgarrd, J.G., Slutter, R.G. (1971). "Shear Strength of Stud Connectors in Lightweight and Normal-Weight Concrete." *AISC Engineering Journal*, 8 (2), 55-64.

Ozbolt, J., Eligehausen, R., Reinhardt, H.W. (1998). "Size effect on the concrete cone pull-out load." *International Journal of Fracture*, 95, 391-404.

Saari, W.K., Hajjar, J.F., Schultz, A.E., Shield, C.K. (2004). "Behavior of shear studs in steel frames with reinforced concrete infill walls." *Journal of Constructional Steel Research*, 60, 1453-1480.

Shaikh, A.F., Yi, W. (1985). "In-Place Strength of Welded Headed Studs." *PCI Journal*, 2, 56-81.

Sharma, A., Eligehausen, R., Asmus, J. (2016). "Experimental investigation of concrete edge failure of multiple-row anchorages with supplementary reinforcement." *Structural Concrete*, 18, 153-163.

Sharma, A., Eligehausen, R., Asmus, J. (2017). "A new model for concrete edge failure of multiple row anchorages with supplementary reinforcement – Reinforcement failure." *Structural Concrete*, 18, 893-901.

Appendix A – Design Tables for the Proposed Standard Embedded Plates

Standard Embedded Plate
Shear Capacity Table (kN)
4 Anchors (SEP 4)

Cracked Concrete
No Reinforcement
f_c'=30 MPa

Case A: In the Field

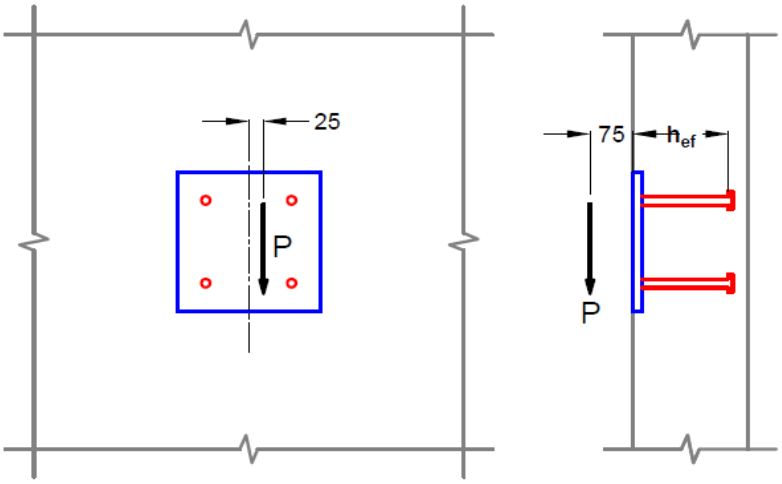

h_{ef} (mm)	n_{stud}	
100	4	86.4
150	4	127.3
200	4	142.0

Standard Embedded Plate | **Cracked Concrete**
Shear Capacity Table (kN) | **No Reinforcement**
4 Anchors (SEP 4) | **f_c'=30 MPa**

Case B: Top of Wall

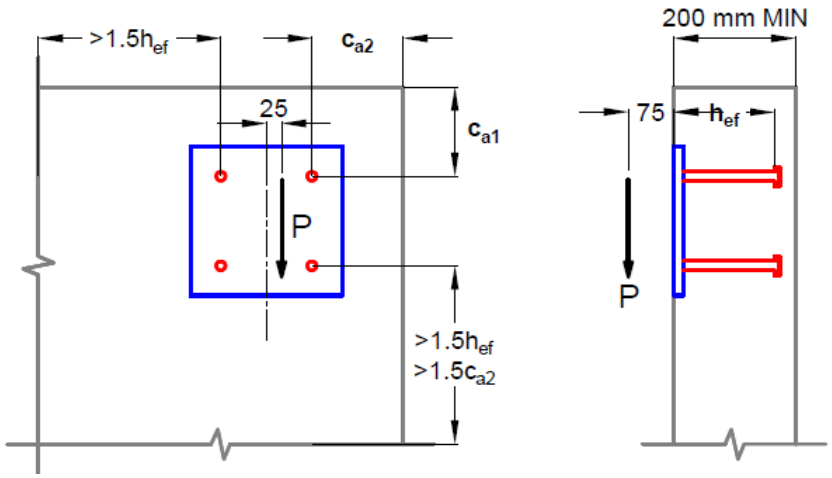

		c_{a1} (mm)							
c_{a2} (mm)	h_{ef} (mm)	50	100	150	200	250	300	350	400
50	100	22.4	25.2	26.0	26.0	26.0	26.0	26.0	26.0
	150	24.2	27.2	27.8	28.3	28.4	28.4	28.4	28.4
	200	24.1	27.5	28.4	28.7	28.9	29.1	29.1	29.1
100	100	34.8	42.9	49.2	49.2	49.2	49.2	49.2	49.2
	150	38.0	46.5	52.7	54.5	55.2	55.2	55.2	55.2
	200	37.7	47.0	54.8	56.0	57.1	57.9	57.9	57.9
150	100	42.1	54.7	64.8	68.7	70.6	70.6	70.6	70.6
	150	43.4	59.4	68.5	75.8	79.5	79.5	79.5	79.5
	200	42.7	59.9	70.9	78.0	82.6	84.4	84.4	84.4
200	100	42.1	59.4	70.6	74.0	77.2	80.2	80.2	80.2
	150	47.6	67.4	77.2	86.8	93.0	97.5	97.5	97.5
	200	46.3	67.7	79.8	88.5	95.9	103.2	103.2	103.2
250	100	42.1	62.7	75.7	78.7	81.5	84.1	86.4	86.4
	150	49.6	73.3	84.5	94.8	102.1	106.5	110.7	112.7
	200	49.8	74.4	88.6	97.8	106.9	114.5	119.6	122.1
300	100	42.1	62.7	80.2	82.9	85.3	86.4	86.4	86.4
	150	49.6	73.3	90.1	101.2	108.7	112.7	116.5	120.2
	200	53.4	79.7	97.2	107.0	116.5	123	127.9	132.6
350	100	42.1	62.7	84.1	86.4	86.4	86.4	86.4	86.4
	150	49.6	73.3	95.2	107.0	114.7	118.4	121.9	125.3
	200	53.4	79.7	103.5	113.8	123.8	130.3	134.9	139.3
400	100	42.1	62.7	86.4	86.4	86.4	86.4	86.4	86.4
	150	49.6	73.3	97.0	112.3	120.2	123.6	126.9	127.3
	200	53.4	79.7	108.9	120.1	130.7	137.1	141.5	142

Standard Embedded Plate | **Cracked Concrete**
Shear Capacity Table (kN) | **No Reinforcement**
4 Anchors (SEP 4) | **f_c'=30 MPa**

Case C: Column

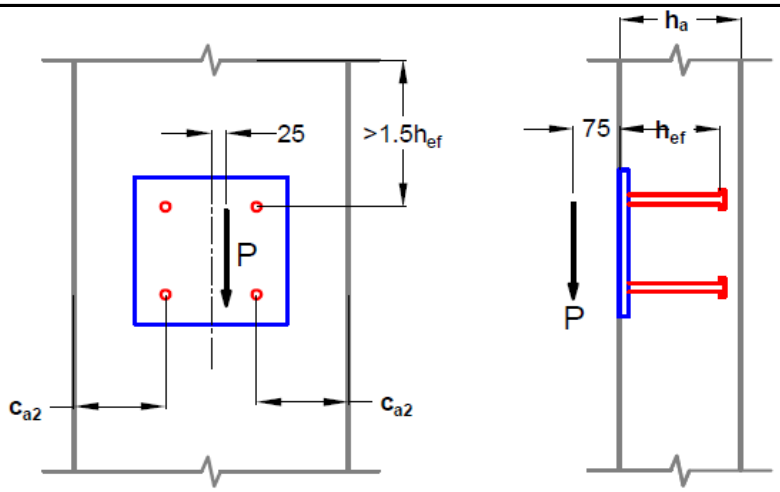

c_{a2} (mm)	h_{ef} (mm)	h_a (mm)				
		200	300	400	500	600
50	100	24.3	24.3	24.3	24.3	24.3
	150	26.2	26.2	26.2	26.2	26.2
	200	26.8	26.8	26.8	26.8	26.8
100	100	47.1	47.1	47.1	47.1	47.1
	150	50.8	50.8	50.8	50.8	50.8
	200	52.4	52.4	52.4	52.4	52.4
150	100	64.8	67.3	67.3	67.3	67.3
	150	75.5	78.3	78.3	78.3	78.3
	200	77.8	80.9	80.9	80.9	80.9
200	100	70.6	79.3	79.3	79.3	79.3
	150	89.4	102.1	102.1	102.1	102.1
	200	98.4	112.0	112.0	112.0	112.0
250	100	75.7	84.2	86.4	86.4	86.4
	150	99.8	114.2	122.1	122.1	122.1
	200	112.3	129.1	136.8	136.8	136.8
300	100	80.2	86.4	86.4	86.4	86.4
	150	106.5	120.9	127.3	127.3	127.3
	200	123.0	141.6	142.0	142.0	142.0
350	100	84.1	86.4	86.4	86.4	86.4
	150	112.7	127.0	127.3	127.3	127.3
	200	130.3	142.0	142.0	142.0	142.0
400	100	86.4	86.4	86.4	86.4	86.4
	150	118.4	127.3	127.3	127.3	127.3
	200	137.1	142.0	142.0	142.0	142.0

Standard Embedded Plate
Shear Capacity Table (kN)
4 Anchors (SEP 4)

Cracked Concrete
No Reinforcement
f_c'=30 MPa

Case D: Beam

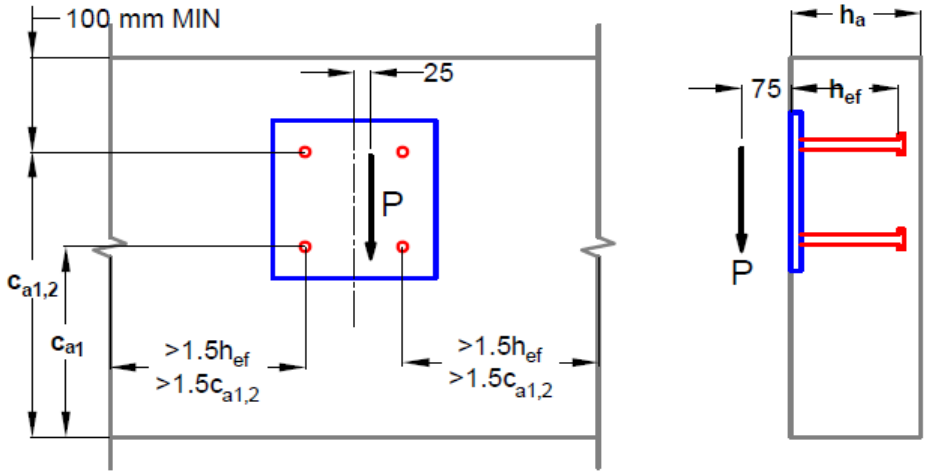

c_{a1} (mm)	h_{ef} (mm)	h_a (mm)				
		200	300	400	500	600
50	100	29.0	34.4	34.4	34.4	34.4
	150	31.0	37.0	37.0	37.0	37.0
	200	31.1	37.2	37.2	37.2	37.2
100	100	34.2	40.1	43.6	43.6	43.6
	150	37.2	44.2	48.3	48.3	48.3
	200	37.8	45.0	49.4	49.4	49.4
150	100	39.0	45.3	49.9	51.8	51.8
	150	42.8	50.4	56.1	58.6	58.6
	200	44.4	52.8	59.4	62.3	62.3
200	100	43.3	49.8	54.5	58.1	58.9
	150	48.0	56.0	62.0	66.8	67.8
	200	50.1	59.3	66.4	72.1	73.4
250	100	47.3	53.8	58.5	62.0	64.8
	150	52.8	61.2	67.3	72.0	75.9
	200	55.6	65.4	72.8	78.7	83.7
300	100	50.8	57.4	62.0	65.4	66.7
	150	57.3	65.8	72.0	76.7	80.5
	200	60.8	71.0	78.6	84.7	89.7
350	100	54.0	60.6	65.0	66.7	66.7
	150	61.4	70.0	76.1	80.8	84.4
	200	65.7	76.2	84.0	90.1	95.1
400	100	57.0	63.3	66.7	66.7	66.7
	150	65.2	73.9	79.9	84.4	85.8
	200	70.3	81.1	88.9	95.0	99.9

Standard Embedded Plate
Shear Capacity Table (kN)
6 Anchors (SEP 6)

Cracked Concrete
No Reinforcement
f_c'=30 MPa

Case A: In the Field

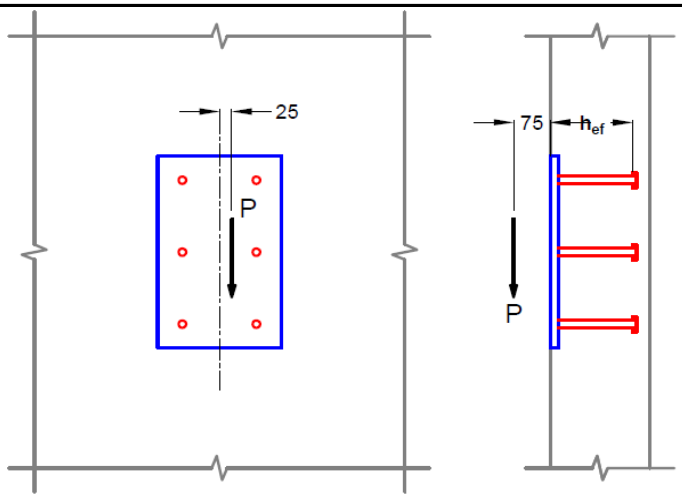

h_{ef} (mm)	n_{stud}	
100	6	135.2
150	6	199.0
200	6	238.9

Standard Embedded Plate
Shear Capacity Table (kN)
6 Anchors (SEP 6)

Cracked Concrete
No Reinforcement
f_c'=30 MPa

Case B: Top of Wall

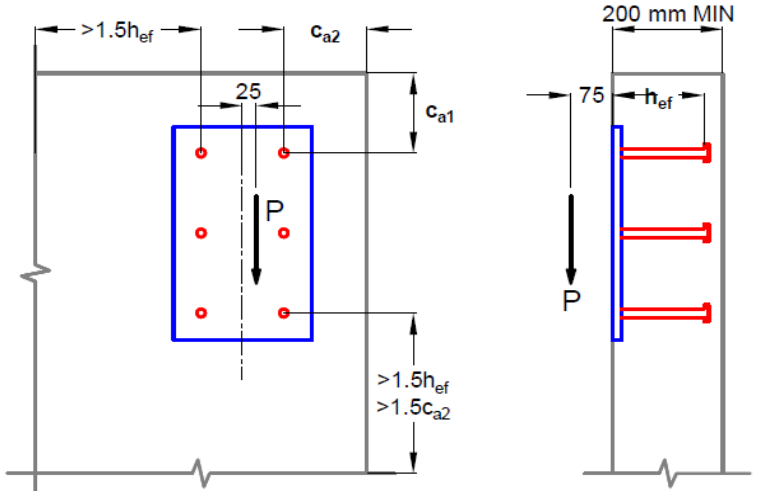

		ca1 (mm)							
ca2 (mm)	hef (mm)	50	100	150	200	250	300	350	400
50	100	39.2	42.0	42.7	42.7	42.7	42.7	42.7	42.7
	150	42.1	44.9	45.5	45.9	46.1	46.1	46.1	46.1
	200	43.1	45.8	46.2	46.5	46.7	48.7	48.7	48.7
100	100	60.0	68.7	75.4	75.4	75.4	75.4	75.4	75.4
	150	65.2	73.3	80.2	81.6	82.2	82.2	82.2	82.2
	200	67.7	75.3	82.1	83.2	84.1	84.8	84.8	84.8
150	100	75.8	86.7	97.1	102.6	105.2	105.2	105.2	105.2
	150	77.8	92.5	102.3	110.4	114.4	114.4	114.4	114.4
	200	80.5	95.4	104.5	112.4	117.2	118.6	118.6	118.6
200	100	76.3	93.9	105.2	110.2	115.1	119.7	119.7	119.7
	150	85.2	103.0	113.3	123.5	130.7	136.7	136.7	136.7
	200	86.9	106.0	115.5	125	133.1	141.3	141.3	141.3
250	100	76.3	100.5	112.7	117.4	121.9	126.2	130.2	132.2
	150	88.9	112.2	123.1	133.7	142	148	153.8	156.6
	200	92.0	116.6	126.5	136.3	146	154.3	160.8	164
300	100	76.3	103.9	119.7	124.1	128.2	132.2	135.2	135.2
	150	88.9	117.1	131.3	142.5	150.9	156.6	162.2	167.5
	200	96.9	127.2	137.5	147.6	157.6	167.4	174.1	180.6
350	100	76.3	103.9	126.2	130.2	134.1	135.2	135.2	135.2
	150	88.9	117.1	139.1	150.9	159.4	164.9	170.1	175.3
	200	96.9	130.2	146.3	156.8	167.2	177.4	183.8	190.1
400	100	76.3	103.9	132.2	135.2	135.2	135.2	135.2	135.2
	150	88.9	117.1	146.3	158.8	167.5	172.7	177.8	182.6
	200	96.9	130.2	154.6	165.7	176.4	187	193.2	199.4

Standard Embedded Plate
Shear Capacity Table (kN)
6 Anchors (SEP 6)

Cracked Concrete
No Reinforcement
f_c'=30 MPa

Case C: Column

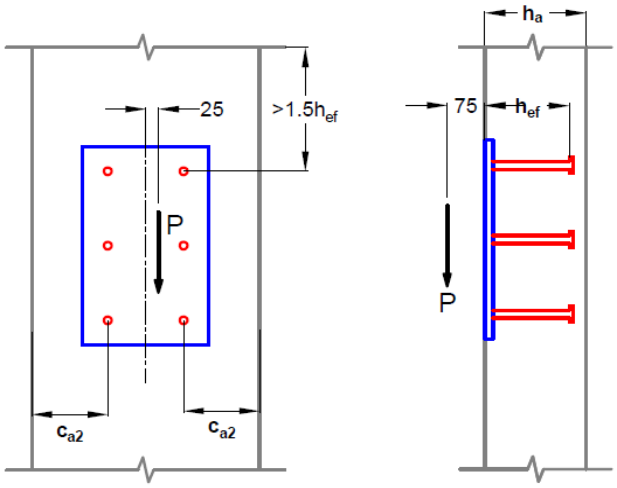

c_{a2} (mm)	h_{ef} (mm)	h_a (mm)				
		200	300	400	500	600
50	100	40.4	40.4	40.4	40.4	40.4
	150	42.9	42.9	42.9	42.9	42.9
	200	43.6	43.6	43.6	43.6	43.6
100	100	73.1	73.1	73.1	73.1	73.1
	150	77.2	77.2	77.2	77.2	77.2
	200	78.5	78.5	78.5	78.5	78.5
150	100	97.1	101.6	101.6	101.6	101.6
	150	110.3	115.1	115.1	115.1	115.1
	200	111.8	116.8	116.8	116.8	116.8
200	100	105.2	121.3	121.3	121.3	121.3
	150	126.5	147.5	147.5	147.5	147.5
	200	136.6	158.9	158.9	158.9	158.9
250	100	112.7	129.1	135.2	135.2	135.2
	150	138.9	162.4	176.0	176.0	176.0
	200	152.3	178.7	194.0	194.0	194.0
300	100	119.7	135.2	135.2	135.2	135.2
	150	148.0	172.1	190.0	197.4	197.4
	200	167.4	197.7	220.9	230.7	230.7
350	100	126.2	135.2	135.2	135.2	135.2
	150	156.6	181.3	199	199	199
	200	177.4	208.6	232.4	238.9	238.9
400	100	132.2	135.2	135.2	135.2	135.2
	150	164.9	189.9	199	199	199
	200	187	219.2	238.9	238.9	238.9

Standard Embedded Plate | **Cracked Concrete**
Shear Capacity Table (kN) | **No Reinforcement**
6 Anchors (SEP 6) | **f_c'=30 MPa**

Case D: Beam

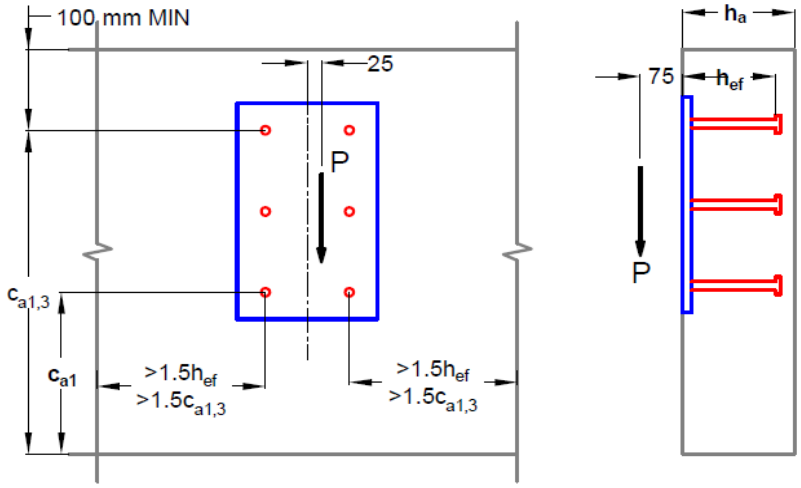

c_{a1} (mm)	h_{ef} (mm)	h_a (mm)				
		200	300	400	500	600
50	100	49.1	58.6	66.2	72.5	73.9
	150	52.3	62.7	71.1	78.1	79.7
	200	52.6	63.2	71.8	79.0	80.7
100	100	54.8	65.1	73.1	79.8	85.4
	150	58.8	70.4	79.6	87.3	93.9
	200	59.4	71.4	81.0	89.1	96.2
150	100	60.2	71.2	79.7	86.6	92.4
	150	64.9	77.3	87.2	95.3	102.3
	200	66.2	79.6	90.3	99.3	107.1
200	100	65.4	77.0	85.8	92.9	98.7
	150	70.7	84.0	94.4	102.9	110.1
	200	72.5	86.8	98.2	107.7	115.9
250	100	70.4	82.4	91.5	98.7	104.6
	150	76.4	90.4	101.2	110.0	117.3
	200	78.6	93.8	105.8	115.8	124.4
300	100	75.2	87.6	96.8	104.1	110.0
	150	81.9	96.5	107.6	116.6	124.1
	200	84.5	100.6	113.2	123.5	132.4
350	100	79.7	92.4	101.7	109.0	110.1
	150	87.2	102.3	113.8	122.9	130.4
	200	90.3	107.1	120.2	130.9	139.9
400	100	84.1	97.0	106.4	110.1	110.1
	150	92.4	107.9	119.5	128.7	135.5
	200	96.0	113.5	126.9	137.9	147.1

Standard Embedded Plate
Shear Capacity Table (kN)
8 Anchors (SEP 8)

Cracked Concrete
No Reinforcement
f_c'=30 MPa

Case A: In the Field

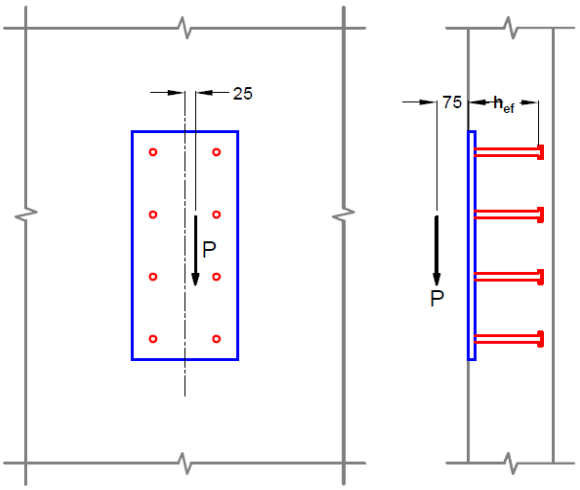

h_{ef} (mm)	n_{stud}	
100	8	178.4
150	8	253.3
200	8	332.2

Standard Embedded Plate
Shear Capacity Table (kN)
8 Anchors (SEP 8)

Cracked Concrete
No Reinforcement
f_c'=30 MPa

Case B: Top of Wall

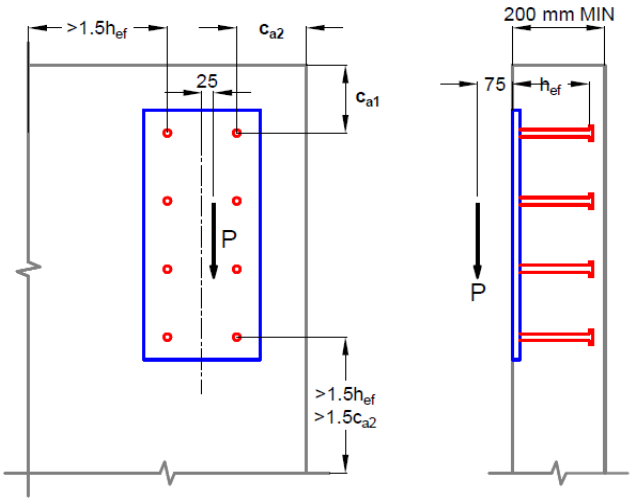

		c_{a1} (mm)							
c_{a2} (mm)	h_{ef} (mm)	50	100	150	200	250	300	350	400
50	100	55.7	58.5	59.2	59.2	59.2	59.2	59.2	59.2
	150	59.4	62.6	63.1	63.5	63.7	63.7	63.7	63.7
	200	59.8	63.2	64	67.1	67.1	67.1	67.1	67.1
100	100	83.7	92.8	99.7	99.7	99.7	99.7	99.7	99.7
	150	89.6	99	106.2	107.4	107.9	107.9	107.9	107.9
	200	90.3	100	108.3	109.3	110.1	110.8	110.8	110.8
150	100	104.2	115.5	126.3	132.4	135.4	135.4	135.4	135.4
	150	109.1	123.1	133.4	141.8	146	146	146	146
	200	109.3	124.4	135.7	144.1	148.9	150.2	150.2	150.2
200	100	109	123.9	135.4	141.2	146.8	152.3	152.3	152.3
	150	119.5	135	145.6	156.1	163.8	170.6	170.6	170.6
	200	118.4	136.1	147.9	157.7	166.3	174.8	174.8	174.8
250	100	109	131.8	144	149.6	154.9	160.1	165.1	167.6
	150	124.7	145.6	156.7	167.5	176.2	183	189.7	192.9
	200	127.5	147.8	160.1	170.1	180.1	188.8	196	199.6
300	100	109	139.2	152.3	157.5	162.6	167.6	172.3	176.9
	150	124.7	154.6	166.2	177.5	186.4	192.9	199.4	205.7
	200	136.6	159.5	172.2	182.6	192.7	202.8	210.2	217.5
350	100	109	141.8	160.1	165.1	170	174.6	178.4	178.4
	150	124.7	158.6	175.4	187.2	196.2	202.5	208.8	214.9
	200	136.6	168.8	182.4	193	203.5	213.8	221.1	228.2
400	100	109	141.8	167.6	172.3	176.9	178.4	178.4	178.4
	150	124.7	158.6	184.2	196.5	205.7	211.8	217.9	223.7
	200	136.6	172.2	192.2	203.2		224.6	231.7	238.7

Standard Embedded Plate
Shear Capacity Table (kN)
8 Anchors (SEP 8)

Cracked Concrete
No Reinforcement
f_c'=30 MPa

Case C: Column

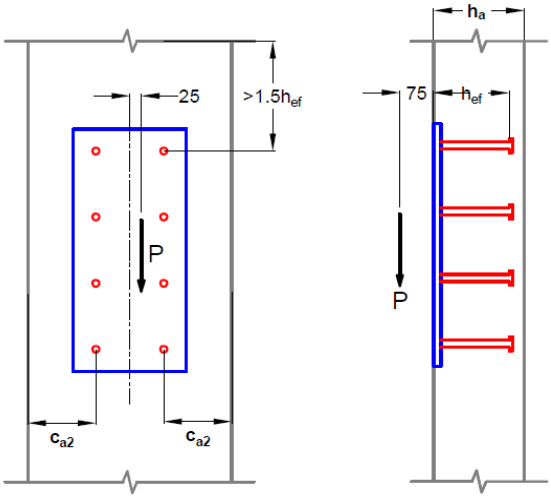

c_{a2} (mm)	h_{ef} (mm)	h_a (mm)				
		200	300	400	500	600
50	100	56.2	56.2	56.2	56.2	56.2
	150	59.5	59.5	59.5	59.5	59.5
	200	60.4	60.4	60.4	60.4	60.4
100	100	97	97	97	97	97
	150	102.1	102.1	102.1	102.1	102.1
	200	103.5	103.5	103.5	103.5	103.5
150	100	126.3	132.4	132.4	132.4	132.4
	150	141.6	148.2	148.2	148.2	148.2
	200	142.9	149.7	149.7	149.7	149.7
200	100	135.4	157.8	157.8	157.8	157.8
	150	159.2	187.4	187.4	187.4	187.4
	200	170.2	199.8	199.8	199.8	199.8
250	100	144	167	178.4	178.4	178.4
	150	172.8	203.9	222.3	222.3	222.3
	200	186.9	221.2	241.6	241.6	241.6
300	100	152.3	175.7	178.4	178.4	178.4
	150	183	215.2	239.7	250	250
	200	202.8	241.4	271.7	284.7	284.7
350	100	160.1	178.4	178.4	178.4	178.4
	150	192.9	226	251	253.3	253.3
	200	213.8	253.9	285.1	310.7	316.4
400	100	167.6	178.4	178.4	178.4	178.4
	150	202.5	236.4	253.3	253.3	253.3
	200	224.6	266	298.1	324.2	332.2

Standard Embedded Plate | **Cracked Concrete**

Shear Capacity Table (kN) | **No Reinforcement**

8 Anchors (SEP 8) | **f_c'=30 MPa**

Case D: Beam

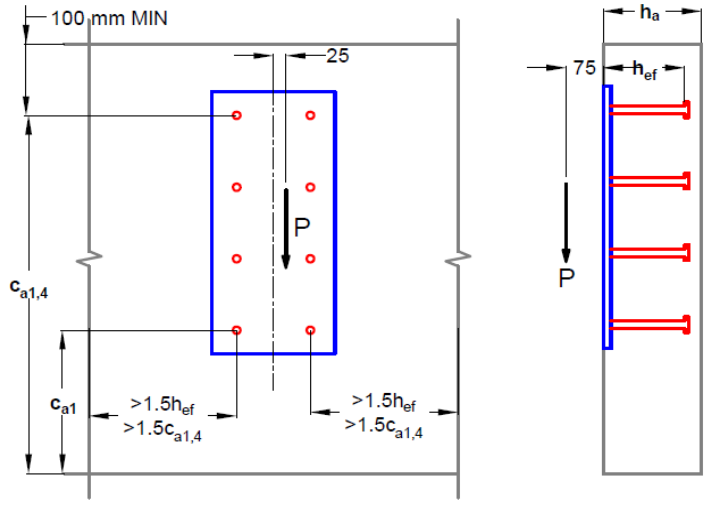

c_{a1} (mm)	h_{ef} (mm)	h_a (mm)				
		200	300	400	500	600
50	100	68.9	82.5	93.4	102.4	110.2
	150	73.6	88.7	100.8	111.1	120.1
	200	76.9	94.2	103.1	114.0	123.7
100	100	74.7	89.2	100.6	110.1	118.2
	150	80.0	96.1	109.1	120.0	129.4
	200	84.2	98.1	111.8	123.6	133.8
150	100	80.4	95.6	107.5	117.4	125.7
	150	86.3	103.4	117.1	128.5	138.3
	200	91.4	105.8	120.4	132.8	143.6
200	100	85.9	101.8	114.2	124.3	132.9
	150	92.4	110.5	124.8	136.7	146.9
	200	94.2	113.3	128.8	141.8	153.1
250	100	91.2	107.8	120.6	130.9	139.6
	150	98.5	117.4	132.3	144.6	155.1
	200	100.5	120.7	136.9	150.6	162.3
300	100	96.4	113.6	126.7	137.2	146
	150	104.4	124.1	139.5	152.2	162.9
	200	106.8	128.0	144.9	159.0	171.2
350	100	101.5	119.1	132.5	143.2	149
	150	110.1	130.6	146.5	159.4	170.4
	200	113.0	135.1	152.6	167.3	179.8
400	100	106.4	124.5	138.1	148.9	149
	150	115.8	136.9	153.2	166.4	177.6
	200	119.0	142.0	160.2	175.3	188.1

Standard Embedded Plate | **Cracked Concrete**

Tension Capacity Table (kN) | **No Reinforcement**

4 Anchors (SEP 4) | **f_c'=30 MPa**

Case A: In the Field

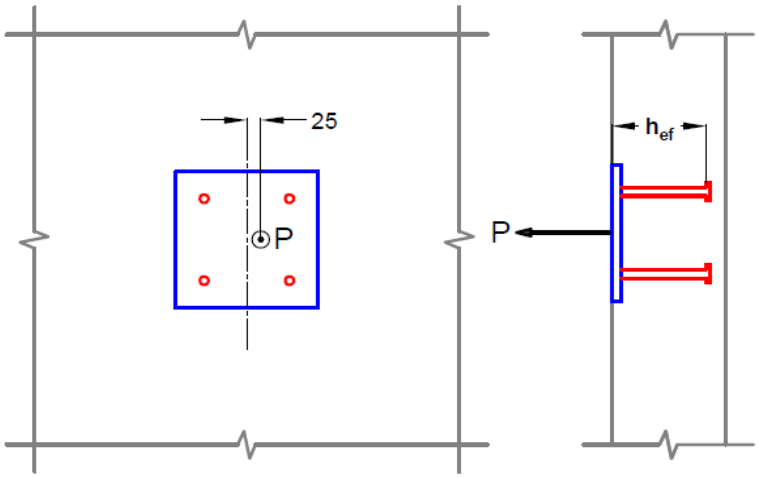

h_{ef} (mm)	n_{stud}	
100	4	68.7
150	4	104.6
200	4	145.2

Standard Embedded Plate | **Cracked Concrete**
Tension Capacity Table (kN) | **No Reinforcement**
4 Anchors (SEP 4) | **f_c'=30 MPa**

Case B: Concrete Corner

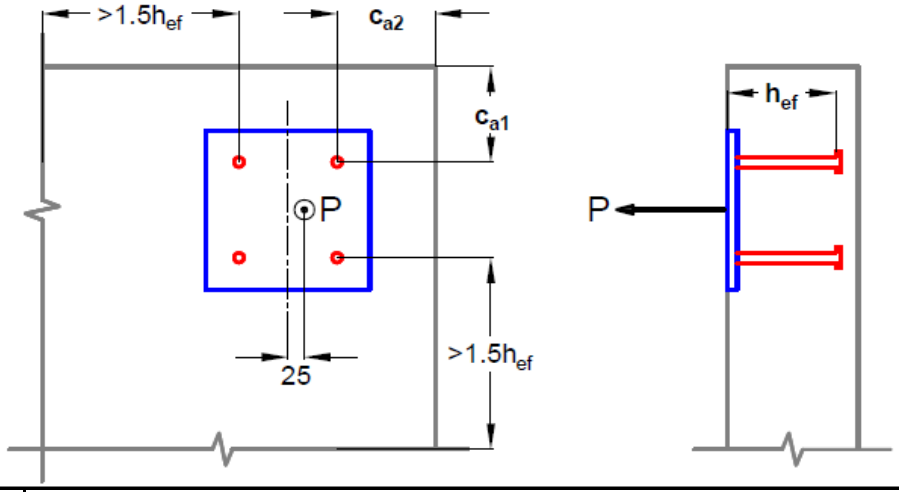

		c_{a2} (mm)							
c_{a1} (mm)	h_{ef} (mm)	50	100	150	200	250	300	350	400
50	100	33.2	38.0	42.7	42.7	42.7	42.7	42.7	42.7
	150	40.3	45.0	49.7	54.5	56.8	56.8	56.8	56.8
	200	48.4	53.3	58.1	62.9	67.8	72.6	72.6	72.6
100	100	38.0	48.8	54.9	54.9	54.9	54.9	54.9	54.9
	150	45.0	54.7	60.4	66.2	69.0	69.0	69.0	69.0
	200	53.3	62.5	68.2	73.8	79.5	85.2	85.2	85.2
150	100	42.7	54.9	68.7	68.7	68.7	68.7	68.7	68.7
	150	49.7	60.4	72.1	79.0	82.4	82.4	82.4	82.4
	200	58.1	68.2	79.0	85.6	92.2	98.8	98.8	98.8
200	100	42.7	54.9	68.7	68.7	68.7	68.7	68.7	68.7
	150	54.5	66.2	79.0	92.9	96.9	96.9	96.9	96.9
	200	62.9	73.8	85.6	98.2	105.7	113.3	113.3	113.3
250	100	42.7	54.9	68.7	68.7	68.7	68.7	68.7	68.7
	150	56.8	69.0	82.4	96.9	104.6	104.6	104.6	104.6
	200	67.8	79.5	92.2	105.7	120.2	128.8	128.8	128.8
300	100	42.7	54.9	68.7	68.7	68.7	68.7	68.7	68.7
	150	56.8	69.0	82.4	96.9	104.6	104.6	104.6	104.6
	200	72.6	85.2	98.8	113.3	128.8	145.2	145.2	145.2
350	100	42.7	54.9	68.7	68.7	68.7	68.7	68.7	68.7
	150	56.8	69.0	82.4	96.9	104.6	104.6	104.6	104.6
	200	72.6	85.2	98.8	113.3	128.8	145.2	145.2	145.2
400	100	42.7	54.9	68.7	68.7	68.7	68.7	68.7	68.7
	150	56.8	69.0	82.4	96.9	104.6	104.6	104.6	104.6
	200	72.6	85.2	98.8	113.3	128.8	145.2	145.2	145.2

Standard Embedded Plate
Tension Capacity Table (kN)
4 Anchors (SEP 4)

Cracked Concrete
No Reinforcement
f_c'=30 MPa

Case C: Column/ End of Wall

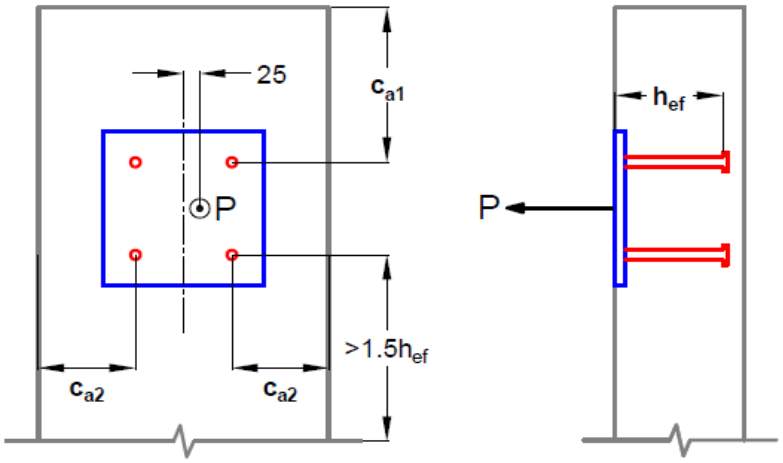

c_{a1} (mm)	h_{ef} (mm)	c_{a2} (mm)							
		50	100	150	200	250	300	350	400
50	100	26.0	34.6	42.7	42.7	42.7	42.7	42.7	42.7
	150	26.0	34.6	42.7	51.9	56.8	56.8	56.8	56.8
	200	26.0	34.6	42.7	51.9	61.9	72.6	72.6	72.6
100	100	28.8	47.5	54.9	54.9	54.9	54.9	54.9	54.9
	150	28.8	47.5	54.9	64.1	69.0	69.0	69.0	69.0
	200	28.8	47.5	54.9	64.1	74.2	85.2	85.2	85.2
150	100	30.5	48.1	68.7	68.7	68.7	68.7	68.7	68.7
	150	30.5	48.1	68.7	77.5	82.4	82.4	82.4	82.4
	200	30.5	48.1	68.7	77.5	87.6	98.8	98.8	98.8
200	100	30.5	48.1	68.7	68.7	68.7	68.7	68.7	68.7
	150	32.4	49.8	69.7	92.1	96.9	96.9	96.9	96.9
	200	32.4	49.8	69.7	92.1	102.1	113.3	113.3	113.3
250	100	30.5	48.1	68.7	68.7	68.7	68.7	68.7	68.7
	150	33.4	50.9	70.6	92.7	104.6	104.6	104.6	104.6
	200	34.4	52.0	71.7	93.6	117.7	128.8	128.8	128.8
300	100	30.5	48.1	68.7	68.7	68.7	68.7	68.7	68.7
	150	33.4	50.9	70.6	92.7	104.6	104.6	104.6	104.6
	200	36.3	54.2	74.1	95.9	119.6	145.2	145.2	145.2
350	100	30.5	48.1	68.7	68.7	68.7	68.7	68.7	68.7
	150	33.4	50.9	70.6	92.7	104.6	104.6	104.6	104.6
	200	36.3	54.2	74.1	95.9	119.6	145.2	145.2	145.2
400	100	30.5	48.1	68.7	68.7	68.7	68.7	68.7	68.7
	150	33.4	50.9	70.6	92.7	104.6	104.6	104.6	104.6
	200	36.3	54.2	74.1	95.9	119.6	145.2	145.2	145.2

Standard Embedded Plate | **Cracked Concrete**

Tension Capacity Table (kN) | **No Reinforcement**

6 Anchors (SEP 6) | **f_c'=30 MPa**

Case A: In the Field

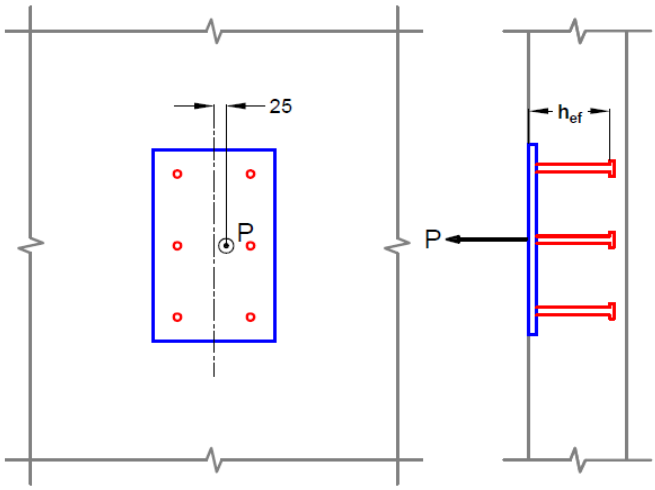

h_{ef} (mm)	n_{stud}	
100	6	91.5
150	6	130.8
200	6	174.3

Standard Embedded Plate | **Cracked Concrete**
Tension Capacity Table (kN) | **No Reinforcement**
6 Anchors (SEP 6) | **f_c'=30 MPa**

Case B: Concrete Corner

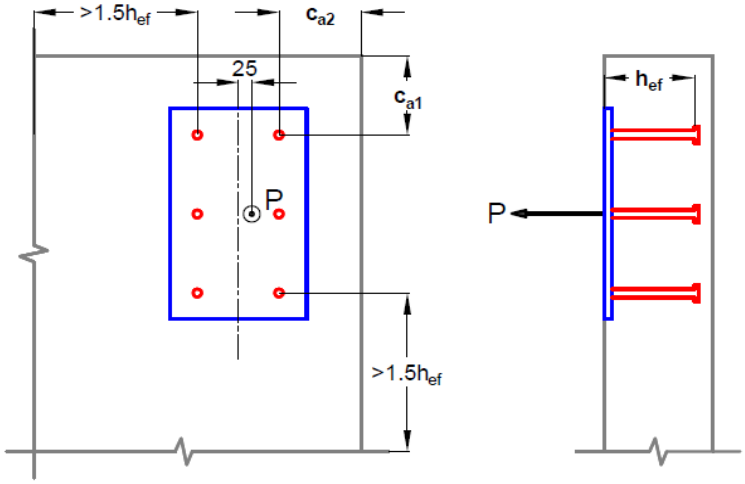

c_{a1} (mm)	h_{ef} (mm)	c_{a2} (mm)							
		50	100	150	200	250	300	350	400
50	100	47.5	54.3	61.0	61.0	61.0	61.0	61.0	61.0
	150	54.5	60.9	67.3	73.7	76.9	76.9	76.9	76.9
	200	62.9	69.2	75.5	81.8	88.1	94.4	94.4	94.4
100	100	52.2	67.1	75.5	75.5	75.5	75.5	75.5	75.5
	150	59.2	71.9	79.5	87.1	90.8	90.8	90.8	90.8
	200	67.8	79.5	86.8	94.0	101.2	108.4	108.4	108.4
150	100	57.0	73.2	91.5	91.5	91.5	91.5	91.5	91.5
	150	63.9	77.7	92.7	101.5	106.0	106.0	106.0	106.0
	200	72.6	85.2	98.8	107.0	115.2	123.5	123.5	123.5
200	100	57.0	73.2	91.5	91.5	91.5	91.5	91.5	91.5
	150	68.7	83.4	99.6	117.1	122.2	122.2	122.2	122.2
	200	77.5	90.9	105.3	120.8	130.1	139.4	139.4	139.4
250	100	57.0	73.2	91.5	91.5	91.5	91.5	91.5	91.5
	150	71.0	86.3	103.0	121.2	130.8	130.8	130.8	130.8
	200	82.3	96.6	111.9	128.4	145.9	156.4	156.4	156.4
300	100	57.0	73.2	91.5	91.5	91.5	91.5	91.5	91.5
	150	71.0	86.3	103.0	121.2	130.8	130.8	130.8	130.8
	200	87.1	102.2	118.5	135.9	154.5	174.3	174.3	174.3
350	100	57.0	73.2	91.5	91.5	91.5	91.5	91.5	91.5
	150	71.0	86.3	103.0	121.2	130.8	130.8	130.8	130.8
	200	87.1	102.2	118.5	135.9	154.5	174.3	174.3	174.3
400	100	57.0	73.2	91.5	91.5	91.5	91.5	91.5	91.5
	150	71.0	86.3	103.0	121.2	130.8	130.8	130.8	130.8
	200	87.1	102.2	118.5	135.9	154.5	174.3	174.3	174.3

Standard Embedded Plate
Tension Capacity Table (kN)
6 Anchors (SEP 6)

Cracked Concrete
No Reinforcement
f_c'=30 MPa

Case C: Column/ End of Wall

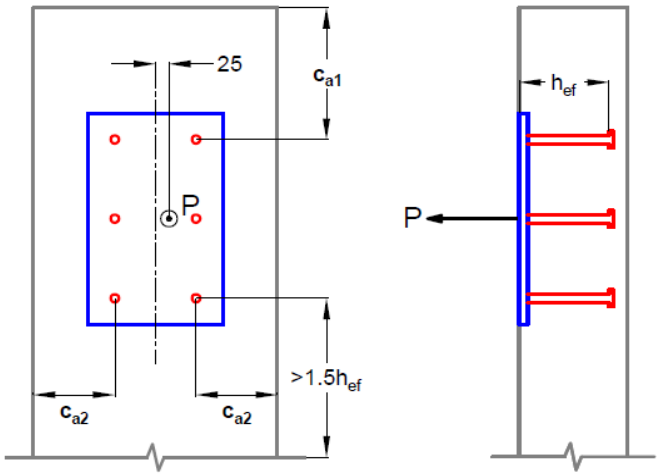

c_{a1} (mm)	h_{ef} (mm)	c_{a2} (mm)							
		50	100	150	200	250	300	350	400
50	100	40.1	51.9	61.0	61.0	61.0	61.0	61.0	61.0
	150	40.1	51.9	61.0	71.4	76.9	76.9	76.9	76.9
	200	40.1	51.9	61.0	71.4	82.6	94.4	94.4	94.4
100	100	41.2	67.8	75.5	75.5	75.5	75.5	75.5	75.5
	150	41.2	67.8	75.5	85.4	90.8	90.8	90.8	90.8
	200	41.2	67.8	75.5	85.4	96.5	108.4	108.4	108.4
150	100	40.7	64.1	91.5	91.5	91.5	91.5	91.5	91.5
	150	40.7	64.1	91.5	100.7	106.0	106.0	106.0	106.0
	200	40.7	64.1	91.5	100.7	111.5	123.5	123.5	123.5
200	100	40.7	64.1	91.5	91.5	91.5	91.5	91.5	91.5
	150	41.3	63.4	88.7	117.2	122.2	122.2	122.2	122.2
	200	41.3	63.4	88.7	117.2	127.6	139.4	139.4	139.4
250	100	40.7	64.1	91.5	91.5	91.5	91.5	91.5	91.5
	150	41.8	63.6	88.3	115.9	130.8	130.8	130.8	130.8
	200	42.3	64.0	88.2	115.2	144.8	156.4	156.4	156.4
300	100	40.7	64.1	91.5	91.5	91.5	91.5	91.5	91.5
	150	41.8	63.6	88.3	115.9	130.8	130.8	130.8	130.8
	200	43.6	65.1	88.9	115.0	143.5	174.3	174.3	174.3
350	100	40.7	64.1	91.5	91.5	91.5	91.5	91.5	91.5
	150	41.8	63.6	88.3	115.9	130.8	130.8	130.8	130.8
	200	43.6	65.1	88.9	115.0	143.5	174.3	174.3	174.3
400	100	40.7	64.1	91.5	91.5	91.5	91.5	91.5	91.5
	150	41.8	63.6	88.3	115.9	130.8	130.8	130.8	130.8
	200	43.6	65.1	88.9	115.0	143.5	174.3	174.3	174.3

Standard Embedded Plate
Tension Capacity Table (kN)
8 Anchors (SEP 8)

Cracked Concrete
No Reinforcement
f_c'=30 MPa

Case A: In the Field

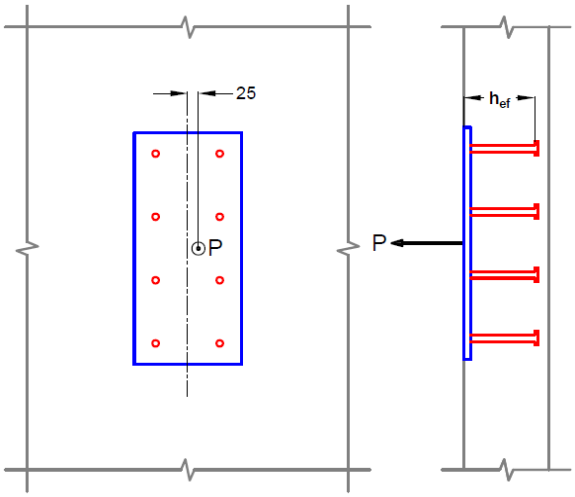

h_{ef} (mm)	n_{stud}	
100	8	114.4
150	8	157
200	8	203.3

Standard Embedded Plate
Tension Capacity Table (kN)
8 Anchors (SEP 8)

Cracked Concrete
No Reinforcement
f_c'=30 MPa

Case B: Concrete Corner

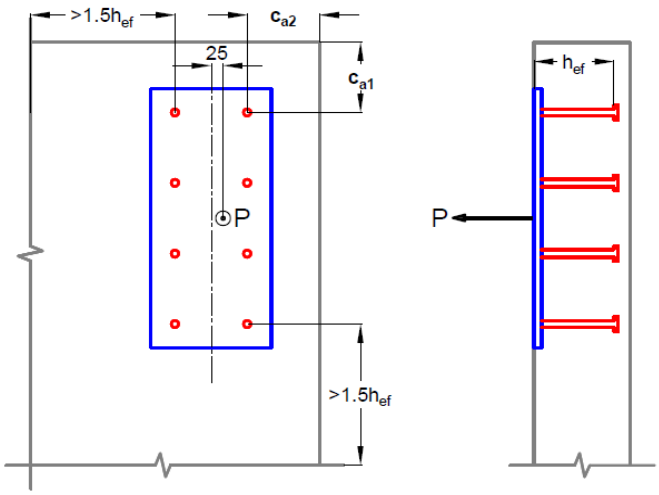

c_{a1} (mm)	h_{ef} (mm)	c_{a2} (mm)							
		50	100	150	200	250	300	350	400
50	100	61.7	70.5	79.3	79.3	79.3	79.3	79.3	79.3
	150	68.7	76.7	84.8	92.9	96.9	96.9	96.9	96.9
	200	77.5	85.2	93	100.7	108.4	116.2	116.2	116.2
100	100	66.5	85.4	96.1	96.1	96.1	96.1	96.1	96.1
	150	73.4	89.2	98.6	107.9	112.6	112.6	112.6	112.6
	200	82.3	96.6	105.3	114.1	122.9	131.7	131.7	131.7
150	100	71.2	91.5	114.4	114.4	114.4	114.4	114.4	114.4
	150	78.1	94.9	113.3	124.1	129.5	129.5	129.5	129.5
	200	87.1	102.2	118.5	128.4	138.3	148.1	148.1	148.1
200	100	71.2	91.5	114.4	114.4	114.4	114.4	114.4	114.4
	150	82.9	100.7	120.2	141.4	147.5	147.5	147.5	147.5
	200	92	107.9	125.1	143.5	154.5	165.6	165.6	165.6
250	100	71.2	91.5	114.4	114.4	114.4	114.4	114.4	114.4
	150	85.2	103.6	123.6	145.4	157	157	157	157
	200	96.8	113.6	131.7	151	171.7	184	184	184
300	100	71.2	91.5	114.4	114.4	114.4	114.4	114.4	114.4
	150	85.2	103.6	123.6	145.4	157	157	157	157
	200	101.7	119.3	138.3	158.6	180.3	203.3	203.3	203.3
350	100	71.2	91.5	114.4	114.4	114.4	114.4	114.4	114.4
	150	85.2	103.6	123.6	145.4	157	157	157	157
	200	101.7	119.3	138.3	158.6	180.3	203.3	203.3	203.3
400	100	71.2	91.5	114.4	114.4	114.4	114.4	114.4	114.4
	150	85.2	103.6	123.6	145.4	157	157	157	157
	200	101.7	119.3	138.3	158.6	180.3	203.3	203.3	203.3

Standard Embedded Plate
Tension Capacity Table (kN)
8 Anchors (SEP 8)

Cracked Concrete
No Reinforcement
f_c'=30 MPa

Case C: Column/ End of Wall

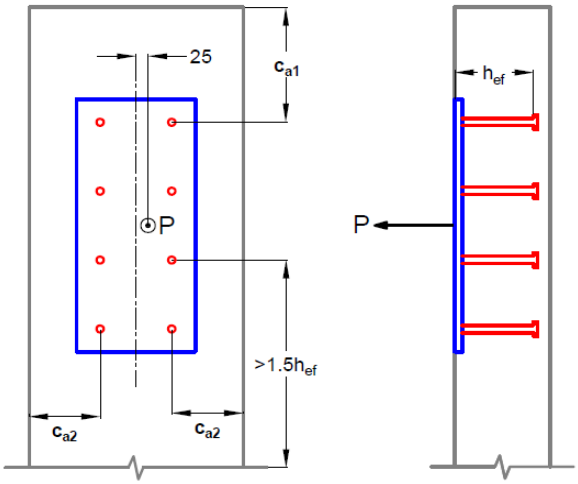

c_{a1} (mm)	h_{ef} (mm)	c_{a2} (mm)							
		50	100	150	200	250	300	350	400
50	100	54.3	69.2	79.3	79.3	79.3	79.3	79.3	79.3
	150	54.3	69.2	79.3	90.9	96.9	96.9	96.9	96.9
	200	54.3	69.2	79.3	90.9	103.2	116.2	116.2	116.2
100	100	53.5	88.2	96.1	96.1	96.1	96.1	96.1	96.1
	150	53.5	88.2	96.1	106.8	112.6	112.6	112.6	112.6
	200	53.5	88.2	96.1	106.8	118.8	131.7	131.7	131.7
150	100	50.9	80.1	114.4	114.4	114.4	114.4	114.4	114.4
	150	50.9	80.1	114.4	123.9	129.5	129.5	129.5	129.5
	200	50.9	80.1	114.4	123.9	135.4	148.1	148.1	148.1
200	100	50.9	80.1	114.4	114.4	114.4	114.4	114.4	114.4
	150	50.1	77	107.7	142.4	147.5	147.5	147.5	147.5
	200	50.1	77	107.7	142.4	153.2	165.6	165.6	165.6
250	100	50.9	80.1	114.4	114.4	114.4	114.4	114.4	114.4
	150	50.1	76.3	106	139.1	157	157	157	157
	200	50.3	75.9	104.8	136.8	172	184	184	184
300	100	50.9	80.1	114.4	114.4	114.4	114.4	114.4	114.4
	150	50.1	76.3	106	139.1	157	157	157	157
	200	50.8	75.9	103.7	134.2	167.4	203.3	203.3	203.3
350	100	50.9	80.1	114.4	114.4	114.4	114.4	114.4	114.4
	150	50.1	76.3	106	139.1	157	157	157	157
	200	50.8	75.9	103.7	134.2	167.4	203.3	203.3	203.3
400	100	50.9	80.1	114.4	114.4	114.4	114.4	114.4	114.4
	150	50.1	76.3	106	139.1	157	157	157	157
	200	50.8	75.9	103.7	134.2	167.4	203.3	203.3	203.3

Appendix B – DIC Test Results

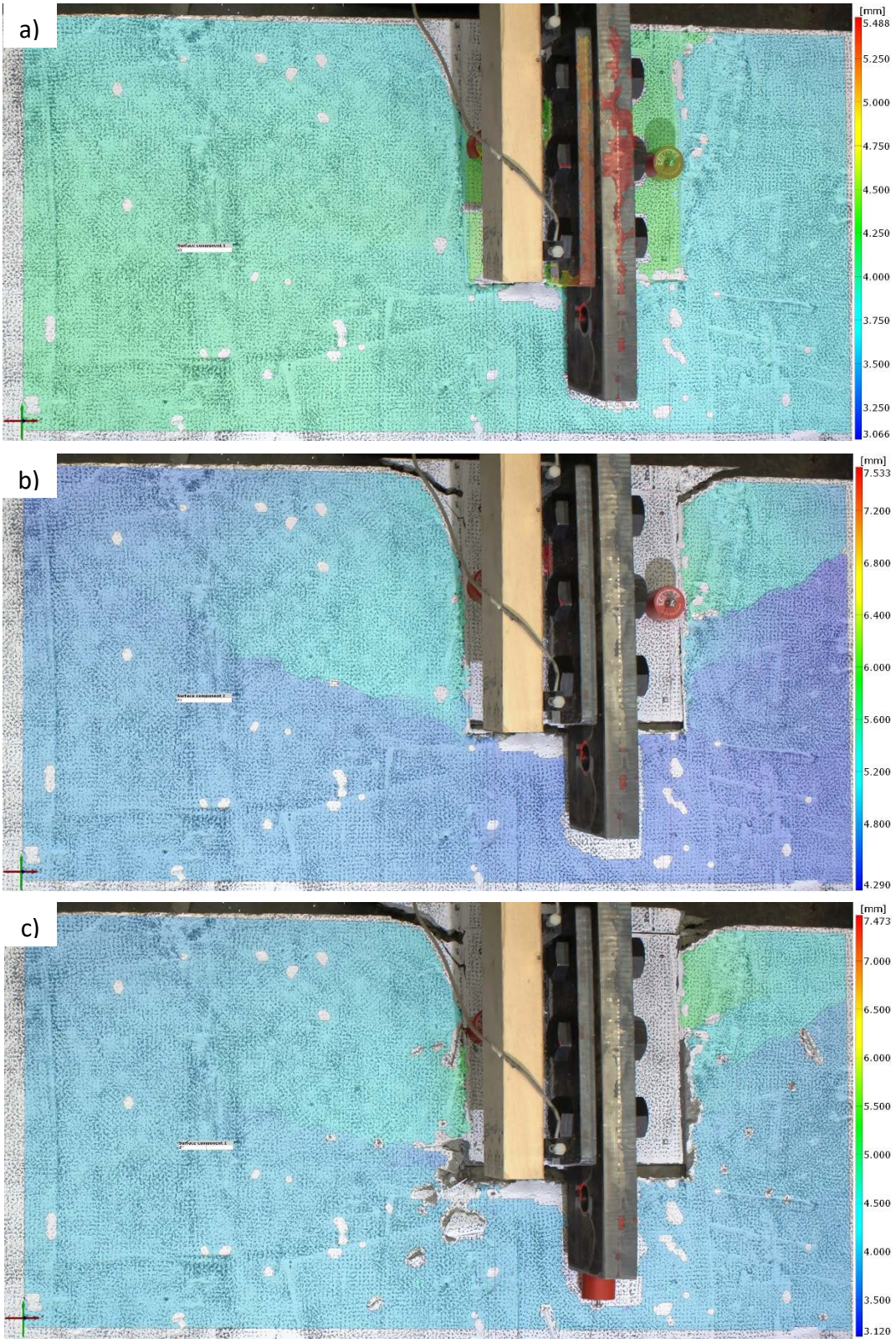

Figure B.1 DIC images of SEP4-150-75 at (a) initial cracking, (b) peak load, (c) after sudden failure (left of connection)

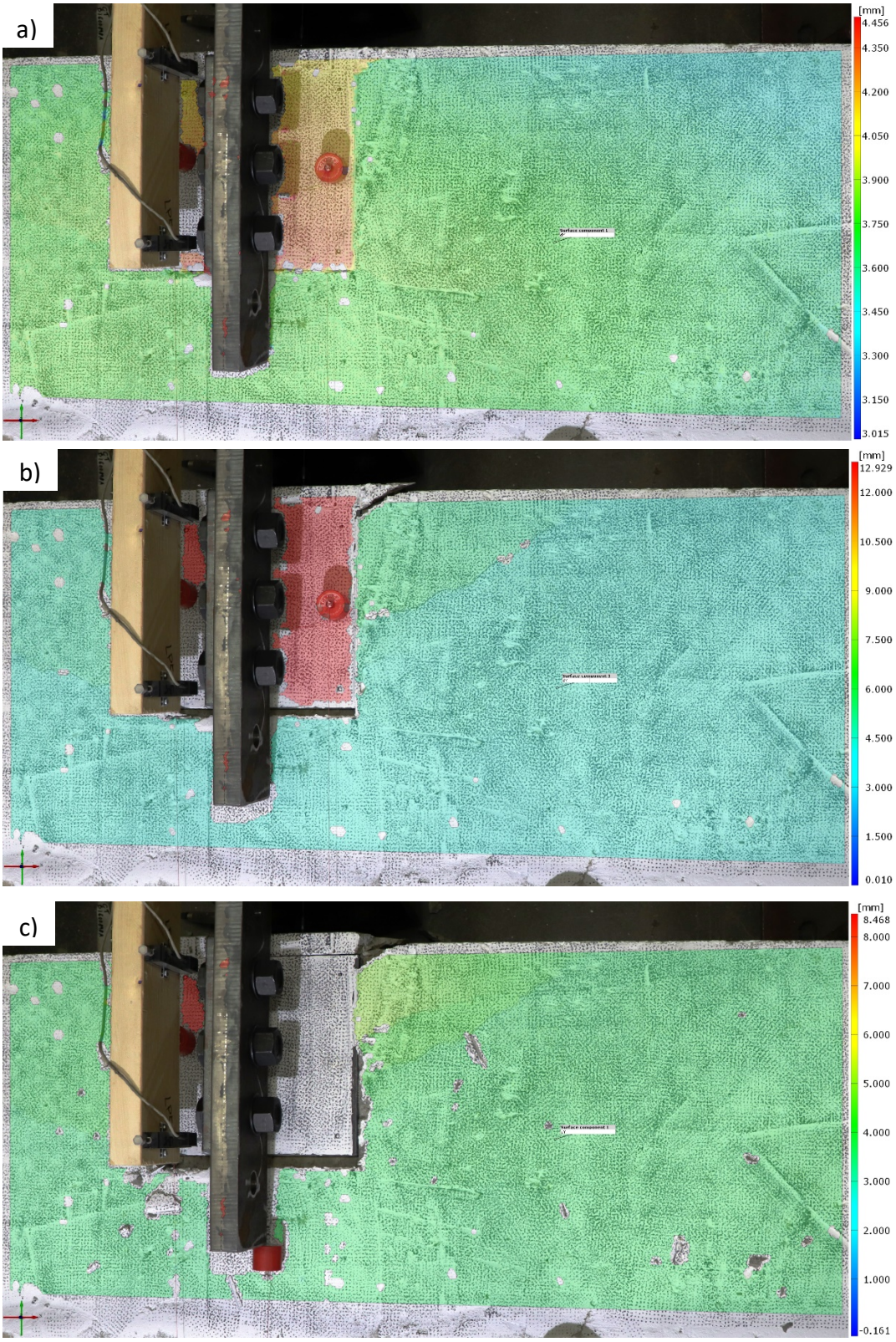

Figure B.2 DIC images of SEP4-150-75 at (a) initial cracking, (b) peak load, (c) after sudden failure (right of connection)

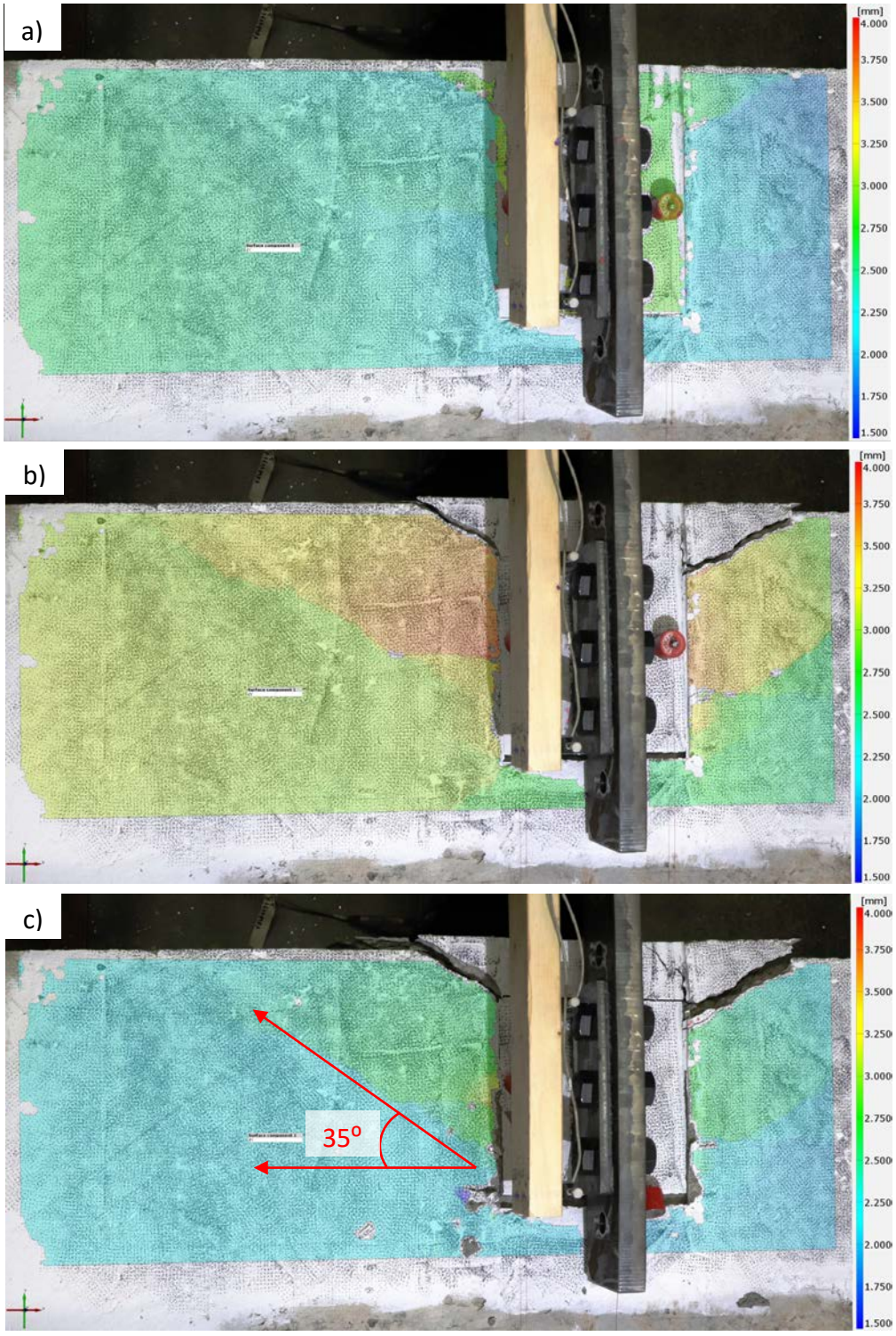

Figure B.3 DIC images of SEP4-150-125 at (a) initial cracking, (b) peak load, (c) net plate displacement of 15 mm (left of connection)

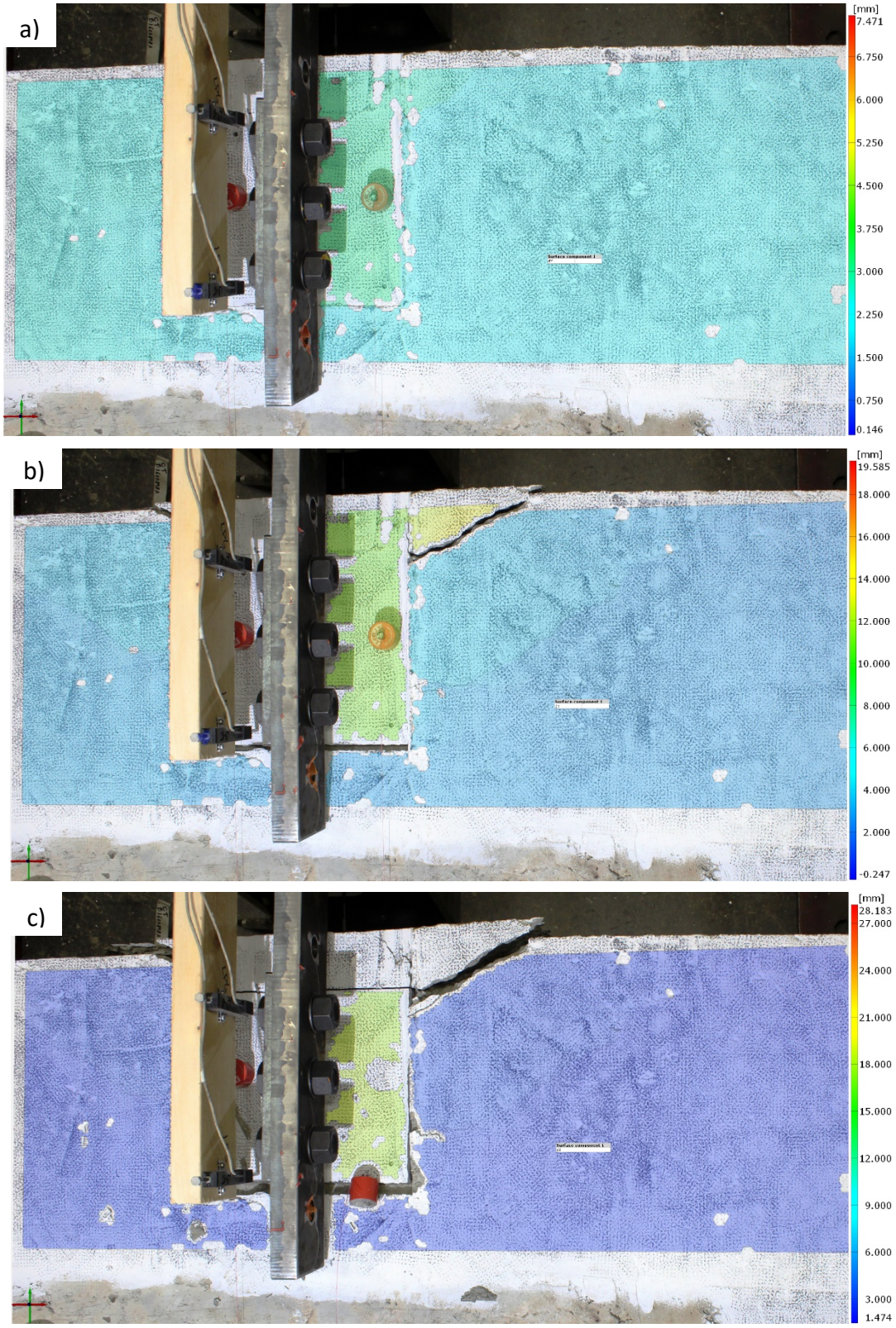

Figure B.4 DIC images of SEP4-150-125 at (a) initial cracking, (b) peak load, (c) net plate displacement of 15 mm (right of connection)

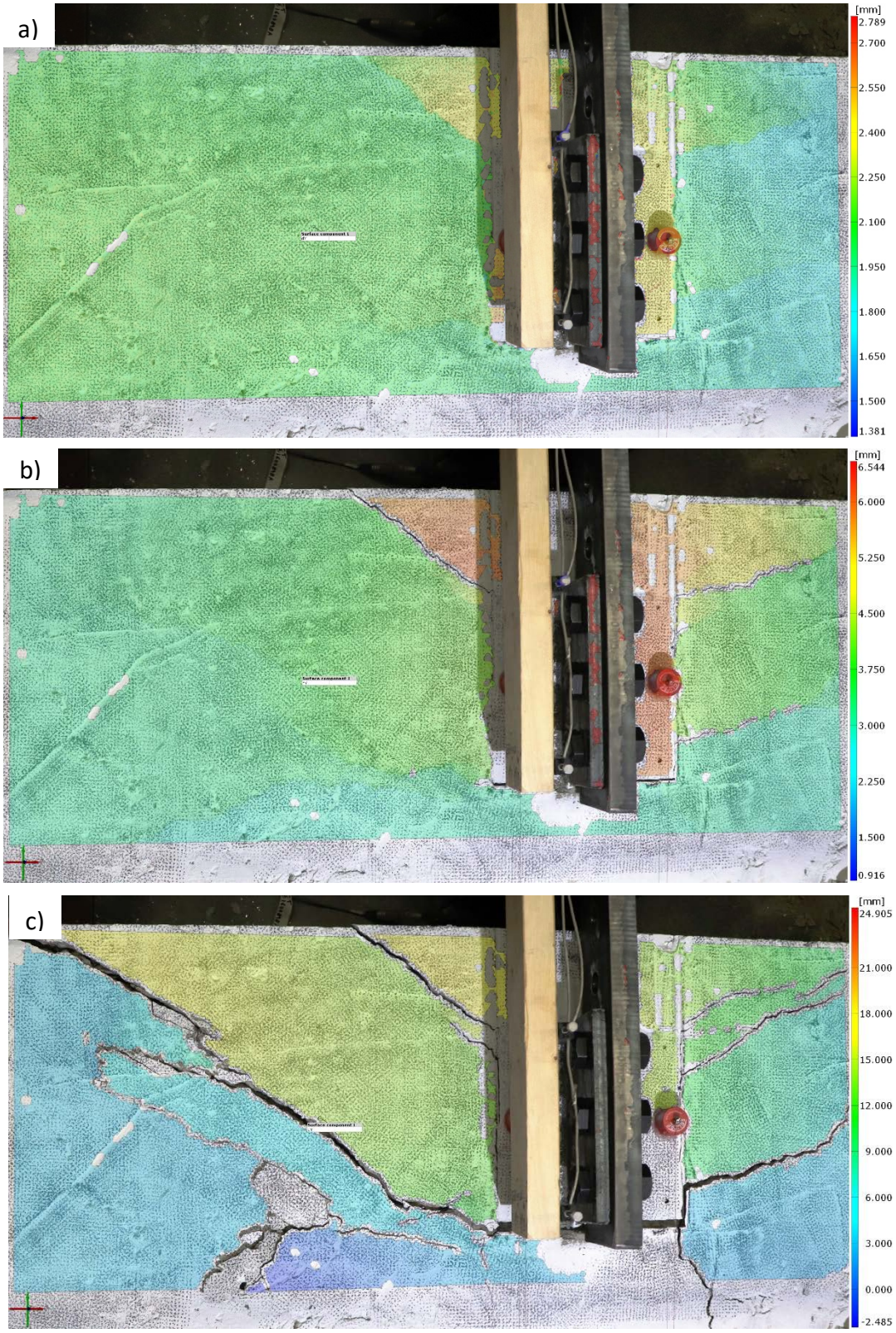

Figure B.5 DIC images of SEP4-150-175 at (a) initial cracking, (b) peak load, (c) net plate displacement of 15 mm (left of connection)

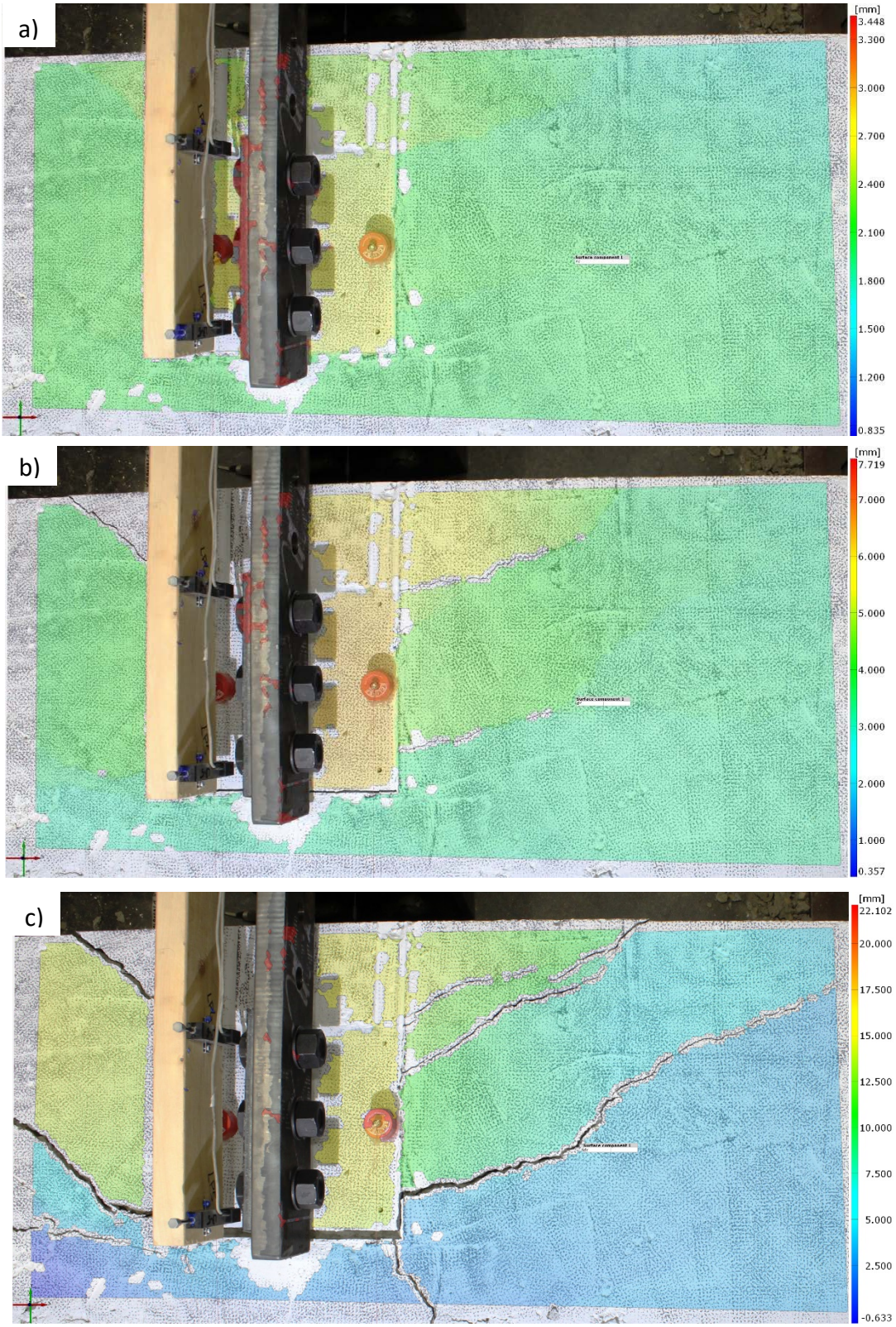

Figure B.6 DIC images of SEP4-150-175 at (a) initial cracking, (b) peak load, (c) net plate displacement of 15 mm (right of connection)

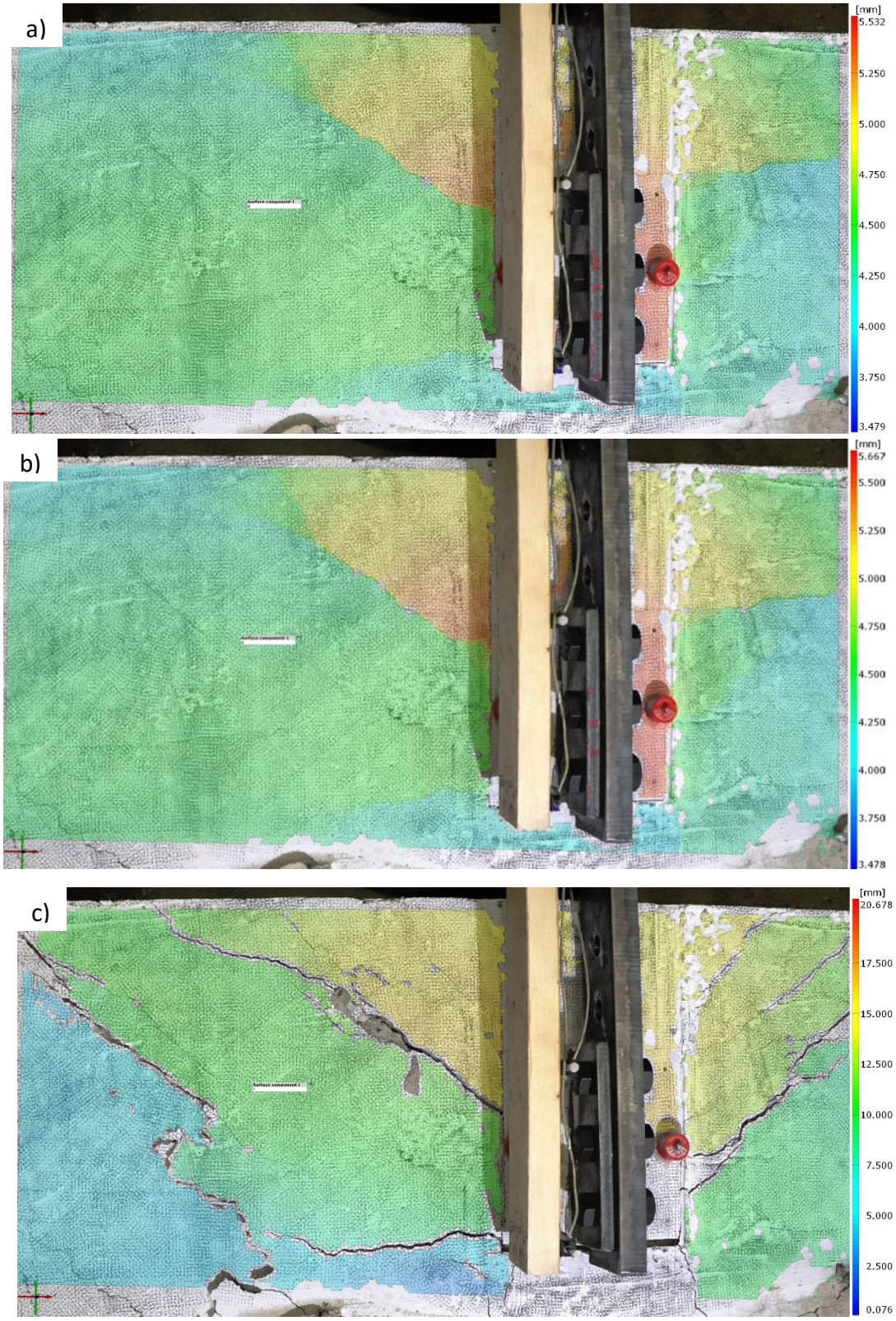

Figure B.7 DIC images of SEP4-150-250 at (a) initial cracking, (b) peak load, (c) net plate displacement of 15 mm (left of connection)

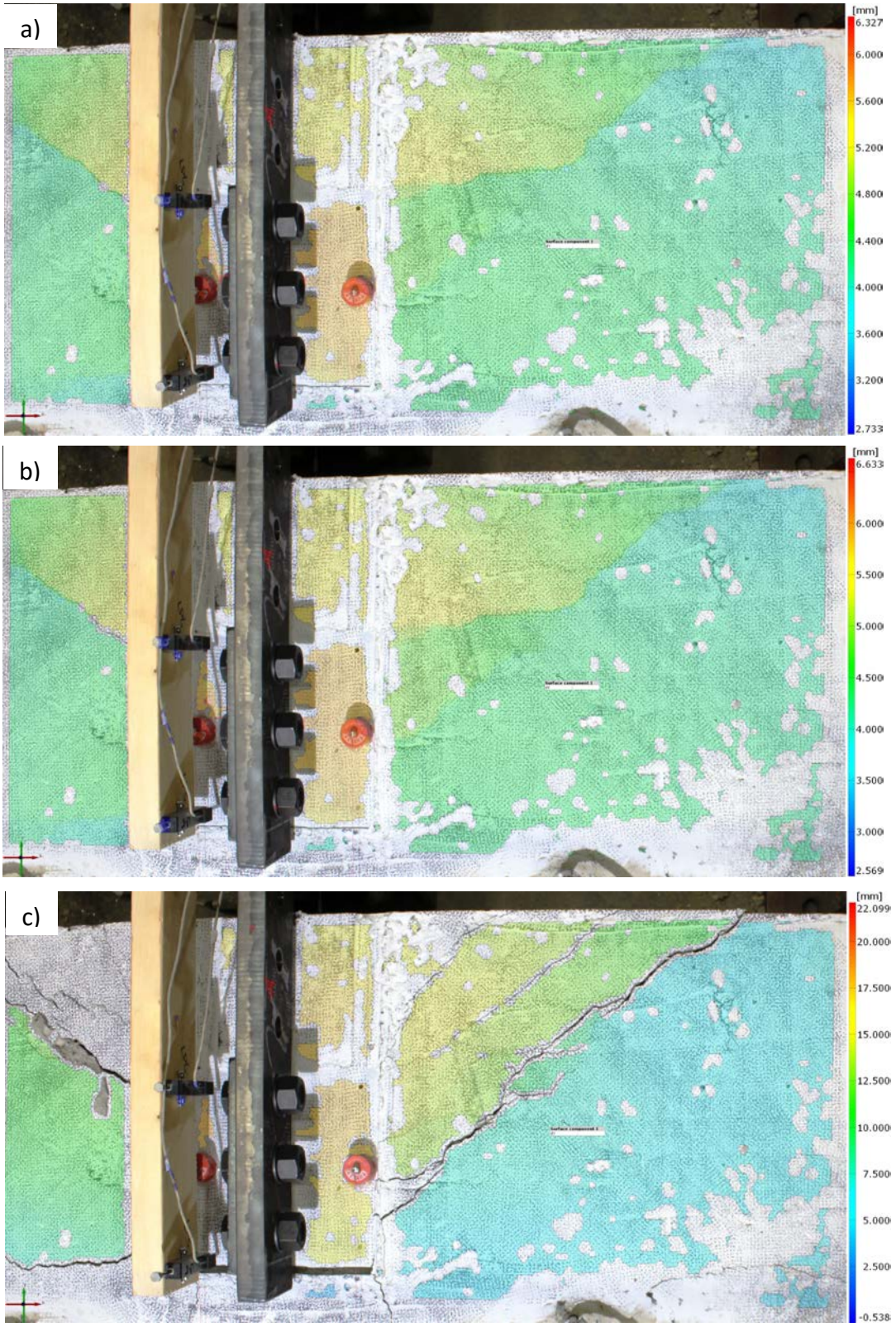

Figure B.8 DIC images of SEP4-150-250 at (a) initial cracking, (b) peak load, (c) net plate displacement of 15 mm (right of connection)

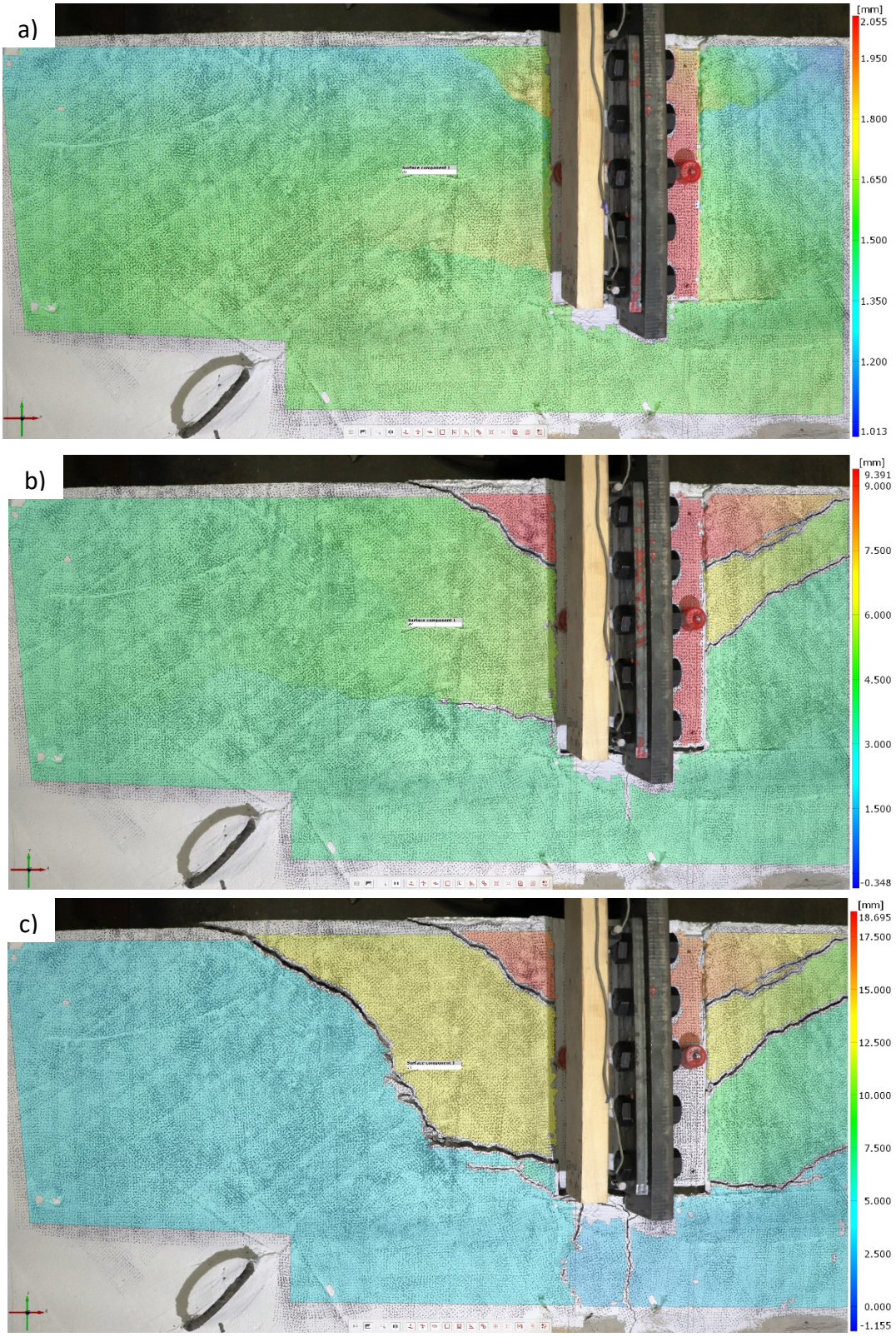

Figure B.9 DIC images of SEP6-150-75 at (a) initial cracking, (b) peak load, (c) net plate displacement of 15 mm (left of connection)

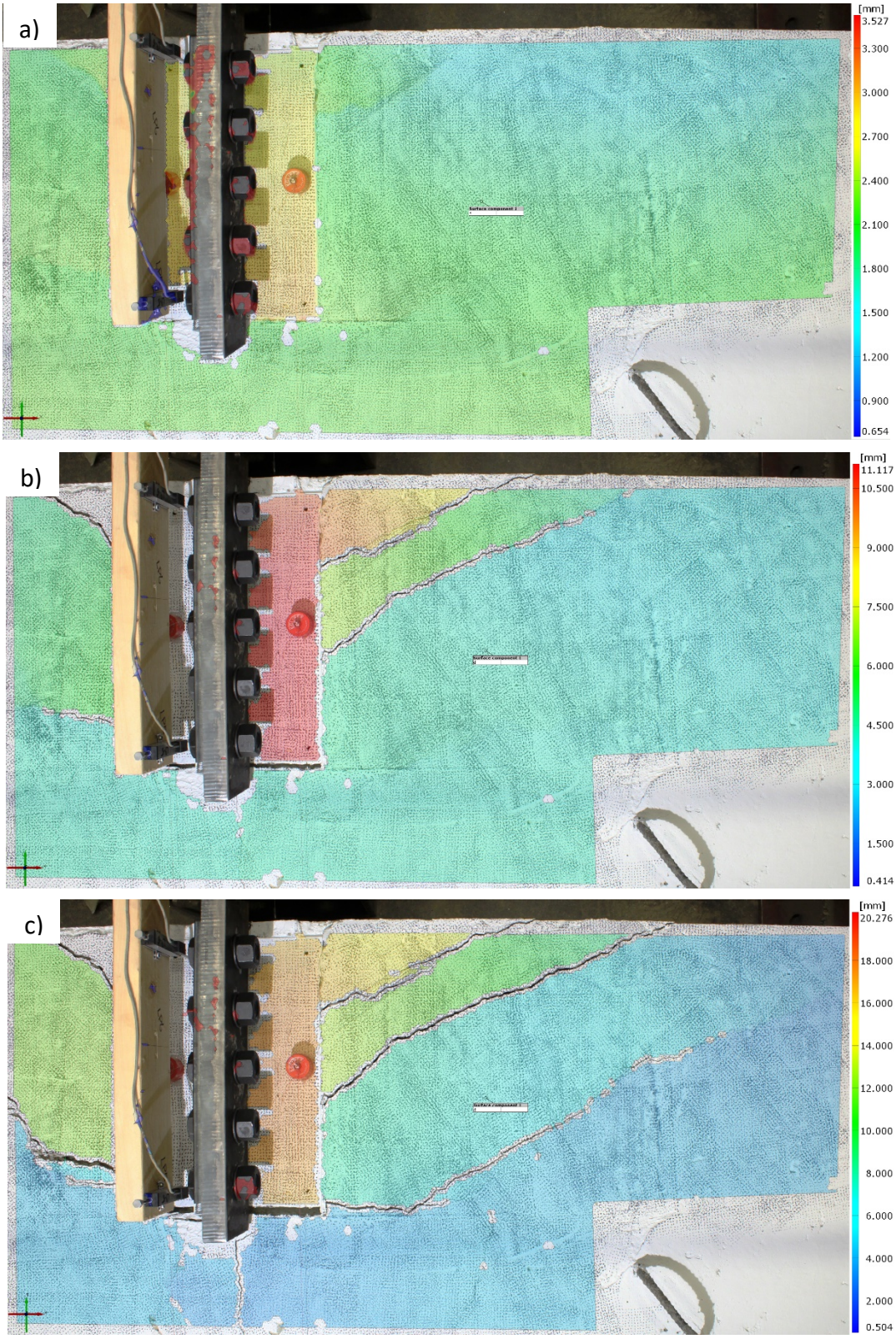

Figure B.10 DIC images of SEP6-150-75 at (a) initial cracking, (b) peak load, (c) net plate displacement of 15 mm (right of connection)

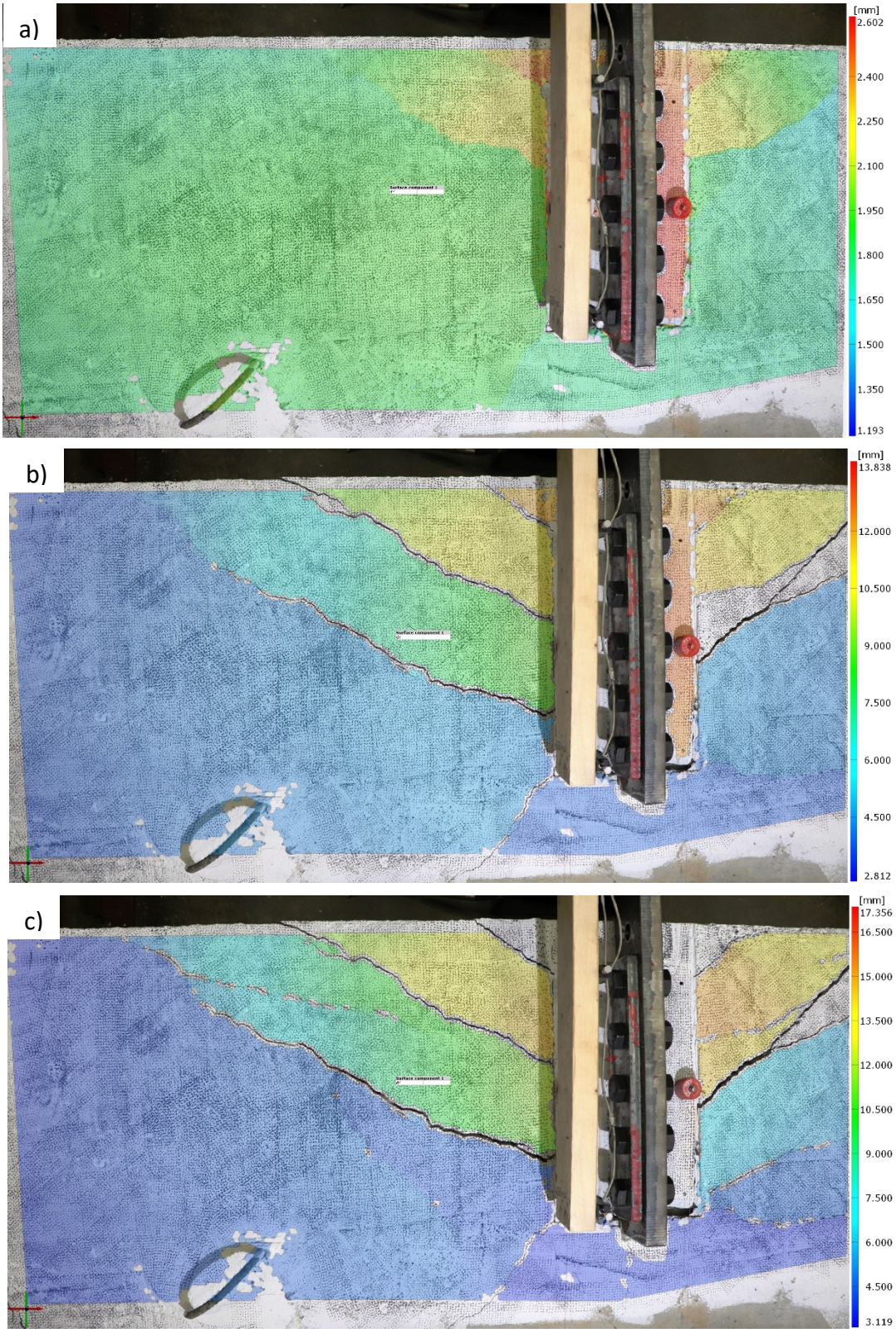

Figure B.11 DIC images of SEP6-150-125 at (a) initial cracking, (b) peak load, (c) net plate displacement of 15 mm (left of connection)

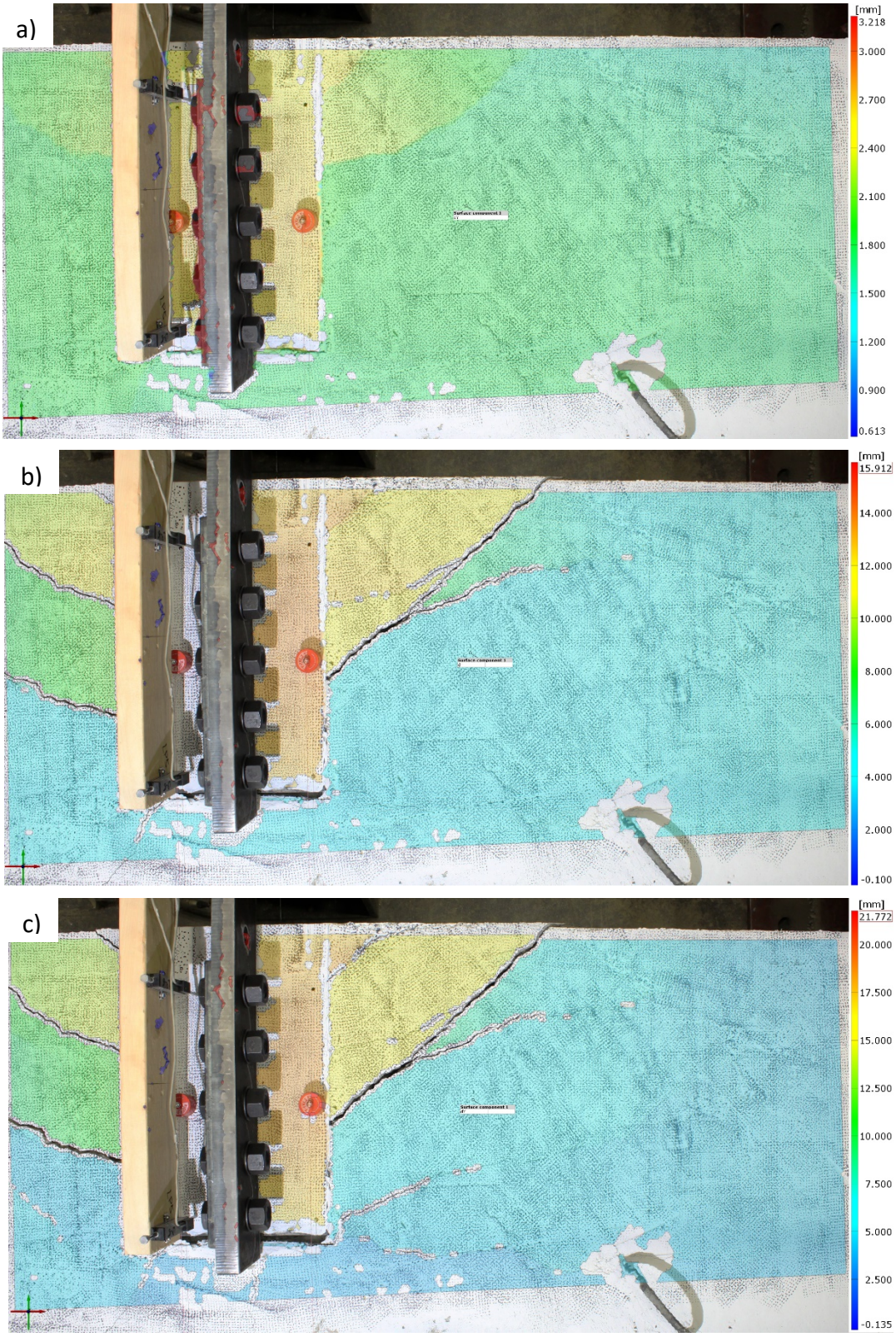

Figure B.12 DIC images of SEP6-150-125 at (a) initial cracking, (b) peak load, (c) net plate displacement of 15 mm (right of connection)

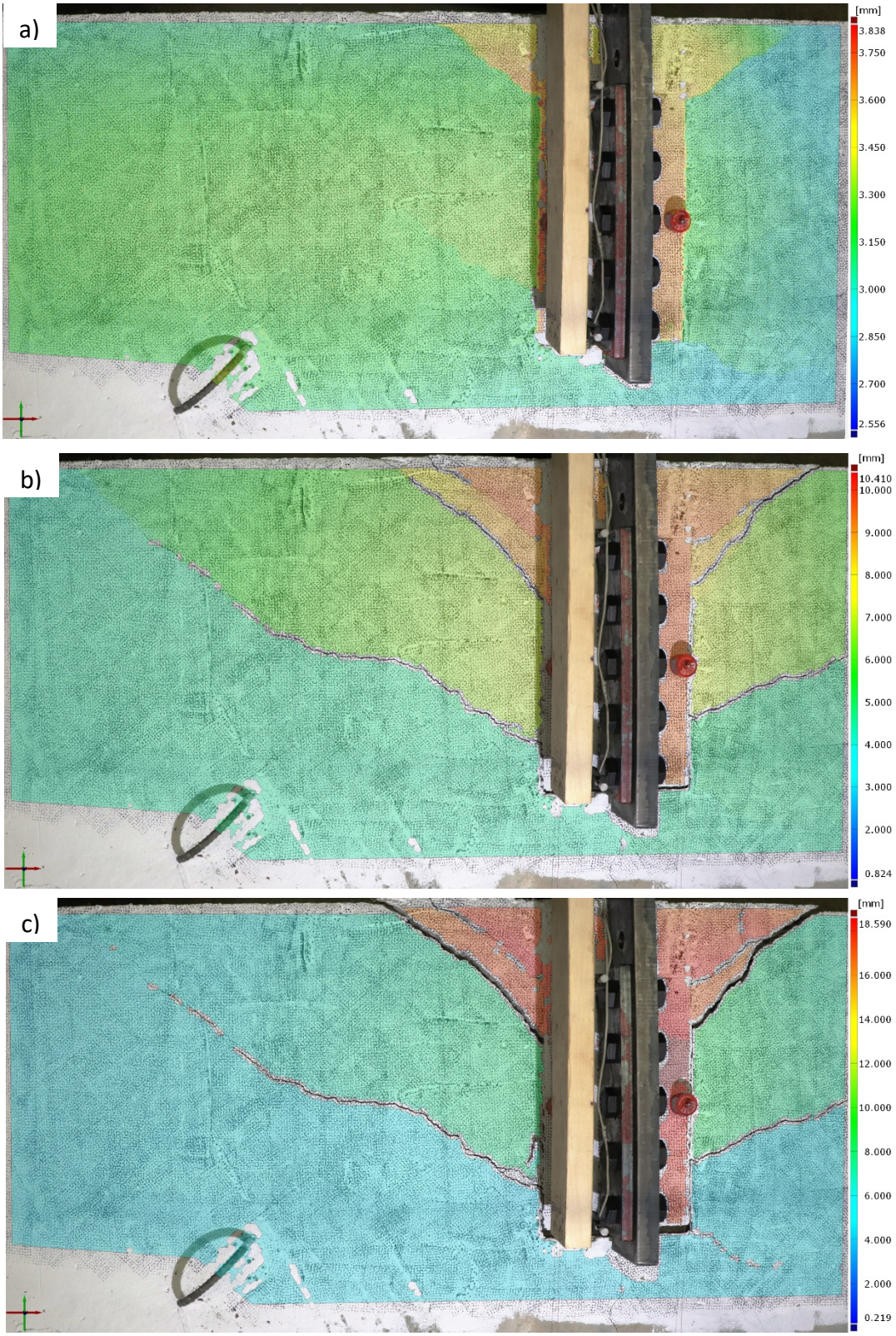

Figure B.13 DIC images of SEP6-150-175 at (a) initial cracking, (b) peak load, (c) net plate displacement of 15 mm (left of connection)

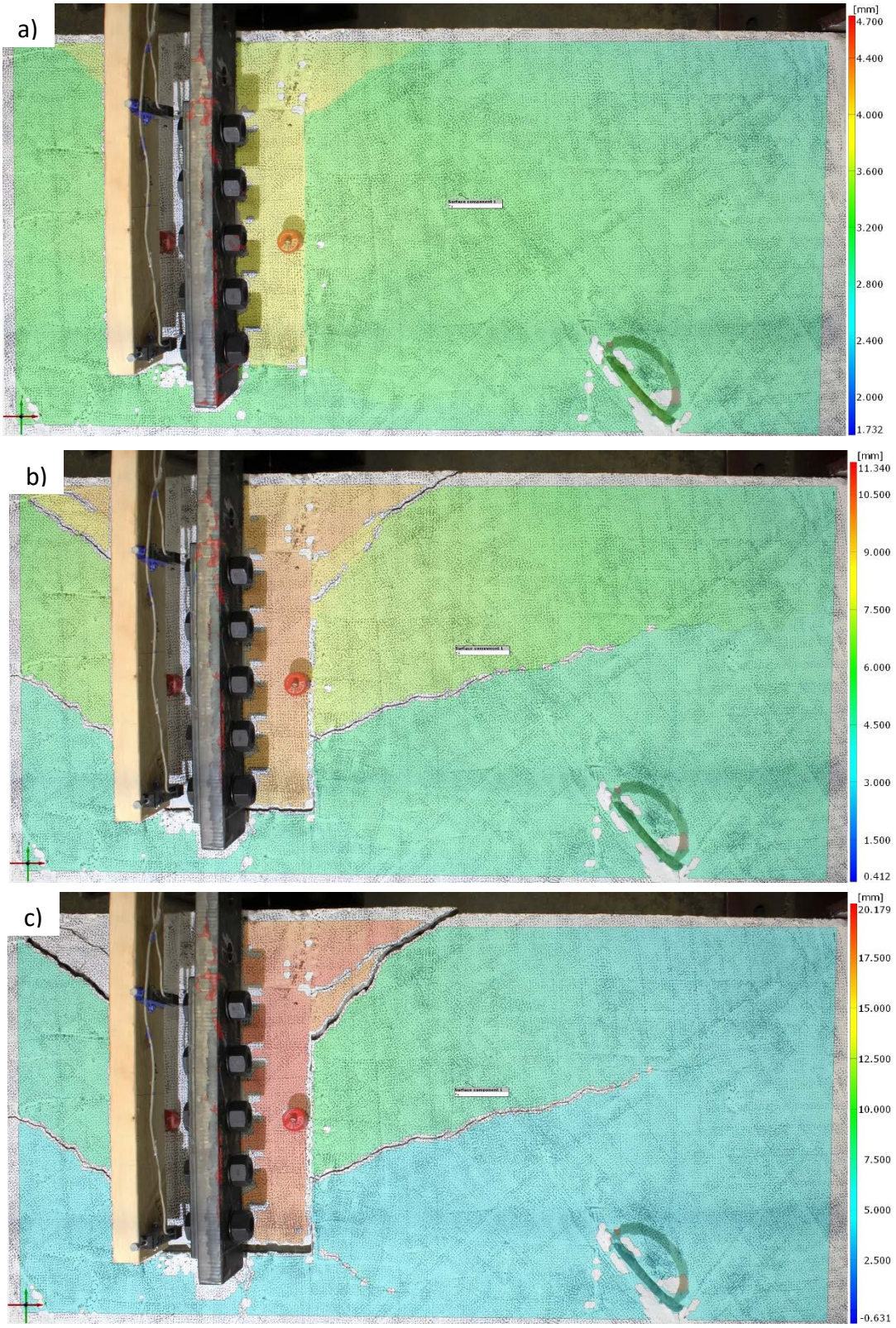

Figure B.14 DIC images of SEP6-150-175 at (a) initial cracking, (b) peak load, (c) net plate displacement of 15 mm (right of connection)

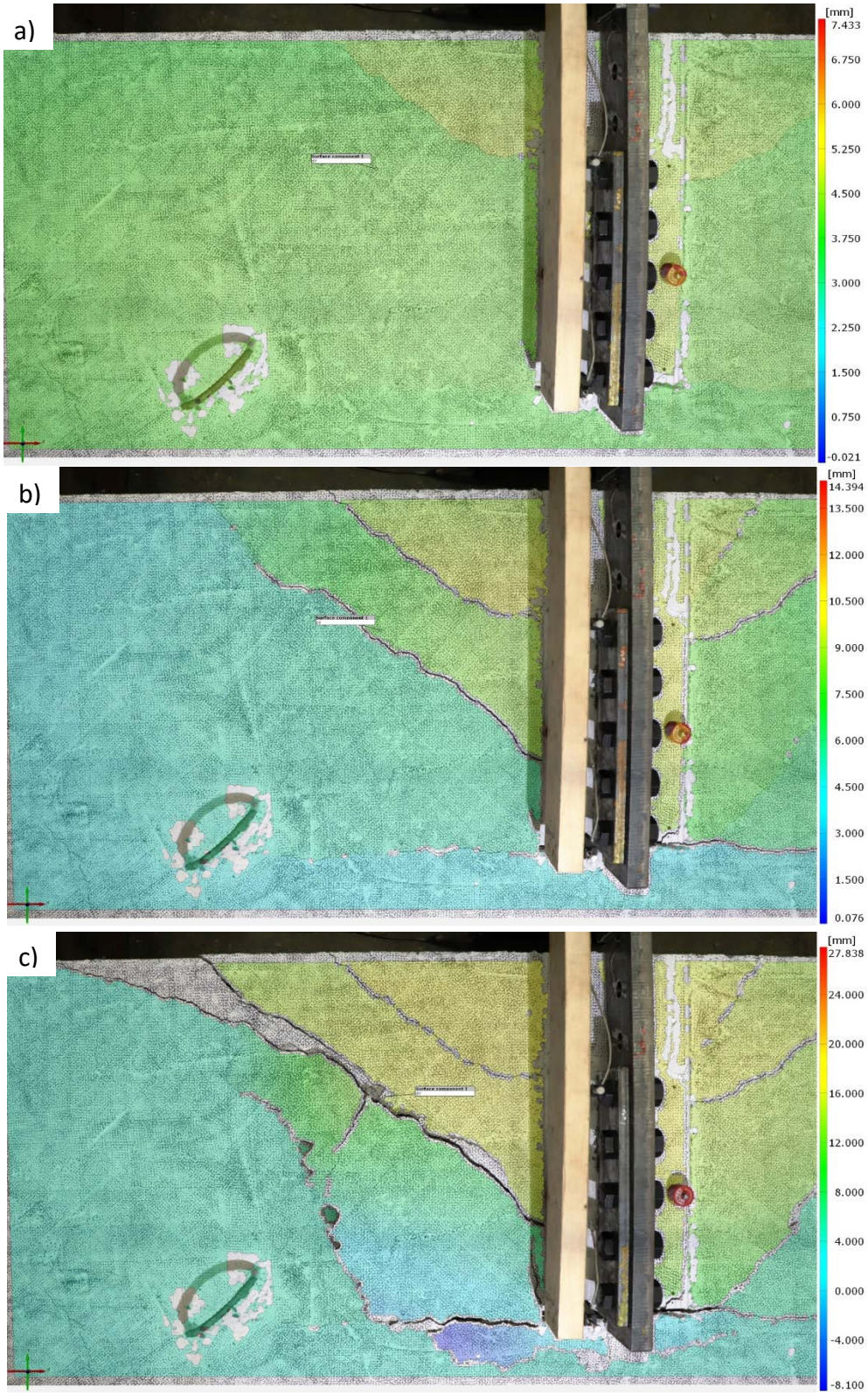

Figure B.15 DIC images of SEP6-150-250 at (a) initial cracking, (b) peak load, (c) net plate displacement of 15 mm (left of connection)

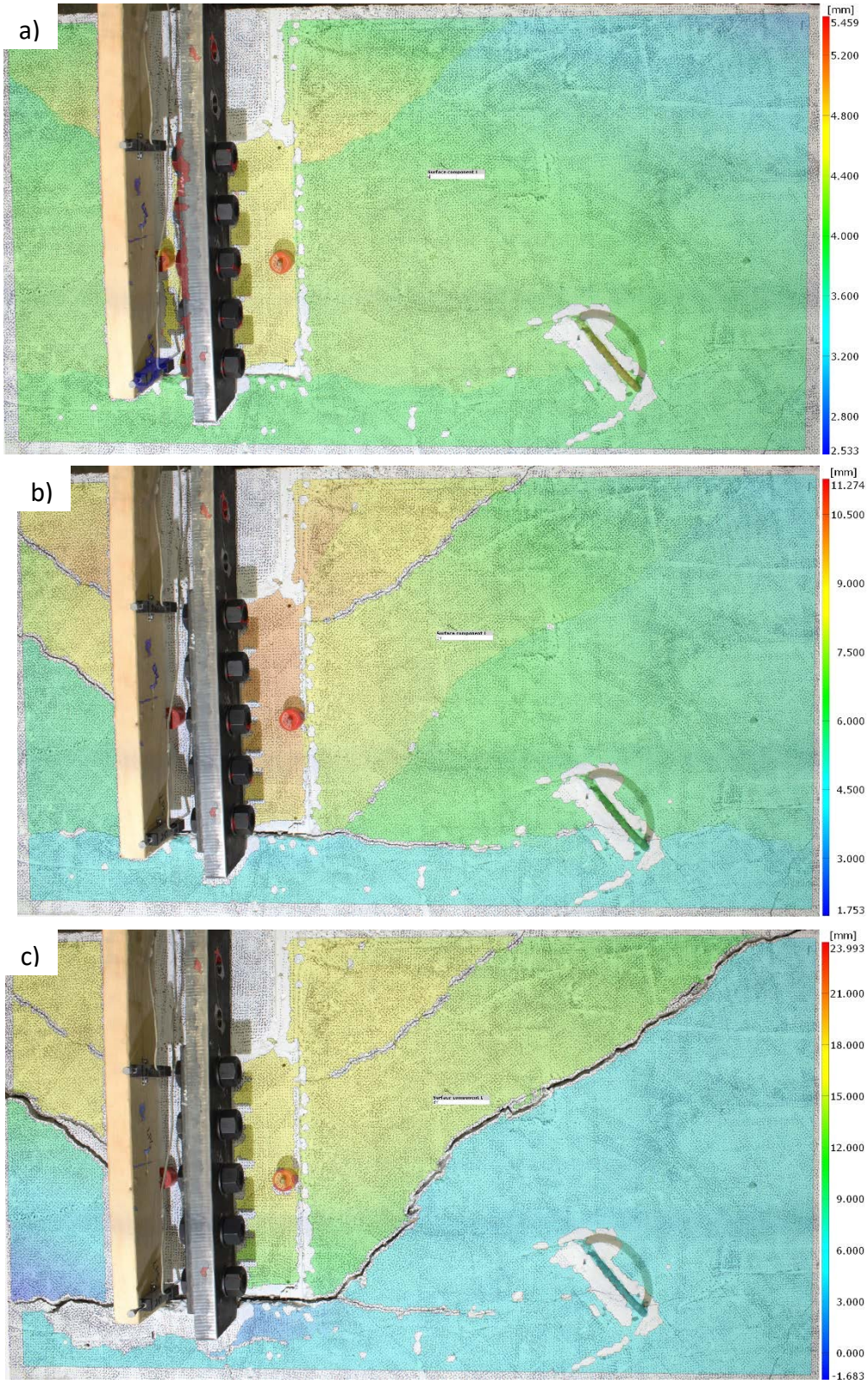

Figure B.16 DIC images of SEP6-150-250 at (a) initial cracking, (b) peak load, (c) net plate displacement of 15 mm (right of connection)

Appendix C – Material Properties

Headed Stud

	Specimen 1	Specimen 2	Specimen 3	Mean	Standard Deviation
E_s (GPa)	200	212	213	208	7.2
f_{uta} (MPa)	504.4	498.1	510.5	504	6.20
Initial Diameter (mm)	9.01	8.95	8.96	8.97	0.032
Initial Area (mm^2)	63.8	62.9	63.1	63.2	0.45
Final Diameter (mm)	5.62	5.48	5.59	5.56	0.072
Final Area (mm^2)	24.8	23.6	24.6	24.3	0.63
% Area Reduction	61.2	62.5	61.1	61.6	0.81
Initial Gauge Length (mm)	50.8	50.8	50.8	50.8	0
Final Gauge Length (mm)	60.81	60.18	60.21	60.4	0.36
% Elongation	19.7	18.5	18.5	18.9	0.70

10M Rebar

	Specimen 1	Specimen 2	Specimen 3	Mean	Standard Deviation
Yield Force (kN)	39.9	40	65.9	48.6	15.0
Peak Load (kN)	58.1	57.8	83.2	66.4	14.6
Initial Gauge Length (mm)	200	200	200	200	0
Final Gauge Length (mm)	225.4	225.5	213.0	221.3	7.19
% Elongation	12.7	12.8	6.5	10.7	3.59

15M Rebar

	Specimen 1	Specimen 2	Specimen 3	Mean	Standard Deviation
Elastic Modulus (GPa)	190	200	200	197	5.8
Yield Strength (MPa)	459	463	457	460	3.1
Ultimate Strength (MPa)	719	720	720	720	0.6
Initial Gauge Length (mm)	200	200	200	200	0
Final Gauge Length (mm)	227.2	225.1	227.0	226.5	1.14
% Elongation	13.6	12.6	13.5	13.2	0.57

Concrete Cylinders

Before testing SEP4 specimens					
	Specimen 1	Specimen 2	Specimen 3	Mean	Standard Deviation
E_c (GPa)	21.6	21.1	20.1	20.9	0.77
f'_c (MPa)	38.9	43.1	40.9	41.0	2.10
In between testing SEP4 and SEP6 specimens					
	Specimen 1	Specimen 2	Specimen 3	Mean	Standard Deviation
E_c (GPa)	20.5	19.2	22.0	20.6	1.37
f'_c (MPa)	40.3	40.5	36.9	39.2	2.02
After testing SEP6 Specimens					
	Specimen 1	Specimen 2	Specimen 3	Mean	Standard Deviation
E_c (GPa)	21.5	22.0	20.6	21.4	0.69
f'_c (MPa)	41.1	41.3	39.3	40.6	1.10

Concrete Beam

	Specimen 1	Specimen 2	Specimen 3	Mean	Standard Deviation
Modulus of Rupture (MPa)	5.3	6.1	6.4	5.9	0.6

Appendix D – Construction Process of Formwork for Specimens

The formwork for the two concrete specimens was constructed from 19 mm (3/4 inch) plywood, and two-by-four (38 × 89 mm) pieces of lumber, shown in Figure D.1. Additionally, metal straps were used to join the plywood pieces in the bottom of the formwork, and to strengthen the corners.

Figure D.1 Formwork for SEP4 concrete specimen

The reinforcement cages used in the concrete blocks were first constructed outside the forms using steel tie wire, shown in Figure D.2. They were then placed into the formwork, and rebar chairs were used to ensure the required cover of 30 mm was achieved, shown in Figure D.3. Tape, and silicone caulking were also used at the interior edges of the formwork, and between plywood sheets to prevent leakage.

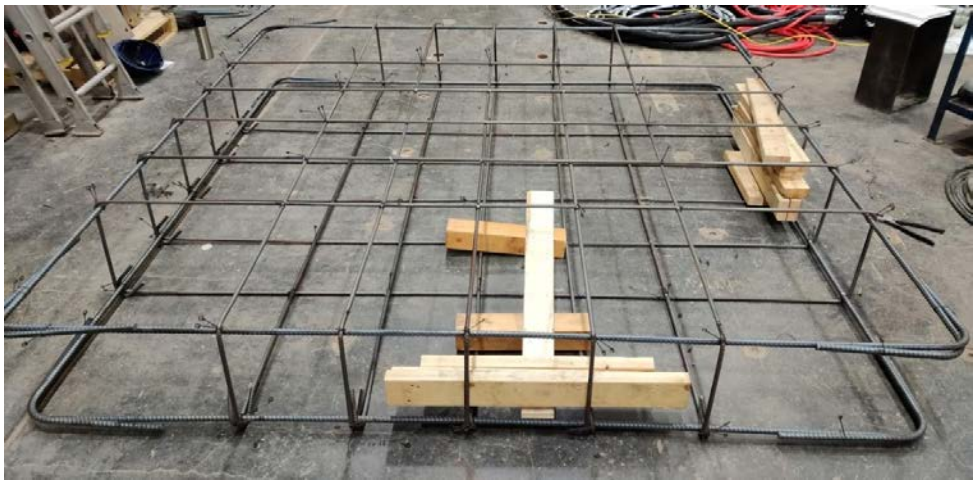

Figure D.2 Reinforcement cage for SEP4 concrete specimen

Figure D.3 Placement of reinforcement into SEP4 concrete specimen formwork

Next, the embedded plates, complete with shear tab and nailer holes, were screwed onto two-by-four pieces of lumber and cantilevered over the walls of the formwork, shown in Figure D.4. After the embedded plates were positioned in the correct location, the cantilevered lumber pieces were then screwed to additional pieces of lumber and screwed into the bottom of the formwork.

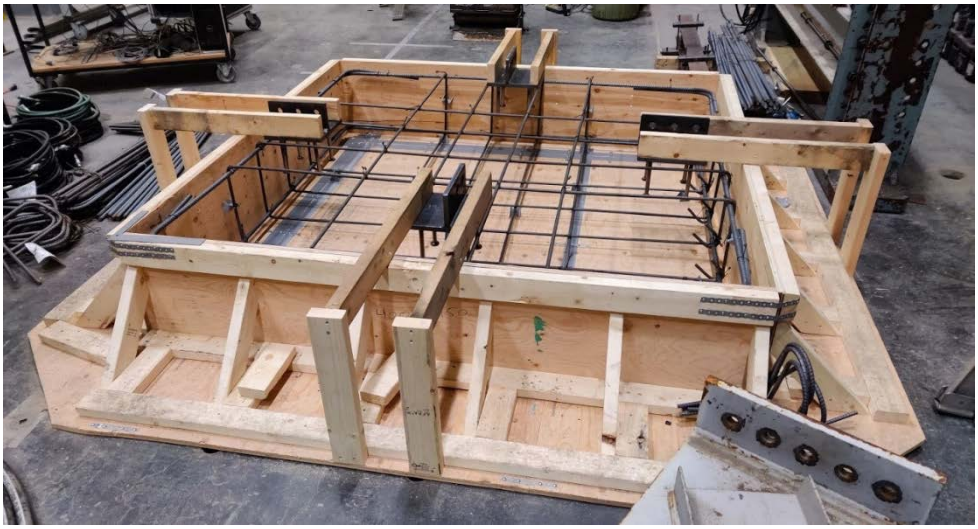

Figure D.4 Installation of SEP4 embedded plates

4.5 m^3 of 30 MPa concrete was ordered, and it was delivered in a single truck for the concrete blocks. During the pour, vibrators were used to ensure concrete flowed around the rebar, and below the embedded plates. 15 cylinders were also cast for materials property tests.

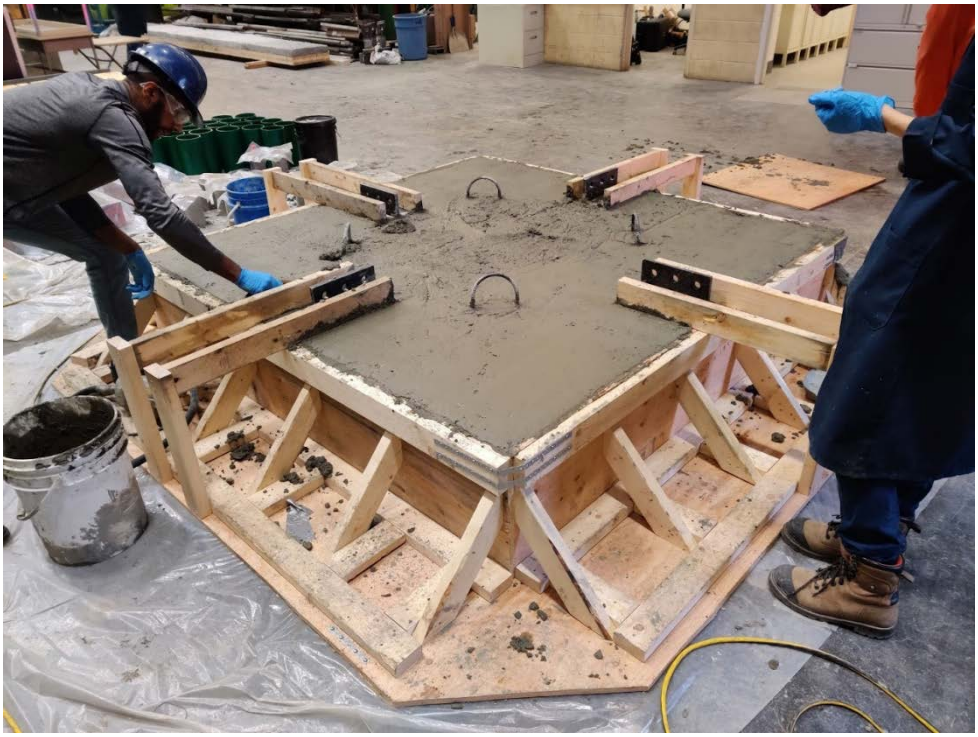

Figure D.5 Finishing of SEP4 concrete specimen

After the concrete was poured, trowels were used to finish the concrete, shown in Figure D.5. A smooth and even surface is desired especially when DIC will be used. A vapour barrier was also placed on top after the finishing. Finally, the specimens were cured for seven days before the forms were stripped and then left to cure indoors for a total of at least 28 days.